Studies on the Rehydration Mechanisms of Expandable Clay Minerals

Motoharu KAWANO

A dissertation submitted to the Doctoral Program
in Geoscience, the University of Tsukuba
in partial fulfillment of the requirements for the
degree of Doctor of Philosophy (in Science)

1993

CONTENTS

ABSTRACT

The rehydration characteristics of expandable clay minerals such as smectite, vermiculite, and rectorite were investigated by X-ray diffraction, infrared absorption, thermal, and chemical analyses to elucidate rehydration mechanisms of the minerals. The behaviors of interlayer cations in the dehydration and rehydration processes were also revealed by means of one-dimensional Fourier analysis and factors affecting the rehydration properties were defined.

The rehydration characteristics of smectites are as follows: (1) the Mg- and K-saturated materials exhibited the slowest and the fastest rehydration rates, respectively, (2) the rehydration ability of beidellite was stronger than that of montmorillonite, and (3) the rehydration ability of trioctahedral smectite was stronger than that of dioctahedral smectite, if both minerals have similar negative charge distribution. Based on the Fourier analysis, it was revealed that interlayer cations of smectites migrated into the hexagonal holes of SiO_4 network by thermal dehydration and returned again to the interlayer space on rehydration. The heating temperatures and sizes of interlayer cations determined the extent of migration. Thus, the smectite heated at lower temperatures or that saturated with large-sized cations (e.g., K^+) exhibited strong rehydration ability because the interlayer cations were located at shallow part of the holes. The migrated cations were attracted by electrostatic force originated from substitution of Mg^{2+} for Al^{3+} in the octahedral sheets, which inhibited rehydration of montmorillonite. However, rehydration of saponite was promoted by a strong repulsive electrostatic force between migrated cations and protons of hydroxyl ions.

The rehydration characteristics of vermiculite are as follows: (1) the Mg- and K-saturated materials exhibited the fastest and the slowest rehydration rates, respectively, and (2) the rehydration ability of vermiculites saturated with any cation other than K^+

were stronger than that of smectite. These rehydration properties of vermiculite appeared to be quite different from those of smectite. The interlayer cations of vermiculite did not migrate into the hexagonal holes and remained at the interlayer space even after thermal dehydration. Consequently, vermiculite exhibited strong rehydration ability and the rehydration rate was strongly affected by hydration energy of interlayer cations. The turbostratic stacking of elementary layer of smectite enhanced migration of interlayer cations into the hexagonal holes, whereas the ordered stacking of vermiculite inhibited cation migration.

Hectorite exhibited weak rehydration ability and slow rehydration rate compared with those of saponite, which can be explained the same reason of montmorillonite. The Mg-saturated hectorite changed through a transitional phase of regular interstratification of dehydrated and rehydrated layers to completely dehydrated structure after heating between 300° and 600°C. The transitional phase was produced by fixation of interlayer Mg^{2+} to the alternating interlayers of hectorite consisting regular distribution of F^- to F^- and OH^- to OH^- facings distinct from the interlayer space.

The rehydration characteristics of rectorite are as follows: (1) the strong rehydration ability was retained until thermal decomposed of crystal structure took place, (2) the Mg- and K-saturated materials heated below 400°C exhibited the slowest and fastest rehydration rates, respectively, and (3) different hydration states appeared on rehydration after heating above 500°C. The strong hydration ability and different hydration rates can be explained by the same reasons as those of beidellite, however the last rehydration property is the most important characteristic which has not been observed in any other expandable clay minerals. The interlayer cations of rectorite migrated into the hexagonal holes by thermal dehydration and returned completely to the interlayer space on rehydration after heating below 400°C. For after heating above 500°C,

however, the migrated cations did not return to the original position and remained around the basal oxygen plane even water molecules were regained in the interlayer space. Consequently, the water molecules coordinated abnormally to the relocated interlayer cations and the different hydration states appeared on rehydration.

In conclusion, the rehydration properties of expandable clay minerals can be explained by the behaviors of interlayer cations in the dehydration and rehydration processes. These behaviors appeared to be controlled by following factors: (1) ionic size of interlayer cations, (2) electrostatic force between the interlayer cations and the octahedral sheet, and (3) nature of stacking of the adjacent silicate layers.

CHAPTER 1 GENERAL INTRODUCTION

Clay minerals can be divided structurally into the amorphous materials (e.g., allophane and imogolite) and the crystalline materials. The most of the crystalline clay minerals belongs to the family of phyllosilicate which is characterized by continuous two-dimensional tetrahedral sheets composed of SiO_4 units linked with neighboring tetrahedra by sharing three oxygens (basal oxygens) in the same horizontal plane. The fourth oxygens (apical oxygens) of each tetrahedra are not shared with another SiO_4 but forms corners of an adjacent octahedral sheet composed of $AlO_4(OH)_2$ units. The tetrahedral cations are Si, Al, or Fe^{3+}, and the octahedral cations normally are Mg, Al, Fe^{2+}, Fe^{3+}, and a small amount of Ti. According to Bailey (1980), the crystalline clay minerals can be classified on the basis of layer type (1:1 or 2:1), layer charge, and type of interlayer into eight major groups as follows: serpentine-kaolin, talc-pyrophyllite, smectite, vermiculite, mica, brittle mica, chlorite, and sepiolite-palygorskite groups. In this classification, the smectite and vermiculite groups fall under the category of expandable clay minerals. Interstratified clay minerals which contain smectite or vermiculite as one of the component layer can also be included in this category.

The structure of smectite and vermiculite consists of negatively charged 2:1 layers and cations located between adjacent 2:1 layers (Figure 1.1). The negative charge originates mainly from substitution of Al^{3+} for Si^{4+} in the tetrahedral sheets or substitution of Mg^{2+} for Al^{3+} in the octahedral sheets, which is electrically balanced by interlayer cations. The values of layer charge in smectites and vermiculites are 0.2 to 0.6 and 0.6 to 0.9 per $O_{10}(OH)_2$ formula unit, respectively (Bailey, 1980). These values are not precisely defined limits but apparently smaller than that of mica group. Therefore,

interlayer bonding of these minerals is relatively weak and the interlayer cations are readily exchangeable. Furthermore, the expandable clay minerals form normally interlamellar complexes with inorganic or organic materials by introduction of such materials into the interlayers. The most common of the interlayer materials is water which coordinate with interlayer cations. The coordination states of water molecules are strongly dependent on the humidity of the ambient atmosphere, and the basal spacing changes stepwise corresponding the hydration states (Glaeser and Méring, 1968; Suquet *et al.*, 1975; Watanabe and Sato, 1988; Matsuda, 1989). When the minerals are heated to successively moderate temperatures (200° to 300°C), the basal spacing contracts due to removal of water molecules from the interlayer space. On exposure to moist air, water molecules are regained in the interlayer space which causes expansion of the basal spacing as illustrated in Figure 1.2.

The studies on the thermal dehydration of expandable clay minerals have been extensively carried out, and details of it are relatively well known (Walker, 1956; Farmer and Russell, 1967). However, the rehydration characteristics and the rehydration mechanisms of the minerals are poorly understood in spite of one of the most fundamental problem of clay mineralogy. It is empirically known that the expandable clay minerals exhibit various rehydration behaviors which are strongly dependent on the crystallochemical characteristics (MacEwan and Wilson, 1980). For example, Li-montmorillonite dehydrates irreversibly after heating at 250°C, whereas Li-beidellite exhibits again expansion of the basal spacing on glycerol solvation after heating at that temperature. There are two reasons which explain this phenomena, one is the migration of Li^+ into empty octahedral sites of montmorillonite where it neutralizes the layer charge

(Hofmann and Klemen, 1950; Greene-Kelly, 1953, 1955; Glaeser and Méring, 1967), and the other is the migration into hexagonal holes rather than the empty octahedral sites (Komarov *et al.*, 1977; Luca and Cardile, 1988, 1989). In any case, the rehydration behaviors seems to be related to fixation of the interlayer cations to the clay structure, and kind of the cations and structures of the clay minerals may affect the fixation.

The expandable clay minerals are widely used for chemical industry to utilize their large surface area which makes it possible to conduct adsorption reaction and catalytic activity in an aqueous system (Barrer, 1978). The clay catalysts produced by cross-linking of expandable clay minerals with organic or inorganic compounds show solution-like catalytic activity and selective adsorption properties (Shabtai, 1979; Lussier *et al.*, 1980, etc.). Such catalysts, so called "Pillared clay", have recently attracted considerably attention, because the pore sizes can be controlled by varying the size or length of the pillar (Rupert *et al.*, 1987). Thus, the elucidation of fundamental properties of expandable clay minerals including rehydration is very important to extend the industrial utilization.

In this study, the rehydration characteristics of expandable clay minerals were examined by means of various physical and chemical methods to elucidate their rehydration mechanisms.

In Chapter 2, the rehydration characteristics of dioctahedral smectites were described and their rehydration mechanisms were discussed.

In Chapter 3, comparative investigation on the rehydration characteristics of saponite and vermiculite were carried out, and the rehydration mechanisms of the minerals were discussed.

In Chapter 4, the rehydration characteristics of hectorite were described and its rehydration mechanism was discussed.

In Chapter 5, the rehydration characteristics of rectorite were described in detail and its rehydration mechanism was discussed.

CHAPTER 2 DIOCTAHEDRAL SMECTITE

2.1 INTRODUCTION

Smectite group has various isomorphous substitutions within both tetrahedral and dioctahedral sites, and it can be divided chemically into two sub-groups as dioctahedral and trioctahedral smectites. Only two out of three octahedral sites of the former are occupied mainly by trivalent cations and all three sites of the later are populated by divalent cations. The dioctahedral smectites commonly contain Si^{4+} and Al^{3+} as tetrahedral cations and Al^{3+}, Mg^{2+}, and Fe^{3+} as dioctahedral cations. Based on chemical compositions, three species are known as end-member of dioctahedral smectites as follows:

Montmorillonite: $M^{+}_{y}(Al_{2-y}Mg_{y})Si_4O_{10}(OH)_2$,

Beidellite: $M^{+}_{x}Al_2(Si_{4-x}Al_x)O_{10}(OH)_2$,

Nontronite: $M^{+}_{x}Fe^{3+}(Si_{4-x}Al_x)O_{10}(OH)_2$.

The negative charge of montmorillonite originates from the substitution of Mg^{2+} for Al^{3+} in octahedral sites, whereas that of beidellite and nontronite arises from the substitution of Al^{3+} for Si^{4+} in tetrahedral sites; M^{+} is a monovalent interlayer cation. Dioctahedral smectites having intermediate compositions between montmorillonite and beidellite are commonly occur in nature and end-menders are rare.

In this Chapter, the rehydration characteristics of dioctahedral smectites which belong to montmorillonite-beidellite series were described and their rehydration mechanisms were discussed. There have been some attempts to investigate the dehydration and rehydration of dioctahedral smectites. Méring (1946) reported that montmorillonite dehydrated irreversibly after heating at 350° to 500°C and pointed out

that kind of interlayer cations influenced the irreversible dehydration temperatures. It is well known that the expansion characteristics of Li-saturated dioctahedral smectites after heating at 250° to 300°C are strongly dependent on charge balance between tetrahedral and octahedral sheets; montmorillonite remains dehydrated but beidellite exhibits expansion of basal spacing to 17.7Å when solvated with glycerol. Similar phenomenon can be observed when exposed to moist air (Russell and Farmer, 1964). Hofmann and Klemen (1950) and Greene-Kelly (1953, 1955) attributed the phenomenon to the migration of small cations into empty octahedral sites of montmorillonite, where they neutralize the octahedral negative charge. However, the rehydration characteristics of dioctahedral smectites saturated with other cations such as Ca^{2+}, Mg^{2+}, Na^{+}, or K^{+} are remain uncertain.

2.2 MATERIALS

Three dioctahedral smectites having different chemical compositions were used in this study, they are from Cheto, U.S.A., Aterasawa, Yamagata Prefecture, Japan, and Sano mine, Nagano Prefecture, Japan. The chemical compositions and numbers of cations are listed in Table 2.1. The chemical composition of Cheto and Sano materials are close to end-member of montmorillonite and beidellite, respectively, and that of Aterasawa material corresponds to intermediate between them. The differential thermal and thermogravimetoric analyses (DTA-TGA) curves of Cheto and Aterasawa materials are shown in Figure 2.1. All of these materials contain homoionic interlayer cation (Ca^{2+}, Mg^{2+}, Na^{+}, or K^{+}). The Cheto material exhibited dehydration of interlayer water below 205°C and dehydroxylation at about 600°-650°C. The TGA curves clearly

showed weight loss due to dehydration and dehydroxylation. The Aterasawa material also gave similar DTA-DTA curves to those of Cheto material (Figure 2.1B).

2.3 EXPERIMENTAL METHODS

The < 2μm fractions of the materials were collected by normal sedimentation methods and were saturated with Ca^{2+}, Mg^{2+}, Na^{+}, or K^{+} by treatment with respective 1 N chloride solutions, and the excess salt was then removed by washing five times with 80% ethanol until complete absence of Cl^{-} ions. These homoionic materials were dried in air, and were heated between 100° to 900°C at intervals of 100°C and then cooled in a desiccator for 1 hr. The relative humidity (RH) in the desiccator was controlled at 0% with di-phosphorus pentanoxide.

These heated materials were used for the following experiment: (1) rehydration ability after heating, (2) rehydration rate after heating, (3) changes in exchangeability of interlayer cations after heating, (4) behaviors of interlayer cations during dehydration and rehydration, and (5) change in d(060) spacing by heating.

The rehydration ability of the materials were examined as follows. The heated materials were re-wetted in deionized water for 1 day and dried in air at 50% RH. These materials were oriented on glass slides by re-suspension in deionized water and allowed to dry again at 50% RH. They were used for X-ray powder diffraction (XRD) analysis.

The rehydration rates were investigated as follows. The unheated homoionic materials oriented on quartz glass slides were heated at 400° or 800°C for 1 hr and then cooled in a desiccator at 0% RH for 1 hr. Changes in XRD patterns for the heated materials on exposure to air at 50% RH for various periods of time were recorded using a

RIGAKU diffractometer, Ni-filtered CuK α radiation, and a scanning speed of 2°2 θ /min.

The changes in exchangeability of interlayer cations were examined by measuring values of exchangeable cations after heating at various temperatures. About 0.5 g of unheated homoionic materials were heated between 100° to 900°C at an intervals of 100°C for 1 hr, and were washed with 0.1N $SrCl_2$ solution more than five times. The extracted cations (Ca^{2+}, Mg^{2+}, Na^{+}, and K^{+}) were measured with an atomic absorption spectrometer (AAS). To confirm that no interlayer cations were lost during heating, the oxide contents of saturated cations (CaO, MgO, Na_2O, and K_2O) in heated materials prepared by the same procedure were measured.

The behaviors of interlayer cations during dehydration and rehydration were examined by one-dimensional Fourier analysis. Materials used this study are Na-saturated Aterasawa smectite: (1) unheated, (2) heated at 600°C, (3) rehydrated after heating at 600°C, and (4) heated at 800°C, and Na-saturated Sano beidellite: (1) unheated, (2) heated at 400°C, (3) heated at 800°C, and (4) rehydrated after heating at 800°C. XRD data were obtained using a RIGAKU diffractometer under relative humidity conditions at 0% and 50% RH for dehydrated and hydrated materials, respectively. Fourier synthesis was made using observed structure factors (Fo) whose signs were driven from calculated structure factors (Fc). The atomic scattering factors were taken from International Tables (1962). The initial structural model used was from Reynolds (1980), and the z-parameters along the c-axis were refined by the least squares method. The minimizing function Rw is given by:

$$Rw = \sum(|Fo| - |Fc|)^2,$$

and reliability factor R is defined as follows:

$$R = \frac{\sum(|Fo| - |Fc|)}{\sum|Fo|} .$$

The changes of d(060) values of homoionic materials before and after heating were examined by XRD. The XRD data were obtained using Ni-filtered CuK α radiation and a scanning speed of 0.5°2 θ /min under 50% RH for the unheated materials and 0% RH for the heated ones.

2.4 RESULTS

2.4.1 Rehydration ability after heating

Figure 2.2A shows variation of d(001) values of the homoionic rehydrated montmorillonite from Cheto after heating at various temperatures. The unheated Ca- and Mg-materials exhibited two-layer hydration having d(001) values of 15.5 and 15.3Å, respectively. On the other hand, the Na- and K-materials showed one-layer hydration with d(001) values of 13.2 and 12.6Å. respectively. These values generally agree with the hydration states of dioctahedral smectite as reported by Suquet *et al.* (1975). After heating at various temperatures and water saturation, the K-material rehydrated slightly after heating at 600°C, whereas the Mg-material remained dehydrated after heating at 400°C. For the Ca- and Na-materials, the rehydration ability was retained up to 500°C. Similar rehydration behaviors were observed in the Aterasawa smectite (Figure 2.2B), however the irreversible dehydration temperatures of the Ca-, Na-, and K-saturated Aterasawa smectite were slightly higher than those of the Cheto montmorillonite. On the other hand, the homoionic beidellite completely rehydrated after heating below 800°C

(Figure 2.2C). After heating at 900°C, the Mg-material did not rehydrate but the Ca-, Na-, and K-materials exhibited segregation structures of rehydrated and dehydrated layers on saturation with deionized water. These results indicate that the rehydration ability of dioctahedral smectite increases with increasing size of the interlayer cations and with decreasing octahedral negative charge.

2.4.2 Rehydration rate in air after heating

Figure 2.3 shows XRD patterns of the homoionic montmorillonite from Cheto heated 400°C and exposure to air at 50% RH for various periods of time. The Mg-material remained dehydrated at least 1 day, whereas the Na- and K-materials exhibited rapid rehydration within a few minutes. On the other hand, the Ca-materials rehydrated progressively through segregation structure of dehydrated and two-layer hydrated forms. Figure 2.4 shows XRD patterns of the homoionic beidellite heated at 800°C and exposure to air at 50 % RH for various periods of time. The Mg-material did not rehydrate, whereas the K-material showed a rapid rehydration and completely rehydrated on exposure to air within about 20 min. The Ca- and Na-materials exhibited progressive rehydration but dehydrated forms remained for 6 and 1 day, respectively. These results strongly indicate that dioctahedral smectites rehydrate more rapidly when the interlayer cations have been exchanged by K^+ rather than Mg^{2+}.

2.4.3 Exchangeability of interlayer cations

Figure 2.5A shows oxide wt.% of CaO, MgO, Na_2O, and K_2O of the representative homoionic montmorillonite from Cheto after heating at various

temperatures. The MgO wt.% represents total value of Mg^{2+} ions located at the interlayer and the octahedral sites. The wt.% values remained constant up to 900°C, suggesting that the interlayer cations are apparently present in the dehydrated structure. The exchangeable cations extracted with 0.1N $SrCl_2$ solution after heating at various temperatures are given in Figure 2.5B. The values of exchangeable Mg^{2+} decreased rapidly by fixation to the structure at temperatures between 300° and 500°C, whereas those of K^+ almost remained up to 600°C and decreased at 600° - 700°C. The Ca^{2+} and Na^+ ions were almost fixed at 600°C. Therefore, the exchangeability of interlayer cations against the heating temperature increases as follows: $Mg^{2+} < Ca^{2+} < Na^+ < K^+$. The oxide wt.% of CaO, MgO, Na_2O, and K_2O of the homoionic smectite from Aterasawa did not change up to 900°C, indicating no interlayer cations were lost during heating (Figure 2.6A). The fixation of interlayer Mg^{2+}, Ca^{2+}, Na^+, and K^+ ions took place at 400°, 700°, 700°, and 800°C, respectively (Figure 2.6B). This result is similar to that of the Cheto montmorillonite, but the Aterasawa smectite requires more higher temperature to fix the Ca^{2+}, Na^+, and K^+ ions. The order of exchangeability of these dioctahedral smectites ($Mg^{2+} < Ca^{2+} < Na^+ < K^+$) is compatible with their rehydration ability as described in previous section.

2.4.4 Behaviors of interlayer cations during dehydration and rehydration

Figure 2.7 shows electron density distribution (ED) and difference synthesis (DS) curves along the *c*-axis for different states of Na-saturated Aterasawa smectite: (1) unheated, (2) heated at 600°C, (3) rehydrated after heating at 600°C, and (4) heated at 800°C. The basal spacings and structure factors for these materials are listed in Table

2.2. The ED curves of the unheated and rehydrated materials gave a broad peak in the interlayer region due to the interlayer Na^+ ions and water molecules. After refinement of the z-parameters, the position of the Na^+ ions was determined as shown in Figures 2.7A and 2.7C. The DS curves showed a nearly flat line, suggesting that the interlayer Na^+ ions of both materials are located at very close to the center of the interlayer space. As for the heated materials at 400° and 800°C, the DS curves (DS2 in Figures 2.7B and 2.7D) calculated by fixing the Na^+ ions at the center of the interlayer space showed a negative peak in interlayer region, suggesting that the Na^+ ions are located at other positions instead of interlayer space. The position of the Na^+ ions, however, was determined to be near the basal oxygen plane by refinement of the z-parameters. The negative peak of the DS curves was also reduced significantly (DS1 in Figures 2.7B and 2.7D), if it was calculated using the refined parameters. Figure 2.8 shows electron density distribution and difference synthesis curves for the Ca- and Mg-saturated Aterasawa smectite heated at 800°C. The basal spacings and structure factors for these materials are listed in Table 2.3. The refined positions of interlayer Ca^{2+} and Mg^{2+} are indicated as arrows on this Figure, in which these cations appeare to migrate to the basal oxygen plane. Pezerat and Méring (1967) reported one-dimensional Fourier synthesis curves of hydrated and dehydrated smectites calculated by using 18 and 14 reflections, respectively. A positive peak due to interlayer cations clearly observed near the surface of the basal oxygen plane. Inasmuch as only 10 or 8 reflections were used in this study, a significant positive peak due to Na^+ ions was not clearly recognized in the ED curves. The position of the ions, however, could be definitely determined by least squares refinement. Insofar as the behavior of the interlayer cations during dehydration and rehydration is concerned, these

results suggest that the cations apparently migrate from the interlayer space toward the hexagonal holes of silicate layers during thermal dehydration and return to the interlayer space on rehydration.

Figures 2.9A to 2.9D show ED and DS curves for the Na-saturated beidellites: (1) unheated, (2) heated at 400°C, (3) heated at 800°C, and (4) rehydrated after heating at 800°C. The basal spacings and structure factors used in this calculation are given in Table 2.4. Arrows on the ED curves indicated positions of the interlayer Na^+ ions of these materials, all of which were determined by the least square refinement. These results also demonstrate that the Na^+ ions migrate into the silicate layer during dehydration and return to the interlayer space on rehydration. Consequently, the behaviors of the interlayer Na^+ ions of the beidellite during dehydration and rehydration are essentially the same as those of the Aterasawa smectite.

2.4.5 Structural rearrangement after heating

The ED curve for the Aterasawa smectite heated at 800°C (Figure 2.7D) showed an increase in electron density near the octahedral cations and a decrease near the octahedral oxygens and hydroxyl ions compared with that of the material heated at 400°C (Figure 2.7B). The beidellite also showed such modification of ED curve after heating at 800°C (Figure 2.9C). Similar results have been reported for sericite by Udagawa (1955), for muscovite by Eberhart (1963) and Udagawa *et al.* (1974), and for pyrophyllite by Wardle and Brindley (1972). These observations have been explained as the removal of hydroxyl ions as H_2O and the relocation of residual oxygens to the same level as that of octahedral cations; $2OH^- \rightarrow H_2O + O^{2-}$. Although the dehydroxylated structure of

smectite is not well known, two types of rearranged octahedral configurations have been considered; a six-fold coordination octahedron (Grim and Bradley, 1948; Bardley and Grim, 1951) and a five-fold coordination octahedron (Wardle and Brindley, 1972).

2.4.6 Change in d(060) spacing after heating

Figure 2.10 shows XRD patterns around the region of (060) reflection for the homoionic montmorillonite from Cheto before and after heating at 400°C. The values of d(060) for the unheated materials were 1.498 - 1.499Å and they were slightly shifted to larger values after heating at 400°C, suggesting expansion of *b*-axis on dehydration. The Aterasawa smectite also showed a slight expansion at 400°C and a further expansion at 800°C (Figure 2.11). The DTA curves (Figure 2.1) confirmed that dehydroxylation of both materials occurred at temperatures between 600° and 700°C. This indicates that the expansion of *b*-axis at 400°C is not attributable to atomic rearrangement of the octahedral sheets. Therefore, the expansion is probably caused by migration of interlayer cations into the hexagonal holes.

2.5 DISCUSSION

The rehydration characteristics of dioctahedral smectites are strongly dependent on their crystal chemistry and kind of interlayer cations. The montmorillonite samples from Cheto saturated with Ca^{2+}, Mg^{2+}, Na^{+}, and K^{+} ions dehydrated irreversibly at 400°, 600°, 600°, and 700°C, respectively. Whereas, the beidellite from Sano mine retained rehydration ability up to 900°C except for K-saturated sample. On the other hand, the rehydration ability of smectite from Aterasawa, having an intermediate composition

between montmorillonite and beidellite, was apparently stronger than that of the Cheto montmorillonite and weaker than that of the beidellite. The irreversible dehydration temperatures of Ca-, Mg-, Na-, and K-saturated Aterasawa smectite were 400°, 700°, 700°, and 800°C. These results indicate that the rehydration ability of dioctahedral smectite increases with decreasing octahedral negative charge and with increasing size of the interlayer cations ($Mg^{2+} < Ca^{2+} < Na^{+} < K^{+}$).

The rehydration of smectite group minerals involves a re-coordination of water molecules to the dehydrated interlayer cations. Therefore, the behavior of interlayer cations during dehydration and rehydration is significant in elucidating the rehydration mechanism. The results of Fourier analysis of Aterasawa smectite and Sano beidellite indicate that interlayer Na^{+} ions of both specimens migrate from interlayer space into the hexagonal holes on thermal dehydration and return to the interlayer space on rehydration as shown in Figure 2.12. Thus, the behaviors of interlayer cations of both specimens during dehydration and rehydration are essentially the same, however the cations migrated into the hexagonal holes of the beidellite tend to be easily extracted.

The negative layer charge of beidellite originates from substitution of Al^{3+} for Si^{4+} in the tetrahedral sheets; the octahedral sheets are almost electrically neutral. This crystallochemical feature indicates that no attractive electrostatic force exists between the octahedral sheets and the migrated interlayer cations. The migrated cations can therefore easily be extracted from the hexagonal holes and then rehydration occurs rapidly. For montmorillonite, however, the migrated interlayer cations are strongly attracted to the octahedral sheets by negative charge originated from substitution of Mg^{2+} for Al^{3+} in the

octahedral sits. This attractive electrostatic force promotes fixation of interlayer cations to the hexagonal holes, which inhibits rehydration of montmorillonite.

The difference in rehydration rates of the homoionic materials is probably due to the size of interlayer cations, rather than to their hydration energy. The small ionic radius of Mg^{2+} allows its easy fixation to the hexagonal holes. On the contrary, the large ionic radius of K^{+} makes its fixation difficult and the cation can easily be extracted from the hexagonal holes. Consiquently, the rehydration rate of K-saturated material is fast, whereas that of Mg-saturated one is slow.

CHAPTER 3 SAPONITE AND VERMICULITE

3.1 INTRODUCTION

Saponite is a trioctahedral smectite with Mg^{2+} as octahedral cation and is the trioctahedral analog of beidellite. The layer charge arises principally from substitution of Al^{3+} for Si^{4+} in the tetrahedral sheets. The theoretical formula of saponite can be written as follows:

$$M^{+}_{x}Mg_3(Si_{4-x}Al_x)O_{10}(OH)_2.$$

Vermiculite is phyllosilicate that consists of 2:1 layer structure with layer charge of 0.6 to 0.9 per $O_{10}(OH)_2$ formula unit (Bailey, 1980). The most of the vermiculite is trioctahedral and is formed mainly by weathering of trioctahedral micas such as phlogopite or biotite. The negative charge on the layers derives from substitution of Al^{3+} for Si^{4+} in the tetrahedral sheets but this is partially compensated by replacement of some divalent octahedral cations by trivalent. The net negative layer charge is balanced by interlayer cations, which are usually hydrated Mg^{2+} and it can be easily exchanged and solvated.

MacEwan and Wilson (1980) reported that, with the exception K- and NH_4-saturated materials, saponite and vermiculite showed similar rehydration characteristics to each other. They also stated that Li-, Na-, and K-saturated saponite rehydrated readily in most air after heating at 700°C, whereas saponite saturated with divalent cations failed to rehydrate after heating above 450°C. These authors, however, did not mention a detailed rehydration mechanism of these minerals. The rehydration characteristics of expandable clay minerals are strongly related to the behaviors of interlayer cations during dehydration and rehydration as described in Chapter 1. If interlayer cations of saponite migrate into

the hexagonal holes on thermal dehydration, strong rehydration ability would be expected because the protons of hydroxyl ions of trioctahedral phyllosilicates are directed toward the interlayer cations (Giese, 1975). Furthermore, K-saturated saponite should more readily rehydrate than Mg-saturated sample because K^+ ions can easily be extracted from the hexagonal holes than the other cations (see Chapter 1). On the other hand, it is well known that K-saturated vermiculite dehydrates irreversibly without heating (Harward *et al.*, 1969); therefore, the rehydration mechanisms of saponite and vermiculite must be quite different.

In this Chapter, the rehydration characteristics of saponite and vermiculite were described and the rehydration mechanisms of both minerals were discussed.

3.2 MATERIALS

Saponite from Ballarat, California, and vermiculite from Llano County, Texas, obtained from the Source Clay Repository of The Clay Minerals Society, were used in this study. Chemical analyses of these materials were reported by Post (1984) and Foster (1963), respectively. The structural formula of the saponite is as follows:

$$(Ca_{0.19}Na_{0.16}K_{0.02})(Al_{0.15}Fe^{3+}_{0.06}Mg_{2.61})(Si_{3.77}Al_{0.23})O_{10}(OH)_2,$$

and that of the vermiculite is:

$$(Mg_{0.48}K_{0.01})(Mg_{2.83}Fe^{3+}_{0.01}Al_{0.15})(Si_{2.86}Al_{1.14})O_{10}(OH)_2.$$

The differential and thermogravimetric analyses (DTA-TGA) curves of these materials saturated with Ca^{2+}, Mg^{2+}, Na^+, or K^+ were shown in Figure 3.1. The DTA-TGA curves of saponite samples indicated that dehydration and dehydroxylation took place completely below 250°C and about 800°-840°C, respectively, accompanying weight

losses due to removal of interlayer water and structural OH. The vermiculite samples also exhibited dehydration below 250°C and dehydroxylation at about 800°C. The exothermic peaks observed at about 840°-880°C are due to recrystallization reaction.

3.3 EXPERIMENTAL METHODS

The < 2μm fractions of saponite and the < 10μm of vermiculite were collected by normal sedimentation methods and were saturated with Ca^{2+}, Mg^{2+}, Na^{+}, or K^{+} by treatment with respective 1N chloride solutions. The excess salt was then removed by washing five times with 80% ethanol until the samples were free from Cl^{-} ions. These homoionic materials were then dried in air and were used following experiments.

About 20 mg of the homoionic materials were heated at temperatures between 100° to 900°C at intervals of 100°C for 1 hr and then cooled in a desiccator of 0% relative humidity (RH) for 1 hr. The RH in the desiccator was controlled with di-phosphorus pentanoxide. The heated materials were oriented on glass slides using deionized water and then dried in air at 50% RH for 1 day. The d(001) values were measured by X-ray powder diffraction (XRD) using a RIGAKU diffractometer, Ni-filtered CuK α radiation, and a scanning speed of 0.5°2 θ /min.

Homoionic materials oriented on quartz glass slides were heated at 700°C for 1 hr and then cooled in a desiccator (0% RH) for 1 hr. XRD patterns were obtained from 14° to 2°2 θ at a scanning speed of 2°2 θ /min during exposure to air at 50% RH for various periods of time.

The positions of interlayer cations for dehydrated saponite and vermiculite were investigated by means of one-dimensional Fourier analysis as described in Chapter 2.

The d(060) values of homoionic materials before and after heating at 400°C were measured by XRD. The XRD data were obtained at a scanning speed of 0.5°2 θ /min under 50% RH for the unheated materials and 0% RH for the heated ones.

3.4 RESULTS

3.4.1 Rehydration ability after heating

Figure 3.2A shows variation of d(001) values of the homoionic rehydrated saponite after heating at various temperatures. The Ca-, Na-, and K-materials retained the same values of d(001) as those of the original hydrated forms until the crystal structure was destroyed by heating. The Mg-material, however, did not rehydrate after heating at 700°C.

Figure 3.2B shows variation of d(001) values of the homoionic rehydrated vermiculite after heating at various temperatures. The Ca-, Mg-, and Na-materials readily rehydrated until the crystal structure was destroyed. The d(001) value of K-material contracted to about 11.0Å before heating and decreased gradually to 10.3Å after heating at 900°C. These results suggest that the saponite and vermiculite have strong rehydration ability, although the detailed rehydration behaviors are slightly different from each other.

3.4.2 Rehydration rate in air after heating

Figure 3.3 shows XRD patterns of the homoionic saponite heated at 700°C followed by exposure to air at 50% RH for various periods of time. The Mg-material remained dehydrated after exposure to air for as long as 1 day. The Ca-material showed a small peak of the two-layer hydrated form (15.5Å), suggesting that the material

rehydrated to a greater extent than did the Mg-material. The Na-material partially rehydrated to a mixture of one-layer hydrated (12.8Å) and dehydrated (9.8Å) layers on exposure to air for a few minutes (0 min in Figure 3.3). The K-material almost completely rehydrated, and the peak of the dehydrated forms was absent from the XRD pattern at 0 min. This observation also suggests that the K-material rehydrates more rapidly than the Na-material. Consequently, the rehydration rates of the homoionic saponite ($K^+ > Na^+ > Ca^{2+} > Mg^{2+}$) are compatible with the ionic radii of saturating cations ($K^+ > Na^+ > Ca^{2+} > Mg^{2+}$; Whittaker and Muntus, 1970), rather than with their hydration energies.

Figure 3.4 shows XRD patterns of the homoionic vermiculite heated at 700°C followed by exposure to air at 50% RH for various periods of time. The d(001) value of Ca-material expanded rapidly to 14.8Å and was enhanced during exposure to air, suggesting that rehydration continued for at least 1 day. The Mg-material rehydrated rapidly and completely within a few minutes. The Na-material showed a segregated structure consisting of one-layer hydrated (11.9Å) and dehydrated (10.0Å) layers. A small peak of the dehydrated layer was noted even after exposure for 1 day. On the other hand, the K-saturated vermiculite remained dehydrated. The rehydration rates of the homoionic vermiculite ($Mg^{2+} > Ca^{2+} > Na^+ > K^+$) were quite different from those of the saponite samples and were compatible with hydration energies of saturating cations ($Mg^{2+} > Ca^{2+} > Na^+ > K^+$; Rosseinsky, 1965), instead of their ionic radii.

3.4.3 Exchangeability of interlayer cations

The variation of oxide wt.% of CaO, MgO, Na_2O, and K_2O of the homoionic saponite saturated with corresponding cations are shown in Figure 3.5A. The values of all elements remained constant, indicating that no interlayer cations were lost during heating. Figure 3.5B shows variation of exchangeable cations extracted with 0.1 N $SrCl_2$ solution after heating at various temperatures. The exchangeability of Mg^{2+} ion decreased successively up to 800°C due to progressive fixation of the ion with temperature. However, the K-saponite retained great exchangeability up to 800°C and it decreased rapidly at 900°C due to thermal decomposition of the saponite structure. The values of exchangeable Ca^{2+} and Na^{+} ions remained unchanged up to 700°C and decreased rapidly at 800°C. The result is similar to that of a dioctahedral smectite from Aterasawa, but the exchangeability of saponite is maintained more higher temperature than that of the Aterasawa smectite. Figure 3.6A shows oxide wt.% of CaO, MgO, Na_2O, and K_2O of the representative homoionic vermiculite after heating at various temperatures. This showed no significant change in the values of oxide wt.%. The variation of exchangeable cations after heating are given in Figure 3.6B. The K-vermiculite gave small value of K-exchangeability before heating and the value decreased after heating up to 800°C. However, the Mg-vermiculite retained great exchangeability up to 800°C and it was lost at 900°C. The exchangeability of Ca^{2+} and Na^{+} ions remained up to 700°C and decreased rapidly at 800°C. This result indicates that the vermiculite retains great exchangeability of interlayer cations at relatively higher temperature as well as saponite.

3.4.4 Position of interlayer cations after dehydration

The positions of interlayer cations of the Na-saturated saponite heated at 400° and 700°C, and the Ca- and Mg-saturated saponite heated at 800°C were examined by means of one-dimensional Fourier analysis. Figure 3.7 shows electron density distribution (ED), and difference synthesis curves calculated by using z-parameters obtained by refinement (DS1) and by assuming that interlayer cations were fixed at center of interlayer space (DS2). The basal spacings and structure factors used in this calculation are listed in Tables 3.1 and 3.2. The DS2 curves for the Na-materials heated at 400° and 700°C showed a negative peak in the interlayer region, suggesting that the interlayer Na^+ ions probably moved from the interlayer space to some other position. After refinement of the z-parameters of atomic planes, the position of interlayer Na^+ ions was determined around the basal oxygen plane as shown in Figures 3.7A and 3.7B. The difference synthesis curve (DS1) calculated by using the refined structure also suggested that the Na^+ ions were apparently located at this position. These results imply that the interlayer Na^+ ions migrated into the hexagonal holes of the SiO_4 network on thermal dehydration. For the Ca- and Mg-materials, similar results were obtained as shown in Figures 3.7C and 3.7D. The positions of interlayer Ca^{2+} and Mg^{2+} ions determined by least squares refinement also indicated that these cations migrated into the hexagonal holes on thermal dehydration.

Figure 3.8 shows ED and DS1 curves for the Ca-, Na-, and K-saturated vermiculite heated at 800°C. The basal spacings and structure factors are listed in Table 3.3. The ED curves of these materials showed sharp peaks around the interlayer region, which are probably due to electron densities of interlayer cations. After refinement of atomic coordinates along the *c*-axis, the DS curves showed no significant residual

electron densities. Consequently, these interlayer cations must have been located at the center of the interlayer space instead of within the hexagonal holes of the silicate network.

3.4.5 Change in d(060) spacing after heating

Figure 3.9 shows XRD patterns around the region of (060) reflection for the homoionic saponite and vermiculite before and after heating at 400°C. The values of d(060) for the unheated saponite were 1.529 - 1.531Å, depending on interlayer cations. After heating at 400°C, the values of d(060) increased slightly suggesting expansion of *b*-axis on thermal dehydration. The expansion of *b*-axis of other phyllosilicates by thermal treatment has been reported (pyrophyllite, Brindley and Wardle, 1970; muscovite, Eberhart, 1963; Vedder and Wilkins, 1969; Udagawa *et al.*, 1974). Udagawa *et al.* (1974) concluded from a three-dimensional structural analysis of dehydroxylated muscovite that the expansion of *b*-axis was caused by atomic rearrangement of the octahedral sheets. The DTA and TGA curves of the present saponite demonstrated that dehydroxylation took place at about 800° - 840°C accompanying a rapid endothermic reaction and weight loss (Figure 3.1). Therefore, the expansion of the *b*-axis of the saponite heated at 400°C may be due to migration of interlayer cation from the interlayer space to the hexagonal holes of the silicate network. The migrated cations probably caused adjustment of the deformed configuration of the tetrahedra. On the other hand, the d(060) values of the homoionic vermiculite, except for the K-saturated material, decreased slightly after heating at 400°C, indicating contraction of the *b*-axis on thermal dehydration. Leonard and Weed (1967) reported a similar behavior of d(060) value of vermiculite saturated with several different cations and heated at 350°C. The behavior of

the d(060) value of vermiculite during thermal dehydration is therefore completely different from that of the saponite, suggesting that the interlayer cations of vermiculite dose not migrate into the hexagonal holes of the silicate network.

3.5 DISCUSSION

Both the saponite and vermiculite samples rehydrated readily and rapidly as described in previous section, however the rehydration characteristics of these minerals were considerably different from each other. The most notable features of rehydration characteristics and behaviors of interlayer cations of saponite were as follows: (1) except for Mg-saturated sample, all saponite samples rehydrated until the crystal structure was destroyed by heating, (2) the rehydration rates decreased in the order: $K^+ > Na^+ > Ca^{2+} > Mg^{2+}$, (3) the interlayer cations migrated into the hexagonal holes of the SiO_4 network on thermal dehydration, and (4) the *b*-axis expanded on thermal dehydration. The most notable features of vermiculite were as follows: (1) except for K-saturated sample, all vermiculite samples rehydrated until the crystal structure was destroyed by heating, (2) the rehydration rates decreased in the order: $Mg^{2+} > Ca^{2+} > Na^+ > K^+$, (3) the interlayer cations remained at the interlayer space even after thermal dehydration, and (4) except for K-saturated sample, the *b*-axis contracted on thermal dehydration.

The rehydration phenomenon can be interpreted as a restoration of the hydrated forms of interlayer cations in the interlayer space. The behaviors of interlayer cations during dehydration is therefore very important in understanding the rehydration mechanism of expandable clay minerals, including saponite and vermiculite. Based on Fourier analysis, it was confirmed that the interlayer cations of saponite migrate into the

hexagonal holes on thermal dehydration. The migrated cations must be extracted from the holes to rehydrate the dehydrated saponite. The factors affecting the extraction of the migrated interlayer cations are: (1) extractive force attributable to hydration of the interlayer cations, (2) attractive electrostatic force of the octahedral sheets attributable to its negative charge, and (3) repulsive electrostatic force of protons of hydroxyl ions located at the bottom of hexagonal holes. The total extractive force is a composite of these electrostatic forces. The following factors also influence the strength of the forces: (1) hydration energy of the interlayer cations, (2) migrated positions of the interlayer cations, (3) negative charge density of the octahedral sheet, and (4) orientation angle of hydroxyl ions. The hydration energy of interlayer cations decreases in the order: Mg^{2+} > Ca^{2+} > Na^{+} > K^{+} (Rosseinsky, 1965). The strength of the extractive force attributed to the hydration energy seems to be dependent on the migrated positions of the interlayer cations. The attractive force caused by the negative charge of the octahedral sheet is also affected by the migrated position of the interlayer cations.

If the cations are located in a shallow part of the hexagonal holes, they are readily extracted in moist air by the force of their hydration energy. The shorter distance from the migrated cations to water molecules increases the extractive force attributable to hydration energy, whereas the longer distance from the migrated cations to the octahedral sheet makes the attractive force to that sheet weaker. If the interlayer cations migrate deep into the holes, the extractive force due to hydration energy of the migrated cations is weaker, and the attractive force to the octahedral negative charge is relatively stronger. A large negative charge of the octahedral sheet increases the attractive force between the migrated interlayer cations and the octahedral sheet. With reference to the orientation of

hydroxyl ions, the protons of the hydroxyl ions of trioctahedral smectites, e.g., saponite, are directed toward the migrated interlayer cations, and the distance from the protons to the migrated cations is at a minimum; therefore, the repulsive force of saponite is relatively stronger. The hydroxyl ions of dioctahedral smectites orient slightly toward the empty octahedral site, and the repulsive force of montmorillonite and beidellite is relatively weaker. The influence of hydroxyl ions on the fixation of interlayer cations in the silicate network has been reported for micas (Bassett, 1960; Newman, 1969; Hoda and Hood, 1972). The negative charge distribution of the present saponite is $-0.13/O_{10}(OH)_2$ in the octahedral sheet and $-0.23/O_{10}(OH)_2$ in the tetrahedral sheet. The octahedral negative charge increases the attractive force between migrated interlayer cations and the octahedral sheet, however protons directed toward the migrated interlayer cations repel the cations toward the interlayer space. Consequently, saponite exhibits strong rehydration compared with a dioctahedral smectite having similar charge distribution.

The rehydration characteristics and behaviors of interlayer cations of vermiculite were completely different from those of saponite as mentioned above. Figure 3.10 shows transmission electron micrographs (TEM) and electron diffraction patterns of Mg-saturated saponite and vermiculite samples. The TEM of saponite clearly showed a particle having euhedral lath-like habits. The diffraction pattern of the particle were distributed uniformly in circles, suggesting a turbostratic stacking of adjacent silicate layers or simply a large number of randomly oriented thin particles. On the other hand, a particle of the vermiculite gave spot diffraction patterns having approximately hexagonal symmetry, implying ordered stacking of adjacent silicate layers. The differences in the

rehydration characteristics of saponite and vermiculite are probably due to the nature of stacking of adjacent silicate layers. The turbostratic stacking of saponite probably enhances migration of interlayer cations into the hexagonal holes as shown in schematically in Figure 3.12A, whereas the ordered stacking of vermiculite inhibits such cation migration (Figure 3.12B). Therefore, the interlayer cations of vermiculite remain at the center of the adjacent silicate layers facing each other even after thermal dehydration, and they rehydrate easily in moist air or on water saturation.

The dehydration of K-saturated vermiculite in moist air without heating is apparently related to the size of the hexagonal holes in the basal oxygen plane and of the interlayer cations. If the interlayer cations are about the same size as the hexagonal holes, the cations are close packed with the basal oxygens, similar to the interlayer configuration of mica. For smaller cations (e.g., Mg^{2+}), however, an incomplete packing is formed after dehydration, and the cations dose not contact the surrounding oxygens. Therefore, rehydration of the cation occurs rapidly in moist air.

Mamy and Gaultier (1976) reported the modification of turbostratic stacking to an ordered stacking by subjecting K-saturated montmorillonite to 100 cycles of alternate wetting and drying at 80°C. They showed a reduction of cation-exchange capacity and a contraction of the basal spacing to about 10Å, indicating that smectites having ordered stacking exhibit vermiculite-like hydration properties (Barshad, 1948, 1950). Thus, the collapse of the interlayer space on K-saturation appears to be restricted to the expandable clay minerals consisting of ordered stacking of adjacent silicate layers, rather than those having greater negative charge density of the silicate layers. Consequently, the most

important factor controlling the rehydration properties of saponite or vermiculite appears to be the nature of stacking of adjacent silicate layers.

CHAPTER 4 HECTORITE

4.1 INTRODUCTION

Hectorite is a trioctahedral smectite with octahedral negative charge arising from substitution of Li^+ for Mg^{2+} in the octahedral sheets, and is the trioctahedral analog of montmorillonite. The theoretical formula of hectorite can be expressed as follows:

$$M^+_x(Mg_{3-x}Li_x)Si_4O_{10}(OH)_2.$$

Hectorites have been synthesized by many investigators (Granquist and Pollack, 1960; Neumann, 1965; Neumann and Sanson, 1970, 1971; Barrer and Jones, 1970, 1971), and used for chemical industry as adsorbers and catalysts. The large surface area of hectorite makes it possible to conduct adsorption reaction and catalytic activity in an aqueous system. Metal complex catalysts intercalated in hectorite show solution-like catalytic activity in its interlayers expanded intermediately (Pinnavaia, 1982). Thus, the interlayer of hectorite plays an important role in industrial utilization. Therefore, dehydration and rehydration characteristics may be provide useful information for further utilization as a functional material. In this Chapter, the rehydration characteristics of hectorite were described.

4.2 MATERIAL

The material used in this study is a hectorite from Hector, California. The chemical composition of this hectorite is:

$$Ca_{0.01}Na_{0.28}K_{0.01}(Mg_{2.65}Al_{0.02}Li_{0.33})Si_{4.00}O_{10}(OH_{0.92}F_{1.08}).$$

The tetrahedral sheets are free from Al^{3+} and the negative layer charge originates mainly from substitution of Li^+ for Mg^{2+} in the octahedral sheets. About one-half of hydroxyl

ion is substituted by fluorine ion. Figure 4.1 shows differential thermal and thermogravimetric analyses (DTA-TGA) curves of the hectorite samples saturated with Ca^{2+}, Mg^{2+}, Na^{+}, or K^{+}. The DTA curves exhibited single or double endothermic peaks due to dehydration of interlayer water between at 93° and 175°C, and a broad endothermic peak due to dehydroxylation at 606° - 622°C. The TGA curves showed rapid weight loss due to dehydration below about 200°C, and gradual weight loss due to removal of hydroxyl and fluorine ions above 600°C.

4.3 EXPERIMENTAL METHODS

The < 2μm fractions collected by normal sedimentation were saturated with Ca^{2+}, Mg^{2+}, Na^{+}, or K^{+} by treatment with 1N chloride solutions, and washed five times with 80% ethanol until complete removal of the excess salt. These homoionic materials were used for following experiments: (1) rehydration ability after heating, (2) rehydration rate after heating, (3) change in exchangeability of interlayer cations, and (4) change in d(060) spacing by heating. Details of experimental methods are described in Chapters 2 and 3.

4.4 RESULTS

4.4.1 Rehydration ability after heating

Figure 4.2 shows variation of d(001) values of the homoionic rehydrated hectorite samples after heating at 100° to 900°C for 1 hr. The d(001) value of Ca-material remained constant up to 400°C and contracted to about 10Å above 500°C. The Na- and K-materials showed similar rehydration behaviors to each other; both materials rehydrated up to 600°C and dehydrated at 700°C. However, the d(001) spacing of K-

material expanded slightly to 10.8Å after heating at 700°C, suggesting that the material retained weak rehydration ability even after heating at 700°C. The d(001) spacing of Mg-material contracted continuously between 300° and 600°C. Figure 4.3 shows XRD patterns of the rehydrated Mg-materials after heating at 200° to 600°C. The fully hydrated structure of the unheated Mg-material changed through a transitional phase of regular interstratification of rehydrated and dehydrated layers to completely dehydrated forms. This transitional interstratified structure probably formed by fixation of the interlayer Mg^{2+} ion to the alternating interlayers.

4.4.2 Rehydration rate in air after heating

Figure 4.4 shows XRD patterns of the hectorite heated at 400°C during exposure to air at 50% RH for various periods of time. All materials showed no significant changes in the XRD patterns during exposure for 1 day, indicating very slow rehydration rate or very weak rehydration ability in air.

4.4.3 Exchangeability of interlayer cations

Figure 4.5A shows oxide wt.% of CaO, MgO, Na_2O, and K_2O of the representative homoionic hectorite samples after heating at various temperatures. The MgO wt.% shows considerably larger value compared with those of other oxides, because the value involves Mg^{2+} ions located at the interlayer and the octahedral sites. No significant changes in values of wt. % were recognized during heating, indicating that the elements remained in the hectorite structure up to 900°C. Figure 4.5B shows variation of exchangeable cations extracted with 0.1N $SrCl_2$ solution from the homoionic

hectorite after heating at various temperatures. The values of exchangeable Na^+ and K^+ ions remained constant at approximately 75 meq/100g up to 500°C and decreased gradually at above temperatures. The Mg^{2+} and Ca^{2+} ions began to fix at 300°C and the values of exchangeability decreased continuously with increasing temperature.

4.4.4 Change in d(060) spacing after heating

XRD patterns around the region of (060) reflection for the homoionic hectorite before and after heating at 400°C are given in Figure 4.6. The values of d(060) for the unheated materials were 1.516 - 1.517Å, depending on saturating cations. These values increased slightly to 1.518Å after heating at 400°C, indicating expansion of *b*-axis on thermal dehydration. The DTA curves of the materials showed an endothermic peak due to dehydroxylation at temperatures above 600°C. Therefore, this expansion is probably caused by migration of interlayer cations into the hexagonal holes instead of the octahedral rearrangements.

4.5 DISCUSSION

The rehydration property of hectorite is strongly influenced by kind of interlayer cations. The K-saturated material appeared to rehydrate completely up to 600°C and decreased in rehydration ability after heating at 700°C. The Na- and Ca-saturated materials rehydrated up to 600° and 400°C, respectively, but remained dehydrated after heating above temperatures. The Mg-materials formed regular interstratified structure of rehydrated and dehydrated layers between 300° and 600°C and tended to decrease continuously in ratio of the rehydrated layer with increasing temperature (Figure 4.3).

The value of exchangeable cation for the Mg-material also decreased continuously between 300° and 600°C, and the d(060) spacing expanded after heating at 400°C. These results suggest that interlayer Mg^{2+} ions migrate into the hexagonal holes by thermal dehydration and fixation of the ions to the alternating interlayers probably occurs. This hectorite sample characteristically contained fluorine ion which replaced for about one-half of hydroxyl ion. It is well known that extraction of interlayer K^+ from trioctahedral mica becomes difficult with increasing fluorine content. This is due to decrease in a repulsive force between interlayer K^+ and proton of hydroxyl ion (Bassett, 1960; Newman, 1969; Hoda and Hood, 1972). The fluorine content of the present hectorite remained unchanged up to 800° and removal from the structure took place at 900°C (Figure 4.7). The crystal structure of the hectorite, especially on the distribution of F^- and OH^- in each elementary layer, remains unclear. However, the regular interstratification produced by heating is attributed to regular distribution of F^- to F^- and OH^- to OH^- facings distinct from the interlayer space as illustrated in Figure 4.8, and Mg^{2+} may be fixed to the hexagonal holes at bottom of which F^- is located.

CHAPTER 5 RECTORITE

5.1 INTRODUCTION

Rectorite is a regular interstratified clay mineral consisting of mica-like and smectite-like layers. The first description of rectorite was carried out by Bradley (1950) for the material from Arkansas, U.S.A., as an interstratification of pyrophyllite and vermiculite layers. On the other hand, Brindley (1956) reported allevardite from Allevard, France, as consisting of pairs of mica-like layers containing two layers of water molecules in alternating layers. Brown and Weir (1963) examined cation-exchange capacities, X-ray properties, electron micrographs, and infrared absorption spectra for allevardite and rectorite. They pointed out that allevardite and rectorite are the same minerals, and these minerals are made up of mica-like and smectite-like layers. Kodama (1966) pointed out that rectorite consists of regular alteration of paragonite-like layers and expandable layers having beidellite- and montmorillonite-like compositions. AIPEA Nomenclature Committee (Bailey, 1981) suggested that rectorite has priority over the name allevardite, and made the following recommendations; "The name rectorite is justified for a 1:1 regular interstratification of dioctahedral mica and dioctahedral smectite. The kind of smectite should not be specified in the definition. A prefix, Na-, K-, or K- can be used to specify the dominant interlayer cation in the mica component".

A large number of papers dealing with description of mineralogical properties of rectorite-type minerals (interstratified mica/smectite having 25-30Å reflection) have been published (Heystek, 1954; Takeshi, 1958; Shimoda and Sudo, 1960; Hayashi, 1961; Sudo *et al.*, 1962; Cole, 1966; Hamilton, 1967; Kodama *et al.*, 1969; Shimoda *et al.*, 1969; Tomita *et al.*, 1969; Tomita and Dozono, 1973, 1974; Pevear *et al.*, 1980; Matsuda *et al.*,

1981a, 1981b; Nishiyama and Shimoda, 1981; Beaufort, 1984; Matsuda, 1984; etc.). There are two reports which noted that rectorite has strong rehydration ability (Shimoda *et al.*, 1969; Tomita and Dozono, 1973), however details of rehydration properties of rectorite remain unclear.

In this Chapter, the rehydration characteristics of rectorite were investigated in detail, and its rehydration mechanism was discussed.

5.2 MATERIALS

The rectorite samples used in this study were from Makurazaki, Kagoshima Prefecture, Japan, and from Arkansas, U.S.A. The chemical compositions of these materials are given in Table 5.1. The structural formula of Makurazaki rectorite can be written as follows:

$$(Na_{0.81}K_{0.40}Mg_{0.07}Ca_{0.05})(Al_{3.66}Fe^{3+}_{0.18}Mg_{0.06}Ti_{0.07})$$

$$(Si_{6.64}Al_{1.36})O_{20}(OH)_4.$$

The cation-exchange capacity is 53.1 meq/100g on the ignited weight basis. The d(060) value is 1.492Å. The structural formulae of component layers were estimated by assuming that all exchangeable cations were located to the interlayer sites of the expandable layer, and the octahedral sheets of both mica and expandable layers have the same composition. The structural formula of the mica layer can be expressed as follows:

$$(Na_{0.71}K_{0.37}Ca_{0.01})(Al_{1.83}Fe^{3+}_{0.09}Mg_{0.03}Ti_{0.04})$$

$$(Si_{2.95}Al_{1.05})O_{10}(OH)_2.$$

and that of expandable layer as:

$$(Na_{0.09}K_{0.01}Mg_{0.07}Ca_{0.05})(Al_{1.83}Fe^{3+}_{0.09}Mg_{0.03}Ti_{0.04})$$

$$(Si_{3.71}Al_{0.29})O_{10}(OH)_2.$$

The structural formula of the mica layer falls under the category of paragonite having layer charge of 1.10 per $O_{10}(OH)_2$ formula unit, and the expandable layer belongs to beidellite having layer charge of 0.34 per $O_{10}(OH)_2$. This Makurazaki rectorite was used for following investigations: (1) rehydration ability, (2) rehydration rate, (3) expansion characteristics under various relative humidities, (4) IR absorption spectra, (5) thermal properties, and (6) exchangeability of interlayer cation after heating.

The mineralogical properties of Arkansas rectorite were reported by Brown and Weir (1963). The structural formula calculated from the chemical analysis is:

$$(Na_{1.02}K_{0.02}Ca_{0.04})(Al_{4.04}Fe^{3+}_{0.06})(Si_{6.59}Al_{1.41})O_{20}(OH)_4.$$

This Arkansas rectoritewas used as material for one-dimensional Fourier analysis to elucidate the behaviors of interlayer cations during dehydration and rehydration.

The differential thermal and thermogravimetric analysis (DTA-TGA) curves of the Makurazaki and Arkansas rectorites saturated with Ca^{2+}, Mg^{2+}, Na^{+}, or K^{+} are given in Figure 5.1. The Makurazaki rectorite exhibited one-, two-, or three-steps of dehydrations below 250° and one- or two-steps of dehydroxylation between approximately 480° and 550°C depending on interlayer cations, and showed stepwise weight losses correspond to the dehydration and dehydroxylation reactions. The Arkansas rectorite gave similar DTA-TGA curves to those of the Makurazaki material but dehydroxylation tended to occur slightly higher temperatures at 575° to 625°C.

5.3 EXPERIMENTAL METHODS

The rehydration ability of the rectorite was examined as follows. The homoionic (saturated with Ca^{2+}, Mg^{2+}, Na^{+}, or K^{+}) materials were heated in air at temperatures between 100° to 900°C at intervals of 100°C for 1 hr. After cooling in a desiccator at 0% RH, the heated materials were re-wetted by adding deionized water for 1 day and dried in air at 50% RH as described in Chapter 3. These materials were oriented on glass slides by re-suspension in deionized water and allowed to dry again at 50% RH. They were used for XRD analysis as rehydrated materials (H_2O-complex). The materials were solvated with ethylene glycol (EG-complex) and glycerol (GL-complex), and then their basal spacings were measured by XRD. The basal spacings of the H_2O-, EG-, and GL-complexes were obtained by averaging the d-values of basal reflections in the < 40° 2θ region. The XRD analysis was undertaken with the use of a RIGAKU diffractometer (CuKα radiation, 30 kV, 100 mA) equipped with a graphite monochromater, 1/2° divergence and scattering slits, using a scanning speed of 0.5° 2θ/min. All materials were kept at 50% RH during X-ray examination.

The rehydration rate of the rectorite was investigated as follows. The homoionic materials oriented on quartz glass slides were heated at 800°C for 1 hr and then cooled in a desiccator at 0% RH for 1 hr. XRD patterns of the heated materials during exposure to air at 50% RH for various periods of time were obtained with a RIGAKU diffractometer using a scanning speed of 2°2θ/min.

The expansion characteristics of the rectorite were examined by XRD using the homoionic unheated materials and rehydrated ones after heating at 800°C. The basal spacings of these unheated and rehydrated materials were measured by XRD under 20%, 30%, 40%, 50%, 60%, 70%, and 80% RH. The materials were kept in the atmosphere at

least 5 hr before X-ray examination. The basal spacings were determined by the same described above.

IR absorption spectra of OH and H_2O vibrations were obtained from the homoionic unheated materials and from the rehydrated materials after heating at 800°C. These materials were kept at 50% RH during measurement. The spectra were recorded with a NIHONBUNKO A302 infrared absorption spectrophotometer using oriented materials on a KBr window.

The H_2O wt.% and OHwt.% of rehydrated materials after heating at various temperatures were measured with a RIGAKU differential thermal and thermogravimetric analysis apparatus. Measurement was made from room temperature to 1100°C with a heating rate of 10°C/min using powdered samples of about 25 mg. The materials were kept at 50% RH before analysis. Weight losses at temperatures below and above 400°C were assigned to H_2O wt.% and OH wt.%, respectively.

The exchangeability of interlayer cations of rehydrated rectorite was examined as follows. About 0.5 g of the homoionic materials were heated in air at temperatures between 100° and 900°C at intervals of 100°C for 1 hr, and were washed with 0.1N $SrCl_2$ solution more than five times. The extracted cations (Ca^{2+}, Mg^{2+}, Na^+, and K^+) were measured with an atomic absorption spectrometer (AAS). To make sure that no interlayer cations were lost during heating, heated materials prepared by the same procedure were dissolved in HF-$HClO_4$ and then the abundance of saturated cations (Ca^{2+}, Mg^{2+}, Na^+, and K^+) was measured by AAS.

The behaviors of interlayer cations during dehydration and rehydration were examined by means of one-dimensional Fourier analysis using Na-saturated rectorite

sample from Arkansas, U.S.A. The XRD data for the dehydrated and rehydrated materials were obtained with a RIGAKU diffractometer in air at 0% and 50% RH conditions. The Na-materials after heating at 400° and 800°C were used as dehydrated samples, and their rehydrated forms prepared by addition of distilled-deionized water as rehydrated samples. The Fourier synthesis was made as described in Chapter 2, and atomic coordinates along the *c*-axis were refined by the least squares method.

5.4 RESULTS

5.4.1 Rehydration ability after heating

Figure 5.2A shows variation of basal spacings of the homoionic rehydrated rectorite (H_2O-complex) after heating at various temperature. The d-values of these materials did not change significantly below 400°C. The Ca- and Mg-materials changed to single layer hydrates after heating above 500° - 600°C, whereas the Na- and K-materials expanded slightly. The transition phases of Ca-material at 500°C and Mg-material at 400°C exhibited two hydration states consisting mainly of 24.7Å layer and a small amount of 22.5Å layer. The basal spacings of all materials became very close to 22.5Å above 500°C, independent of saturating cation. Figures 5.2B and 5.2C show variation of basal spacings of the rehydrated materials after solvation with ethylene glycol (EG-complex) and glycerol (GL-complex), respectively. The d-values of EG-complexs of the unheated materials are slightly different from each other ($Mg^{2+} > Na^{+} > K^{+} > Ca^{2+}$), suggesting that the kind of interlayer cations also affects the expansion on EG-solvation. The basal spacings of the materials almost remained constant below 400°C, and increased with increasing

temperature between 400° and 800°C to about 26.8Å at 800°C. The GL-cpmplexes exhibited similar behavior with the d-values increasing to about 27.7Å at 800°C.

5.4.2 Rehydration rate in air after heating

The rehydration rate of the homoionic rectorite heated at 800°C followed by exposure to air at 50% RH was examined by XRD. Figure 5.3 shows variation of XRD patterns of the materials heated at 800°C during exposure for various periods of time. The XRD patterns of Ca-material showed a slight increase in intensity of first-order reflection and a broadening of second-order reflection during exposure to air, suggesting that rehydration proceeded slowly. For the Mg-material, the XRD patterns did not change significantly indicating that the dehydrated forms remained for 2 days. The Na-material exhibited progressive rehydration within 1 day, whereas the K-material rehydrated rapidly and completely within a few minutes. These results suggests that the rehydration rates of the homoionic rectorite samples are strongly dependent on their interlayer cations. The rehydration rates increase with increasing the ionic radii ($K^+ > Na^+ > Ca^{2+} > Mg^{2+}$) of saturating cations rather than their hydration energies.

5.4.3 Expansion characteristics of rehydrated materilas

Figure 5.4 shows variation of basal spacings of the homoionic unheated rectorite and its rehydrated forms after heating at 800°C under various RH conditions. The basal spacings of the unheated Ca- and Mg-materials increased slightly and continuously with increasing the humidity. However, the rehydrated Ca- and Mg-materials exhibited a single layer hydrate between 20% and 70% RH and a double layer hydrate at 80% RH. For the

Na-material, transition of single to double layer hydrate occurred at 70% RH for the unheated material and 80% RH for the rehydrated one. The unheated K-material showed a single layer hydrate with basal spacing of approximately 22Å between 20% and 80% RH. Whereas, the rehydrated K-material expanded slightly to 22.5Å between 20% and 70% RH and changed to a double layer hydrate with a basal spacing of 25.2Å at 80% RH. The expansion characteristics of these unheated materials are very similar to those of homoionic rectorites reported by Matsuda (1984, 1989), whereas those of the rehydrated materials are quite different.

5.4.4 Infrared absorption analysis of rehydrated materials

The IR spectra of unheated rectorite exhibited strong absorptions due to OH vibration at 3645 - 3637 cm^{-1} and broad absorptions due to H_2O stretching vibration at 3455 - 3390cm^{-1}. The rehydrated rectorite after heating below 400°C showed the same spectra as those of unheated materials. Whereas, the rehydrated materials after heating above 500°C exhibited pronounced absorption bands due to OH and H_2O but the absorption frequencies and intensities changed slightly from those of unheated materials (Figure 5.5). Figure 5.6A shows the relationship between absorption frequencies of H_2O and hydration energies of saturating cations (Rosseinsky, 1965). The samples plotted are homoionic (Ca^{2+}, Mg^{2+}, Na^{+}, or K^{+}) unheated materials and homoionic materials rehydrated after heating at 800°C. The absorptions of the unheated materials shifted to lower frequency with increasing hydration energy. On the other hand, the absorption frequencies of the rehydrated materials were nearly constant at 3440 cm^{-1}.

Figure 5.6B shows the relationship between absorption intensity ratios of I_{H_2O}/I_{OH} and hydration energies. The same materials as Figure 5.6A were plotted on this figure. The amounts of rehydroxylated OH were estimated to be approximately one-half of the original OH (Figure 5.8B) . Therefore, the I_{OH}-values of rehydrated materials were normalized to completely rehydroxylated state with the values of OH wt. % obtained by TGA. The I_{H_2O}/I_{OH} ratios of unheated materials shifted to larger values with increasing hydration energy, whereas those of rehydrated ones exhibited nearly constant values.

5.4.5 Thermal analysis of rehydrated materials

Figure 5.7 shows DTA curves of the homoionic rehydrated rectorite after heating at various temperatures. The DTA curves of rehydrated Ca-material after heating below 400°C did not change significantly. However, a first dehydration peak (82°C) was shifted to a slightly lower temperature, a secondary dehydration peak (168°C) disappeared, and a dehydroxylation peak (547°C) was shifted to a considerably lower temperature after heating above 500°C. Similar phenomena were also observed in the Mg-, Na-, and K-materials. The results suggests that original hydration states have been completely restored on rehydration after heating below 400°C, but different hydration states appears after heating above 500°C.

The variations of H_2O wt.% and OH wt.% of the rehydrated rectorite are presented in Figure 7.7A and 5.7B, respectively. The H_2O wt.% of rehydrated Ca- and Mg-materials decreased continuously, whereas that of rehydrated Na- and K-materials remained almost unchanged. However, the values of these materials converged to about 4 - 5 wt.% OH, independent on saturation cation. The OH wt.% of these materials

decreased rapidly at 500°C , and continued to decrease slightly when they were heated at higher temperatures. At 500°C and above, about one-half of original OH appeared to be regained in the dehydroxylated structure after leaving in the wet state for 1 day. No significant change of OH wt.% was observed after leaving it wet for 2 months.

5.4.6 Exchangeability of interlayer cations

Figure 5.9A shows oxide wt.% of CaO, MgO, Na_2O, and K_2O of the representative homoionic rectorite after heating at various temperatures. The values remained constant, suggesting that no interlayer cations were lost during heating up to 900°C. The exchangeable cations extracted with 0.1N $SrCl_2$ solution after heating at various temperatures are given in Figure 5.9B. The exchangeability of Ca^{2+}, Mg^{2+}, and K^+ ions decreased rapidly at temperatures about 400° - 600°C. The magnitude of decrease for the Na^+ ion was less than for the other cations. Figure 5.10 shows variations of exchangeable cations of the Ca-material after heating at various temperatures. The exchangeable Ca^{2+} ion decreased rapidly above 500° C, but the exchangeable Na^+ and K^+ ions increased between 500° and 800°C. This means that the interlayer Ca^{2+} ions begin to fix to the expandable layer above 500°C, whereas the Na^+ and K^+ ions tend to be extracted from the interlayer sites of the mica layers. A similar phenomenon was also observed in the K-material (Figure 5.10B): exchangeable K decreased and exchangeable Na increased.

5.4.7 Behaviors of interlayer cations during dehydration and rehydrtion

The behaviors of interlayer cations of rectorite during dehydration and rehydration were examined by one-dimensional Fourier analysis. The rectorite sample used this

analysis is from Arkansas, U.S.A. This material also exhibited similar rehydration characteristics to those of the Makurazaki rectorite as shown in Figure 5.11. The basal spacings and structure factors of the unheated Na-rectorite are listed in Table 5.2. The electron density distribution (ED) and difference synthesis (DS) curves along the *c*-axis for the material are shown in Figure 5.12. The left portion of the ED curve corresponds to mica layer and the right portion to smectite layer. The ED curve showed a large positive peak due to water molecules and Na^+ ions around the interlayer region of the smectite layer. The z-parameters of the silicate layer and interlayer Na^+ ions obtained by the least squares refinement indicated that the Na^+ ions were located at position slightly deviated from the center of the interlayer space.

Figures 5.12A and 5.12B show ED and DS curves for the dehydrated Na-rectorite after heating at 400° and 800°C, respectively. The basal spacings and structure factors used in this calculation are listed in Tables 5.3 and 5.4, respectively. For the material heated at 400°C, a negative peak appeared in the interlayer region of the DS curve (DS2 in Figure 5.13A) which obtained by fixing the Na^+ ions at the center of interlayer space. This result probably implies that the Na^+ ions are not located at the interlayer space. When the z-parameters were refined using that of the Na^+ ions as variable as well as other atomic places, the position of the ions moved toward the basal oxygen plane and the DS curve improved considerably (DS1 in Figure 5.13A). The dehydrated material after heating at 800°C exhibited similar behaviors of the Na^+ ions. These results suggest that the interlayer Na^+ ions migrates into the hexagonal holes of the SiO_4 network by thermal dehydration.

Figures 5.13A and 5.13B show ED and DS curves for the rehydrated Na-rectorite after heating at 400° and 800°C, respectively. The basal spacings and structure factors for

the materials are listed in Tables 5.5 and 5.6, respectively. The electron density distribution for the rehydrated material after heating at 400°C showed a very similar curve to that for the original unheated material, suggesting that the original hydrated structure of interlayer space was restored on rehydration. The z-parameters obtained by the least squares refinement indicated that the Na^+ ions was located at slightly deviated position from the center of interlayer space as shown in Figure 5.14. The DS curve which calculated using the refined z-parameters also showed no significant residual electron density. For the rehydrated material after heating at 800°C, a broad positive peak was observed around the basal oxygen plane in the DS curve (DS2 in Figure 10.13B) which was calculated by assuming that the Na^+ ions were located at the center of the interlayer space. Then, the z-parameters were again refined using the position of Na^+ ions as variable. The z-parameters obtained by this refinement showed that the ions were located near the basal oxygen plane, and the positive peak completely disappeared in DS curve (DS1 in Figure 5.14B) recalculated by using the parameters. These results imply that the migrated Na^+ ions of the dehydrated material at 400°C return to the same position as that of the original unheated materials on rehydration. However, the Na^+ ions of the dehydrate material at 800°C do not return to the interlayer space but remain near the basal oxygen plane on rehydration.

5.5 DISCUSSION

The rehydration properties of rectorite after heating below and above dehydroxylation temperatures are distinctly different each other. The rehydrated materials after heating below dehydroxylation temperatures exhibited no significant changes in the

basal spacings, endothermic peaks due to removal of interlayer water, and IR absorption frequencies of interlayer water compared with those of original unheated materials. The rehydrated H_2O wt.% and amounts of exchangeable cations also remained unchanged. Based on Fourier analysis, it was confirmed that the interlayer cations of expandable layers of rectorite migrated into the hexagonal holes of the SiO_4 network during thermal dehydration, and they returned to the original positions in the interlayer space on rehydration. Therefore, the original hydrated configurations of interlayer space are completely restored on rehydration.

The rehydrated materials after heating above dehydroxylation temperatures showed very unique expansion characteristics (Figure 5.2). The basal spacings of expandable clay minerals are mainly influenced by the following factors: (1) the nature of interlayer cations (e.g., hydration energy and ionic radius), (2) negative layer charge of silicate layer, (3) orientation of OH, and (4) relative humidity of atmosphere. If negative layer charge and/or orientation angle of OH change, the basal spacings should behave similarly to each other. Namely, if the negative layer charge and/or the orientation angle increase, some contraction of the basal spacings may be occurred. On the contrary, if the above properties decrease, some expansion can be expected (Suquet *et al.*, 1975). According to Figure 5.2, the basal spacings of Ca- and Mg-materials contracted drastically, whereas those of Na- and K-materials expanded slightly. These results indicate that factors other than those mentioned above can be considered to explain the behaviors of basal spacings. Furthermore, the EG- and GL-complexes showed expansion of basal spacings after heating above 500°C (Figures 5.2B and 5.2C). It is well known that greater negative layer charge and large ionic radii of interlayer cations inhibit the expansion of EG- and GL-complexes (MacEwan

and Wilson, 1980). Based on this fact, these expansion characteristics suggest that the negative layer charge decreased by heating above 500°C. However, the H_2O-complexes of Ca- and Mg-materials contracted rapidly at 500°C which can not be explained by reduction of the layer charge. The correlation relationship observed in the IR spectra of unheated materials disappeared in those of rehydrated materials, suggesting reduction of electrostatic effects of interlayer cations on rehydration. The results of Fourier analysis showed that the migrated cations into the hexagonal holes by thermal dehydration did not return to the interlayer space and remained at the holes. Therefore, these unique expansion characteristics may be due to reduction of electrostatic effects of interlayer cations rather than structural changes of the silicate layer. It is also well known that the adsorption of water, ethylene glycol, and glycerol molecules are due to dipole attractions to the interlayer cations and also to hydrogen bonding to the oxygen surfaces (Emerson, 1957; Brindley and Roy, 1964; Bissada *et al.*, 1967; Dowdy and Mortland, 1967, 1968). Consequently, the reduction of electrostatic effects can be attributed to a decrease in dipole attraction by migration of the interlayer cations into the hexagonal holes.

A decrease in exchangeable Ca^{2+} of the Ca-material at temperatures between 500° and 600°C (Figure 5.9B) is due to fixation to the hexagonal holes, because no removal of the cation took place up to 900°C (Figure 5.9A). An increase in exchangeable Na^+ and K^+ ions between 500° and 800°C is due to extraction of the ions from the interlayer sites of mica-layer components (Tomita and Sudo, 1968; Scott *et al.*, 1972; Smith and Scott, 1974), because interlayer cations of expandable layers have been completely exchanged by Ca^{2+} ions. The amounts of extracted Na^+ ions are considerably larger than those of K^+ ions compared with their atomic abundance ratio (Na/K = 2.0). This is probably due to

larger hydration energy of Na^+ ion. Therefore, the small decreasing value of exchangeable Na^+ ions was compensated by Na^+ ions extracted from the mica layers. Consequently, the interlayer cations of expandable layers were fixed by heating at 500°-600°C, regardless of which cation was present. However, water molecules were regained in the interlayer space with the cations remaining in the hexagonal holes. This relocation of interlayer cations perhaps reduced the dipole attraction between the interlayer cations and the water molecules.

After leaving in the wet state for 1 day under room temperature, about one-half of OH^- was immediately regained in dehydroxylated rectorite structure. Further rehydroxylation could not be recognized after leaving in a wet state for two months. The removal of rehydroxylated OH^- took place at slightly lower temperature than original OH^-. Illite and montmorillonite regain very small amounts of OH^- on exposure to moist air for long periods of time after complete dehydroxylation (Grim and Bradley, 1948). Larger amounts of OH^- can be regained in the dehydroxylated structure under a high temperature water vapor condition (Jonas, 1955; Heller *et al.*, 1962; Vedder and Wilkins, 1969). A 2*M* mica exhibits rehydration and rehydroxylation behaviors similar to those of rectorite after boiling in acid solution (Tomita, 1974). For rectorite, however, remarkable rehydroxylation occurred simply by leaving in a wet state at room temperature for at least 1 day. No clay minerals having such a strong rehydroxylation property have been reported yet.

CONCLUSION

The rehydration characteristics of expandable clay minerals such as smectite, vermiculite, and rectorite after heating at various temperatures were examined by various physical and chemical methods to elucidate their rehydration mechanisms. The rehydration ability was determined by changes in d(001) values or basal spacings after solvation with water, and the rehydration rate was evaluated by changes in XRD patterns during exposure to air. The variation of exchangeable cation was obtained from the values of extracted cation from the heated materials with 0.1N $SrCl_2$ solution. The behaviors of interlayer cations during dehydration and rehydration were investigated by means of one-dimensional Fourier analysis.

The expandable clay minerals showed various rehydration characteristics depending on kind of interlayer cations and on their crystallochemical properties. Smectite group minerals showed following rehydration characteristics: (1) the rehydration rate increases with increasing size of the interlayer cations ($Mg^{2+} > Ca^{2+} > Na^{+} > K^{+}$), (2) the rehydration ability of beidellite is considerably stronger than that of montmorillonite, and (3) the rehydration ability of saponite is apparently stronger than that of dioctahedral smectite having similar negative charge distribution. The rehydration phenomenon of expandable clay minerals is caused by a re-coordination of water molecules to the dehydrated interlayer cations in the interlayer space. Therefore, the behaviors of interlayer cations during dehydration and rehydration are a significantly important problem to understand the rehydration mechanism. The results of Fourier analysis confirmed that the interlayer cations of smectites migrated into the hexagonal holes of SiO_4 network on thermal dehydration and returned again to the interlayer space on rehydration. The large-sized cation is difficult to fix to the hexagonal holes because the cation migrates to the shallow part of the holes. It is a reason for fast rehydration rate

of smectite containing large-sized cation. The migrated cations are attracted by electrostatic force originated from substitution of Mg^{2+} for Al^{3+} in the octahedral sites, which inhibits rehydration of montmorillonite. However, rehydration of saponite is promoted by a strong repulsive electrostatic force between migrated cations and protons of hydroxyl ions.

In contrast to the smectite, vermiculite except for K-saturated material exhibited strong rehydration ability, and the rehydration rate tended to increase with decreasing size of interlayer cations. These rehydration properties of vermiculite appeared to be quite different from those of smectite. Based on Fourier analysis, the interlayer cations of vermiculite did not migrate into the hexagonal holes and remained at the interlayer space even after thermal dehydration. Consequently, vermiculite exhibits strong rehydration ability and the rehydration rate is compatible with the hydration energy of interlayer cations instead of their size. The turbostratic stacking of smectite enhanced migration of interlayer cations into the hexagonal holes, whereas the ordered stacking of vermiculite inhibited cation migration.

Hectorite exhibited weak rehydration ability and very slow rehydration rate compared with those of saponite. Hectorite and saponite are trioctahedral analog of montmorillonite and beidellite, respectively. Therefore, the rehydration of hectorite is inhibited by an attractive electrostatic force between migrated interlayer cations and the negatively charged octahedral sheets as well as montmorillonite. The Mg-saturated hectorite changed through regular interstratification of dehydrated and rehydrated layers to completely dehydrated structure after heating between 300° and 600°C. This interstratified structure was produced by fixation of interlayer Mg^{2+} to the alternating interlayers of hectorite consisting regular distribution of F^- to F^- and OH^- to OH^- facings distinct from the interlayer space.

Rectorite retained strong rehydration ability until the crystal structure was destroyed by heating, and the rehydration rate increased with increasing size of interlayer cations. These observations can be explained by the same reasons as those of beidellite. However, the effect of interlayer cations on formation of water molecules layers in the interlayer space decreased considerably after heating above 500°C. This is the most important characteristic which has not been observed in any other expandable clay minerals. The interlayer cations of rectorite migrated into the hexagonal holes on thermal dehydration and returned completely to the interlayer space on rehydration after heating below 400°C. For after heating above 500°C, however, the migrated cations did not return to the original position and remained around the basal oxygen plane even water molecules were regained in the interlayer space. Consequently, the water molecules coordinate abnormally to the relocated interlayer cations and the effect of the cations reduces considerably on rehydration.

ACKNOWLEDGMENTS

The author wishes to express his sincere gratitude to Profs. K. Tomita (Kagoshima University), S. Shimoda (University of Tsukuba), T. Nishiyama (Toyo University), and Dr. D. L. Bish (Los Alamos National Laboratory) for valuable comments and suggestions. Assoc. Prof. T. Matsuda (Okayama University) kindly supplied the author with a beidellite sample used in this study. The author also thank Mr. T. Kakoi (Kagoshima University) for technical assistance in the transmission electron microscopy. Thanks are due to the staff of the Institute of Earth Sciences, Faculty of Science, Kagoshima University for their generosities.

REFERENCES

Ames, L. L. and Goldich, S. S. (1958) A contribution on the Hector, California, bentonite deposit. *Econ. Geol.* **53**, 22.

Bailey, S. W. (1980) Structures of layer silicates: in *Crystal Structures of Clay Minerals and Their X-ray Identification*, G. W. Brindley and G. Brown. eds., Mineralogical Society, London, 1-124.

Barrer, R. M. (1978) *Zeolites and Clay Minerals as Sorbents and Molecular Sieves.* Academic Press, New York, pp. 407-483.

Barrer, R. M. and Jones, D. L. (1970) Synthesis and properties of fluorhectorites. *J. Chem. Soc., A.* 1531-1537.

Barrer, R. M. and Jones, D. L. (1971) Shape-selective sorbents derived from fluorhectorite. *J. Chem. Soc., A.* 2594-2603.

Barshad, I. (1948) Vermiculite and its relation to biotite as revealed by base-exchange reactions, X-ray analysis, diffraction thermal curves and water content. *Amer. Mineral.* **33**, 655-678.

Barshad, I. (1950) The effect of interlayer cations on the expansion of mica-type crystal lattice. *Amer. Mineral.* **35**, 225-238.

Barshad, I. (1952) Factors affecting the interlayer expansion of vermiculite and montmorillonite with organic substance. *Proc. Soil Sci. Amer.* **16**, 176-182.

Bassett, W. A. (1960) Role of hydroxyl orientation in mica alteration. *Bull. Geol. Soc. Amer.* **71**, 449-456.

Beaufort, D. (1984) An interstratified illite/smectite mineral from the hydrothermal deposit in Sibert, Rhone, France. *Clays Clay Minerals* **32**, 154-156.

Ben Hadj-Amara, A., Besson, G., and Tochoubar, C. (1987) Characteristiques structurales d'une smectite dioctahedriqe en fonction de l'order-desorder dans la distribution des charges eletriques: I. Etudes des reflections 001. *Clay Miner.* **22**, 305-318.

Bissada, K. K., Johns, W. D., and Cheng, F. S. (1967) Cation-dipole interactions in clay organic complexes. *Clay Miner.* **7**, 155-166.

Bradley, W. F. and Grim, R. E. (1951) High temperature thermal effects of clay related materials. *Amer. Mineral.* **36**, 182-201.

Brindley, G. W. and Roy, S. (1964) Complexes of Ca-montmorillonite with primary monohydric alcohols. *Amer. Minerl.* **49**, 106-115.

Brindley, G. W. and Wardle, R. (1970) Monoclinic and triclinic forms of pyrophyllite and pyrophyllite anhydride. *Amer. Mineral.* **55**, 1259-1272.

Brown, G. and Weir, A. H. (1963) The identity of rectorite and allevardite. *Proc. In. Clay Conf. Stockholm* **14**, 27-35.

Cole, W. F. (1966) A study of a long-spacing mica-like mineral. *Clay miner.* **6**, 261-281.

Dowdy, R. H. and Mortland, M. M. (1967) Alcohol-water interactions on montmorillonite surface. I. Ethanol. *Clays Clay Minerals* **15**, 259-271.

Dowdy, R. H. and Mortland, M. M. (1967) Alcohol-water interactions on montmorillonite surface. II. Ethylene glycol. *Soil Sci.* **105**, 30-43.

Eberhart, L. P. (1963) Transformation du mica en muscovite par chauffage entre 700° et 1200°C. *Bull. Soc. Franc. Miner. Cristallogr.* **86**, 213-251.

Emerson, W. W. (1957) Organo-clay complexes. *Nature* **180**, 48-49.

Farmer, V. C. and Russell, J. D. (1967) Infrared absorption spectrometry in clay studies. *Clays Clay Minerals* **15**, 121-142.

Foster, M. D. (1963) Interpretation of the composition of vermiculites and hydrobiotite: in *Clays and Clay Minerals, Proc. 10th Nat. Conf., Austin, Texas, 1961*, Ada, Swineford and P. C. Franks, eds., Pergamon Press, New York, 70-89.

Glaeser, R. and Méring, J. (1967) Effet du chauffage sur les montmorillonites saturees de cations de petit rayon. *C. R. Acad. Sci. Paris* **265**, 833-835.

Glaeser, R. and Méring, J. (1968) Homogeneous hydration domains of the smectites. *C. R. Acad. Sci. Paris* **267**, 436-466.

Granquist, W. T. and Pollack, S. S. (1960) A study of the synthesis of hectorite. *Clays Clay Minerals* **8**, 150-169.

Greene-Kelly, R. (1953) The identification of the montmorillonoids in clays. *J. Soil Sci.* **4**, 233-237.

Greene-Kelly, R. (1955) Dehydration of the montmorillonite minerals. *Mineral. Mag.* **30**, 604-615.

Grim, R. E. and Bradley, W. F. (1948) Rehydration and dehydration of the clay minerals. *Amer. Mineral.* **33**, 50-59.

Hamilton, J. D. (1967) Partially-ordered mixed-layer mica-montmorillonite from Maitland, New South Wales. *Clay Miner.* **7**, 63-78.

Hayashi, H. (1961) Mineralogical study on alteration products from altered aureole of some Kuroko deposits. *J. Miner. Soc. Japan* **5**, 101-125.

Hayashi, H. (1963) Montmorillonite from some bentonite deposits in Yamagata Prefecture, Japan. *Clay Science* **1**, 176-182.

Heller, L., Farmer, V. C., Mackenzie, R. C., Mitchell, B. D., and Taylor, H. F. W. (1962) The dehydroxylation and rehydroxylation of triphomic dioctahedral clay minerals. *Clay minerals Bull.* **5**, 56-72.

Heystek, H. (1954) An occurrence of a regular mixed-layer clay-mineral. *Mineralog. Mag.* **30**, 400-408.

Hoda, S. N. and Hood, W. C. (1972) Laboratory alteration of trioctahedral micas. *Clays Clay Minerals* **20**, 343-358.

Hofmann, U. and Klemen, E. (1950) Loss of exchangeability of lithium ions in bentonite on heating. *Z. Anorg. Allg. Chem*, **262**, 95-99.

Jonas, E. C. (1955) The reversible dehydroxylization of clay minerals: in *Clays and Clay Minerals, Proc. 3rd Nat. Conf., Texas, 1954*, W. O. Milligan, eds., Nat. Acad. Sci.-Nat. Res. Counc., Washington, D.C., 66-72.

Komarov, V. S., Rozin, A. T., and Akulich, N. A. (1977) Sites of localization of exchange cations of heat-treated montmorillonite. *Zh. Prikl. Spektrosk.* **26**, 1099-1103.

Leonard, R. A. and Weed, S. B. (1967) Infuence of exchange ions on the b-dimensions of dioctahedral vermiculite. *Clays Clay Minerals* **15**, 149-161.

Luca, V. and Cardile, C. M. (1988) Thermally induced cation migration in Na and Li montmorillonite. *Phys. Chem. Minerals* **16**, 98-103.

Luca, V. and Cardile, C. M. (1989) Cation migration in smectite minerals: Electron spin resonance of exchanged Fe3+ probes. *Clays Clay Minerals* **37**, 325-332.

Lussier, R. J., Magee, J. S., and Vaughan, D. E. W. (1980) Pillared interlayered clay cracking catalyst - preparation and properties. Reprints, 7th Can. Sym. Catal.,

Edmonton, Alberta, 88-95.

MacEwan, D. M. C. and Wilson, M. J. (1980) Interlayer and intercalation complexes of clay minerals: in *Crystal Structures of Clay Minerals and Their X-ray Identification*, G. W. Brindley anf G. Brown. eds., Mineralogical Society, London, 197-248.

Matsuda, T., Henmi, K., Nagasawa, K., and Honda, S. (1981a) Chemical compositions and X-ray properties of regularly interstratified mica-smectites. *J. Miner. Soc. Japan* **16**, 91-102.

Matsuda, T., Nagasawa, K., Tsuzuki, Y., and Henmi, K. (1981b) Regulary interstratified dioctahedral mica-smectite from Roseki deposits in Japan. *Clay Miner.* **16**, 91-102.

Matsuda, T. (1984) Mineralogical study on regularly interstratified dioctahedral mica-smectites. *Clay Science* **6**, 117-148.

Matsuda, T. (1988) Beidellite from Sano mine, Nagano Prefecture, Japan. *Clay Science* **7**, 151-159.

Matsuda, T. (1989) Expansion characteristics of rectorite. *Clay Science* **7**, 297-306.

Méring, J. (1946) On the hydration of montmorillonite. *Trans. Faraday Soc.* **42B**, 205-219.

Neumann, B. S. (1965) Behavior of a synthetic clay (fluor-hectorite) in pigment dispersions. *Rheologica Acta.* **4**, 250-255.

Neumann, B. S. and Sansom, K. G. (1970) The formation of stable sols from laponite, a synthetic hectorite-like clay. *Clay Miner.* **8**, 389-404.

Neumann, B. S. and Sansom, K. G. (1971) Rheological properties of dispersions of

laponite. *Clay Miner.* **9**, 231-243.

Newman, A. C. D. (1969) Cation exchange properties of micas. I. The relation between mica composition and potassium exchange in solutions of different pH. *J. Soil Sci.* **20**, 357-373.

Nishiyama, T. and Shimoda, S. (1981) Ca-bearing rectorite from Tooho mine, Japan. *Clays Clay Minerals* **29**, 236-240.

Pevear, D. R., Williams, V. E., and Mustoe, G. E. (1980) Kaolinite, smectite and K-rectorite in bentonites: Relation to coal rank at Tulameen, British Columbia. *Clays Clay Minerals* **28**, 241-254.

Pezerat, H. and Méring, J. (1967) Recherches sur la position des cations echangeables et de leau dans les montmorillonites. *C.R. Acad. Sci. Paris* **265**, 529-532.

Pinnavaia, T. J. (1982) Intercalation of molecular catalysts in layered silicates. *ACS Symp. Ser.* **192**, 242-253.

Post, J. L. (1984) Saponite from near Ballarat, California. *Clays Clay Minerals* **32**, 147-153.

Rosseinsky, D. R. (1965) Electrode potentials and hydration energies. Theories and correlations. *Chemical Reviews* **65**, 467-490.

Rupert, J. P., Granquist, W. T., and Pinnavaia, T. J. (1987) Catalytic properties of clay minerals: in *Chemistry of Clays and Clay Minerals*, A. C. D. Newman, eds., Mineralogical Society, London, 275-318,

Russell, J. D. and Farmer, V. C. (1964) Infrared spectroscopic study of the dehydration of montmorillonite and saponite. *Clay Miner. Bull.* **5**, 443-464.

Scott, A. D., Ismail, F. T., and Locatis, R. R. (1972) Changes in interlayer potassium

exchangeability induced heating micas: in *Proc. Inter. Clay Conf., Madrid*, M. M. Mortland and V. C. Farmer, eds., **2**, 143-158.

Shabtai, J. (1979) Zeolites and cross-linked silicates as media for selective catalysis. *Chem. L"Indust.* **61**, 734-741.

Shimoda, S. and Sudo, T. (1960) An interstratified mixture of mica clay minerals. *Amer. Mineral.* **45**, 1069-1077.

Shimoda, S., Oinuma, K., and Negishi, T. (1969) Interstratified minerals of illite and montmorillonite. *J. Geol. Soc. Japan* **75**, 591-599.

Smith, S. J. and Scott, A. D. (1974) Exchangeability of potassium in heated fine-grained micaceous minerals. *Clays Clay Minerals* **22**, 263-270.

Sudo, T., Hayashi, H., and Shimoda, S. (1962) Mineralogical problems of intermediate clay minerals. *Clays Clay Minerals* **9**, 378-392.

Suquet, H., de la Calle, C., and Pezerat, H. (1975) Swelling and structural organization of saponite. *Clays Clay Minerals* **23**, 1-9.

Takeshi, H. (1958) Kaolin minerals in "Roseki". *J. Miner. Soc. Japan* **5**, 388-404.

Tomita, K. (1974) Similarities of rehydration and rehydroxylation properties of rectorite and 2*M* clay micas. *Clays Clay Minerals* **22**, 79-85.

Tomita. K., Yamashita, H., and Oba, N. (1969) An interstratified mineral found in altered andesite. *J. Japan Assoc. Miner. Pet. Econ. Geol.* **61**, 25-34.

Tomita, K. and Dozono, M. (1973) An expansible mineral having high rehydration ability. *Clays Clay Minerals* **21**, 185-190.

Tomita, K. and Dozono, M. (1974) An interstratified mineral of mica and montmorilonite found in an altered tuff. *J. Japan Assoc. Miner. Pet. Econ. Geol.* **69**, 147-154.

Tomita, K. and Sudo, T. (1968) Interstratified structure formed from a pre-heated mica by acid treatments. *Nature* **217**, 1043-1044.

Udagawa, S. (1955) X-ray studies on thermal transformations in sericite. *J. Ceram. Assoc. Japan* **63**, 517-523.

Udagawa, S., Urabe, K., and Hasu, H. (1974) The crystal structure of muscovite dehydroxylate. *J. Japan Assoc. Min. Petr. Econ. Geol.* **69**, 381-389.

Uno, Y., Kohyama, N., Sato, M., and Takeshi, H. (1986) High-temperature phase transformation of montmorillonite. *J. Miner. Soc. Japan* **17**, Spec. Issue, 155-161.

Vedder, W. and Wilkins, R. W. (1969) Dehydroxylation and rehydroxylation, oxidation and reduction of micas. *Amer. Mineral.* **54**, 482-509.

Walker, G. F. (1956) The mechanism of dehydration og Mg-vermiculite. *Clays Clay Minerals* **4**, 101-115.

Wardle, R. and Brindley, G. W. (1972) The crystal structures of pyrophyllite, 1Tc, and of its dehydroxylate. *Amer. Mineral.* **57**, 732-750.

Watanabe, T. and Sato, T. (1988) Expansion characteristics of montmorillonite and saponite under various relative humidity conditions. *Clay Science* **7**, 129-138.

Whittaker, E. J. W. and Muntus, R. (1970) Ionic radii for use in geochemistry. *Geochim. Cosmochim. Acta* **34**, 945-956.

TABLES

Table 2.1. Chemical analyses and numbers of cations on the basis $O_{20}(OH)_4$ for dioctrahedral smectites.

	1	2	3
SiO_2	48.24	51.62	45.27
TiO_2	0.02	0.07	0.09
Al_2O_3	17.01	24.31	26.62
Fe_2O_3	0.81	0.88	0.08
FeO	0.15	0.41	-
MgO	4.05	1.36	1.13
CaO	3.03	1.52	1.81
Na_2O	0.34	1.06	0.63
K_2O	0.16	0.16	0.49
$H_2O(+)$	8.59	6.46	7.93
$H_2O(-)$	17.21	12.68	16.02
Total (%)	99.30	100.53	100.07
Tetrahedral			
Si	7.76	7.44	7.00
Al	0.24	0.56	1.00
Octahedral			
Al	2.99	3.58	3.84
Fe^{3+}	0.10	0.10	0.00
Fe^{2+}	0.02	0.04	-
Mg	0.95	0.28	0.14
Ti	-	-	0.02
Sum	4.06	4.00	4.00
Interlayer			
Ca	0.49	0.24	0.30
Mg	0.02	-	0.12
Na	0.02	0.30	0.18
K	0.01	0.02	0.10
H	0.03	-	-
Sum	0.57	0.56	0.70

1 = Montmorillonite from Cheto, U.S.A. (Uno *et al.*, 1986)
2 = Dioctahedral smectite from Aterasawa, Yamagata Prefecture, Japan (Hayashi, 1963).
3 = Beidellite from Sano mine, Nagano Prefecture, Japan (Matsuda, 1988).

Table 2.2. Basal spacings and structure factors for various states of Na-saturated smectite from Atarasawa.

	Unheated			Heated at 600°C		
00 *l*	d(Å)	|Fo|	Fc	d(Å)	|Fo|	Fc
1	12.6	160.7	-110.1	9.7	53.5	-50.3
2	6.25	45.2	-41.8	4.79	62.4	-47.1
3	4.19	23.2	-21.1	3.19	135.3	-133.0
4	3.12	154.2	153.7	2.383	16.2	-15.1
5	2.485	14.0	-13.2	1.917	86.5	99.7
6	2.078	77.1	-78.7	1.595	23.6	24.5
7	1.786	39.8	37.0	1.370	53.1	-55.8
8	1.555	31.6	32.6	1.206	28.4	34.0
9	1.385	51.6	-49.3			
10	1.249	34.4	34.4			
	Rehydrated			Heated at 800°C		
00 *l*	d(Å)	|Fo|	Fc	d(Å)	|Fo|	Fc
1	12.6	103.2	-114.1	9.8	45.6	-40.2
2	6.24	51.0	-43.4	4.83	49.6	-44.8
3	4.21	20.0	-24.0	3.22	132.2	-150.5
4	3.12	161.2	154.7	2.421	21.0	21.4
5	2.462	15.6	-14.9	1.931	56.5	66.8
6	2.075	74.7	-76.2	1.603	40.3	37.9
7	1.789	38.5	39.2	1.362	62.3	-63.2
8	1.554	29.0	32.8	1.205	42.5	46.5
9	1.386	46.0	-45.8			
10	1.248	35.5	35.8			

|Fo| = observed structure factors. Fc = calculated structure factors.

Table 2.3. Basal spacings and structure factors for Ca- and Mg-saturated smectite from Aterasawa heated at 800°C.

	Ca-saturated			Mg-saturated		
00 *l*	d(Å)	|Fo|	Fc	d(Å)	|Fo|	Fc
1	9.7	41.8	-38.2	9.7	41.7	-37.7
2	4.82	51.4	-51.6	4.79	48.2	-38.5
3	3.21	144.0	-142.0	3.19	149.6	-147.4
4	2.383	17.7	19.2	2.383	17.7	19.2
5	1.924	58.7	64.6	1.924	58.7	64.6
6	1.599	44.4	46.6	1.599	44.4	46.6
7	1.375	81.5	-78.4	1.375	81.5	-78.4
8	1.206	47.1	51.4	1.206	47.1	51.4

|Fo| = observed structure factors. Fc = calculated structure factors.

Table 2.4. Basal spacings and structure factors for various states of Na-saturated beidellite from Sano mine.

	Unheated			Heated at 400°C		
00 *l*	d(Å)	|Fo|	Fc	d(Å)	|Fo|	Fc
1	12.7	109.8	-112.3	9.96	58.1	-43.5
2	6.23	45.9	-47.0	4.86	59.1	-56.9
3	4.16	23.8	-20.6	3.23	122.6	-126.6
4	3.097	152.2	154.9	2.442	19.3	-13.3
5	2.459	14.4	-9.7	1.936	84.4	87.9
6	2.059	81.8	-76.6	1.603	31.3	31.9
7	1.766	43.7	43.2	1.379	67.3	-69.4
8	1.544	44.9	42.1	1.204	30.9	35.9
9	1.376	41.2	-43.6			
10	1.239	40.1	36.3			

	Heated at 800°C			Rehydrated		
00 *l*	d(Å)	|Fo|	Fc	d(Å)	|Fo|	Fc
1	9.89	45.9	-36.3	12.66	95.9	-90.2
2	4.90	63.1	-57.8	6.27	49.3	-46.1
3	3.25	149.1	-147.9	4.18	16.1	-21.7
4	2.442	19.5	21.7	3.116	168.9	167.7
5	1.951	64.7	74.0	2.495	19.2	-24.2
6	1.622	44.6	44.1	2.074	49.1	-57.8
7	1.389	75.1	-76.4	1.775	24.1	27.0
8	1.228	39.0	44.9	1.551	40.2	43.2
9				1.382	56.8	-53.7
10				1.249	36.9	44.6

|Fo| = observed structure factors. Fc = calculated structure factors.

Table 3.1. Basal spacings and structure factors for Na-saturated saponite after heating at 400° and 700°C.

	Heated at 400°C			Heated at 700°C		
00 *l*	d(Å)	|Fo|	Fc	d(Å)	|Fo|	Fc
1	9.91	78.3	-70.6	9.86	77.6	-69.5
2	4.920	53.9	-40.8	4.906	53.4	-41.3
3	3.269	150.3	-149.1	3.263	150.5	-150.8
4	2.470	14.2	19.9	2.465	14.1	17.5
5	1.961	76.0	85.0	1.959	82.1	88.0
6	1.627	34.8	38.6	1.624	42.4	44.1
7	1.399	68.8	-73.1	1.401	69.7	-76.5
8	1.222	28.5	36.8	1.228	23.9	30.6

|Fo| = observed structure factors. Fc = calculated structure factors.

Table 3.2. Basal spacings and structure factors for Ca- and Mg-saturated saponite after heating at 800°C.

	Ca-saturated			Mg-saturated		
00 *l*	d(Å)	|Fo|	Fc	d(Å)	|Fo|	Fc
1	9.62	70.7	-70.1	9.53	70.3	-69.4
2	4.783	44.0	-38.1	4.740	43.5	-38.1
3	3.178	146.3	-145.7	3.153	144.0	-144.7
4	2.383	23.3	22.3	2.356	26.9	22.2
5	1.908	69.5	69.8	1.896	69.2	67.3
6	1.589	41.3	38.0	1.575	53.2	47.3
7	1.363	61.9	-69.0	1.353	64.7	-76.2
8	1.194	44.5	46.2	1.185	39.2	39.8

|Fo| = observed structure factors. Fc = calculated structure factors.

Table 3.3. Basal spacings and structure factors for Ca-, Na-, and K-saturated vermiculite after heating at 800°C.

	Ca-saturated			Na-saturated			K-saturated		
00 *l*	d(Å)	|Fo|	Fc	d(Å)	|Fo|	Fc	d(Å)	|Fo|	Fc
1	9.63	54.4	-59.2	9.94	59.0	-54.7	10.35	49.6	-43.6
2	4.783	22.6	17.9	4.914	24.2	4.2	5.053	23.8	6.9
3	3.178	158.6	-159.3	3.267	132.0	-142.9	3.387	112.2	-124.3
4	2.106	35.4	35.9	2.478	21.1	19.8	2.536	47.7	45.5
5	1.910	63.0	61.0	1.959	84.8	80.7	2.024	105.5	102.5
6	1.590	33.9	35.1	1.631	36.6	36.9	1.684	59.1	56.8
7	1.363	41.0	-38.0	1.399	56.3	-48.4	1.443	52.1	-49.1
8	1.188	44.2	42.5	1.222	40.6	43.1	1.267	56.9	57.8

|Fo| = observed structure factors. Fc = calculated structure factors.

Table 5.1. Chemical analyses for rectorites.

	1	2*
SiO_2	46.46	55.20
TiO_2	0.67	-
Al_2O_3	29.75	38.7
Fe_2O_3	1.65	0.59
MgO	0.58	-
CaO	0.34	0.33
Na_2O	2.92	4.40
K_2O	2.17	0.11
$H_2O(+)$	6.01	-
$H_2O(-)$	8.96	-
Total (%)	99.51	99.33

1 = Rectorite from Makurazaki, Kagoshima Prefecture, Japan. 2 = Rectorite from Arkansas, U.S.A. (Brown and Weir, 1963). * Ignited weight basis.

Table 5.2. Basal spacings and structure factors for Na-saturated rectorite from Arkansas without heating.

00 *l*	d(Å)	d(Å)× *l*	|Fo|	Fc
1	22.2	22.2	66.3	65.6
2	11.13	22.26	146.0	-137.6
3	7.420	22.26	31.9	45.2
4	5.543	22.17	66.3	-64.4
5	4.442	22.21	22.3	-57.5
7	3.162	22.13	260.5	-257.0
10	2.217	22.17	43.7	57.1
11	2.010	22.11	129.6	135.0
12	1.844	22.13	94.1	95.0
14	1.578	22.09	63.7	54.3
16	1.382	22.11	77.3	-75.9
17	1.304	22.17	33.8	41.4
18	1.228	22.10	50.9	51.9
19	1.170	22.23	37.6	-41.4
Average basal spacing (Å)		22.167		

|Fo| = observed structure factors. Fc = calculated structure factors.

Table 5.3. Basal spacings and structure factors for Na-saturated rectorite from Arkansas after heating at 400°C.

00 *l*	d(Å)	d(Å)× *l*	|Fo|	Fc
1	20.3	20.3	20.3	-14.6
2	9.76	19.52	91.5	-102.0
3	6.49	19.47	20.5	22.2
4	4.83	19.32	99.3	-96.3
5	3.858	19.29	22.5	17.5
6	3.209	19.25	218.3	-213.7
9	2.129	19.16	19.5	21.6
10	1.908	19.08	161.0	163.5
12	1.601	19.21	39.4	44.7
14	1.376	19.26	72.2	-69.3
16	1.203	19.25	51.7	53.1
Average basal spacing (Å)		19.281		

|Fo| = observed structure factors. Fc = calculated structure factors.

Table 5.4. Basal spacings and structure factors for Na-saturated rectorite from Arkansas after heating at 800°C.

00 *l*	d(Å)	d(Å)× *l*	|Fo|	Fc
1	21.0	21.0	21.5	21.8
2	9.83	19.66	79.8	-75.3
3	6.48	19.44	26.7	36.8
4	4.86	19.40	107.9	-93.5
5	3.904	19.52	36.2	32.9
6	3.210	19.26	266.5	-262.6
8	2.415	19.32	55.4	58.0
9	2.141	19.27	32.5	34.1
10	1.928	19.28	132.6	147.1
12	1.616	19.39	91.2	92.4
14	1.384	19.38	87.7	-88.7
16	1.206	19.30	58.5	67.4
	Average basal spacing (Å)	19.384		

|Fo| = observed structure factors. Fc = calculated structure factors.

Table 5.5. Basal spacings and structure factors for Na-saturated rectorite from Arkansas rehydrated after heating at 400°C.

00 *l*	d(Å)	d(Å)× *l*	|Fo|	Fc
1	22.2	22.2	58.2	58.5
2	11.13	22.26	113.7	-121.1
3	7.42	22.26	27.4	33.6
4	5.55	22.20	59.7	-53.1
5	4.444	22.22	53.6	-57.1
7	3.166	22.16	252.3	-254.7
10	2.217	22.17	38.4	41.5
11	2.013	22.14	141.7	133.6
12	1.846	22.15	112.6	106.6
14	1.580	22.12	57.0	55.4
16	1.383	22.13	76.9	-86.8
17	1.303	22.15	43.8	37.8
18	1.229	22.12	65.9	65.0
19	1.163	22.10	49.0	-47.4
	Average basal spacing (Å)	22.170		

|Fo| = observed structure factors. Fc = calculated structure factors.

Table 5.6. Basal spacings and structure factors for Na-saturated rectorite from Arkansas rehydrated after heating at 800°C.

00 *l*	d(Å)	d(Å)× *l*	|Fo|	Fc
1	22.9	22.9	44.5	30.8
2	11.41	22.82	85.2	-86.0
3	7.65	22.96	40.2	45.1
4	5.69	22.76	65.3	-70.6
5	4.56	22.80	47.3	-48.5
6	3.776	22.66	12.5	-15.1
7	3.250	22.75	285.2	-281.8
8	2.838	22.70	17.0	12.4
9	2.531	22.78	38.4	39.9
10	2.293	22.93	16.9	16.5
11	2.075	22.83	98.6	102.0
12	1.904	22.85	64.5	66.9
14	1.623	22.72	80.4	87.4
16	1.433	22.93	119.4	-116.2
18	1.251	22.52	49.3	54.1
Average basal spacing (Å)		22.794		

|Fo| = observed structure factors. Fc = calculated structure factors.

FIGURES

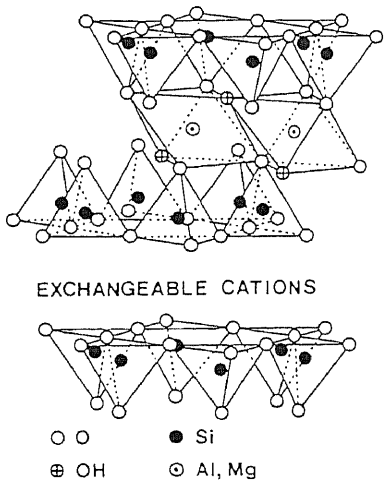

Figure 1.1. Schematic representation of the structure of expandable clay minerals.

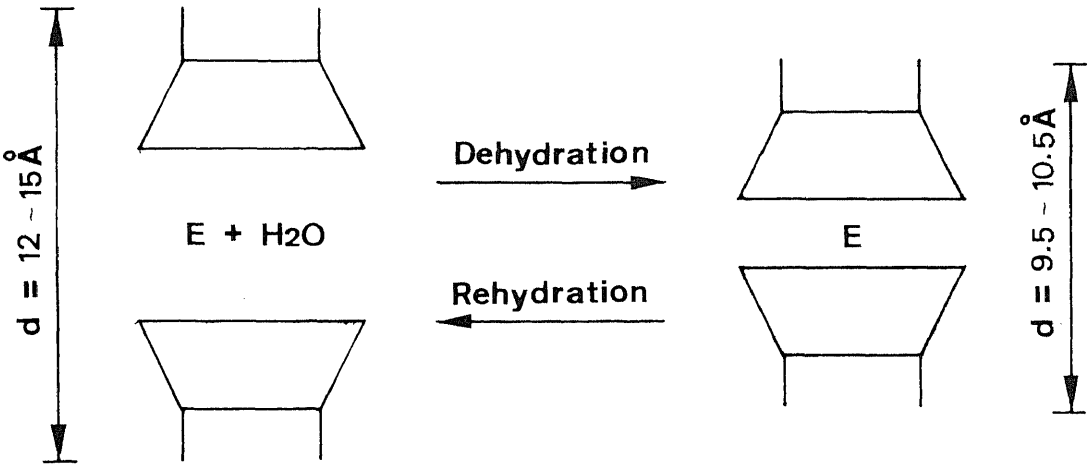

Figure 1.2. Schematic representation of dehydration and rehydration processes of smectite. The hydrated smectite shows 12 to 15Å of basal spacing depending on the hydration states of interlayer cation. E = exchangeable interlayer cation.

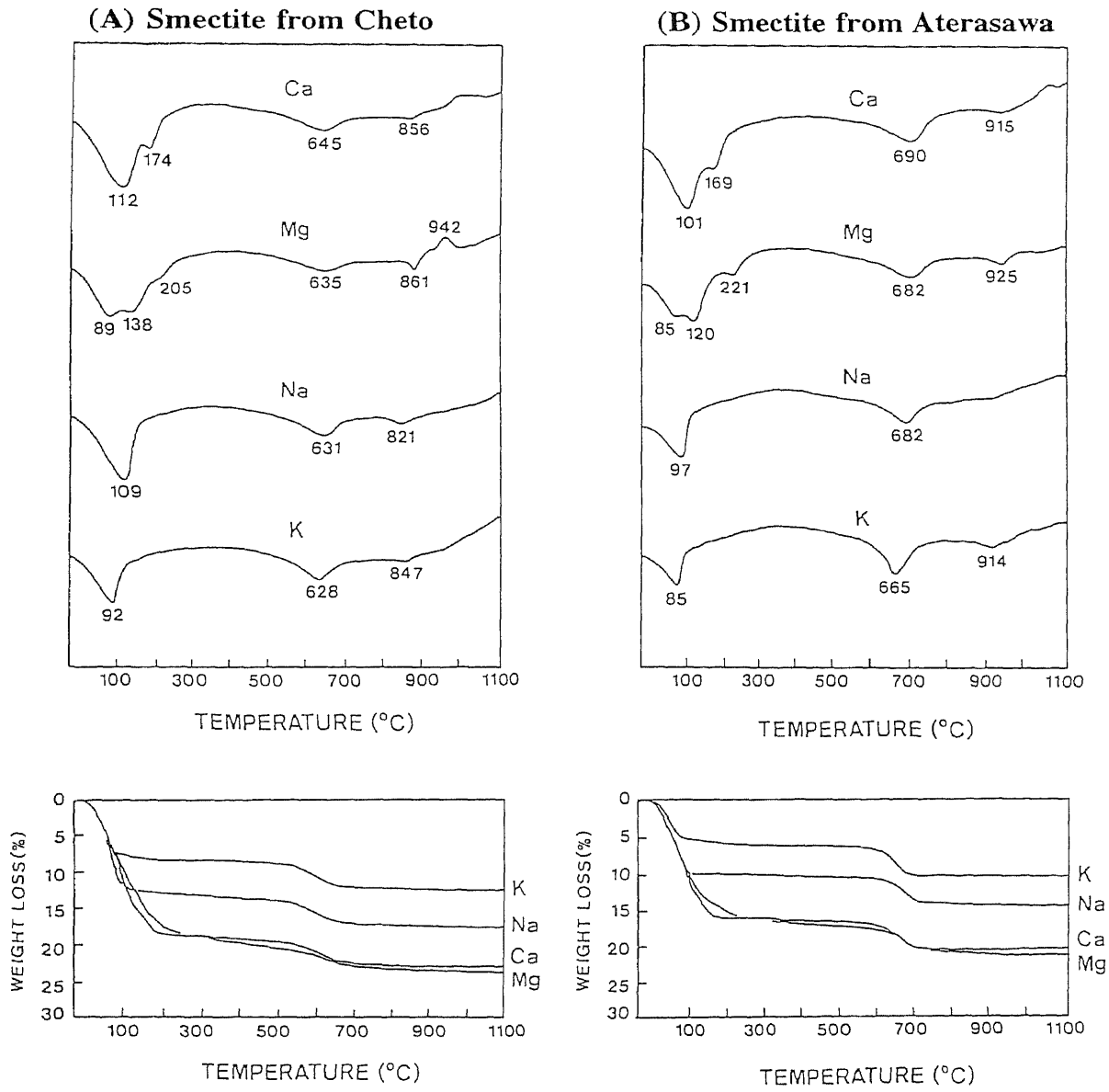

Figure 2.1. Differential thermal and thermogravimetric analysis curves of homoionic smectites from (A) Cheto and (B) Aterasawa. Ca, Mg, Na, and K represent Ca-, Mg-, Na-, and K-saturated materials, respectively.

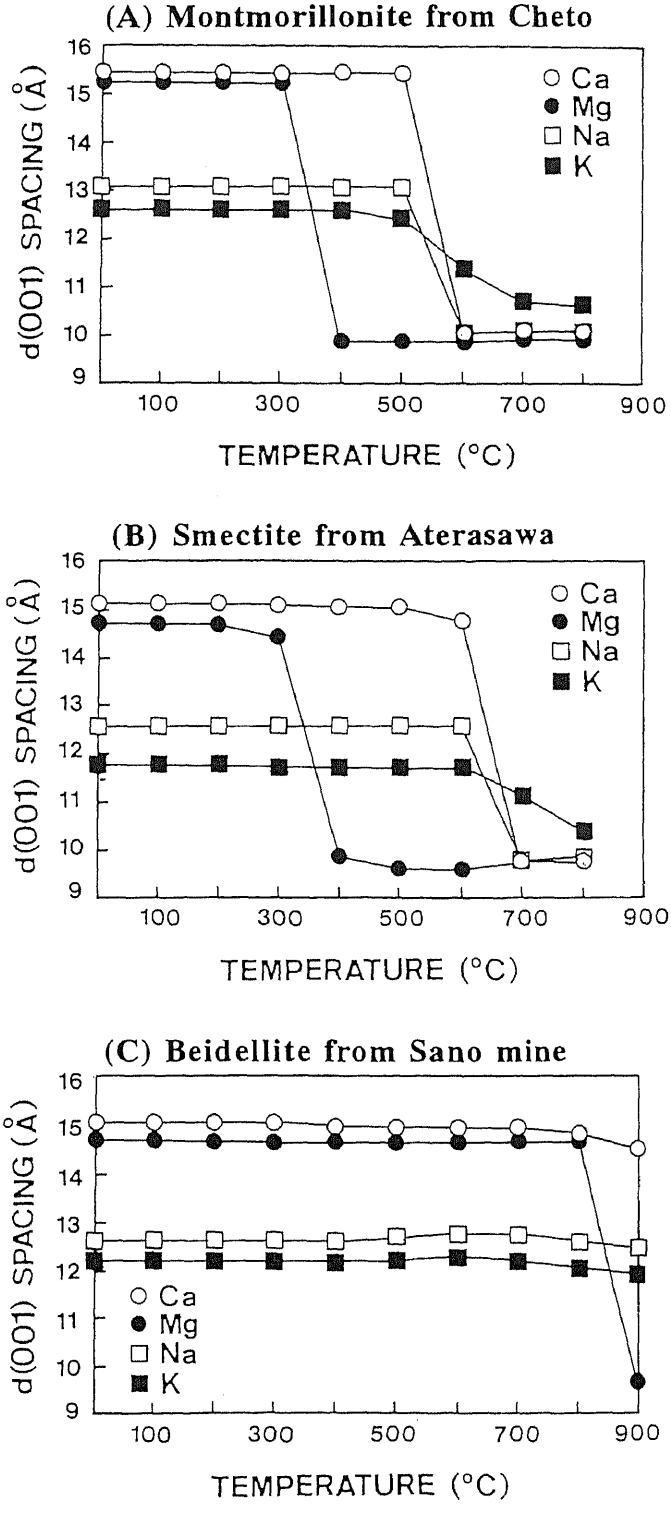

Figure 2.2. Variation of d(001) values for rehydrated homoionic smectites from (A) Cheto, (B) Aterasawa, (C) Sano mine after heating at various temperatures.

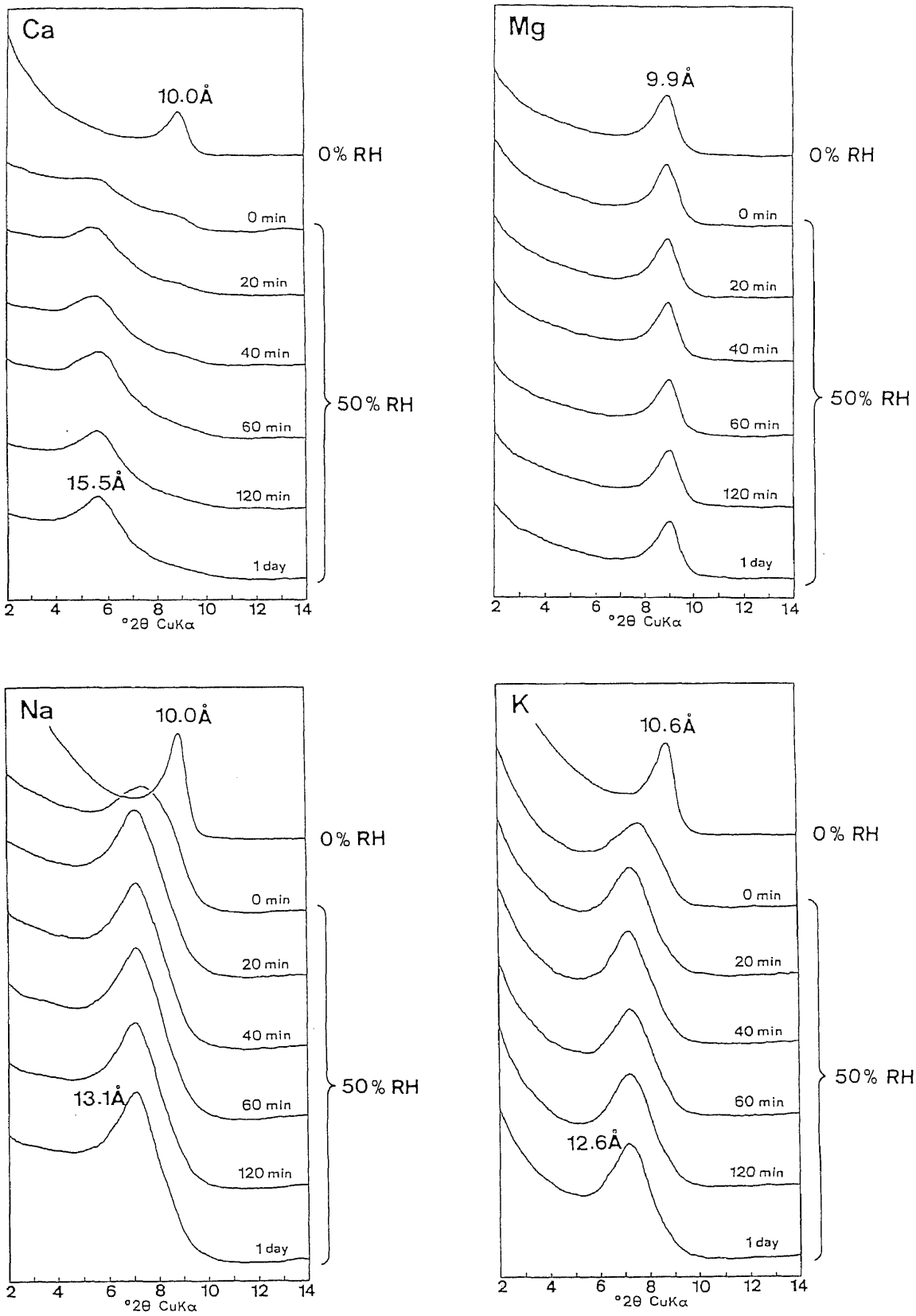

Figure 2.3. Changes in (001) reflections for homoionic montmorillonite from Cheto heated at 400°C during rehydration in air at 50% RH. Ca, Mg, Na, and K represent Ca-, Mg-, Na-, and K-saturated materials, respectively. 0% and 50% RH signify relative humidity of atmosphere.

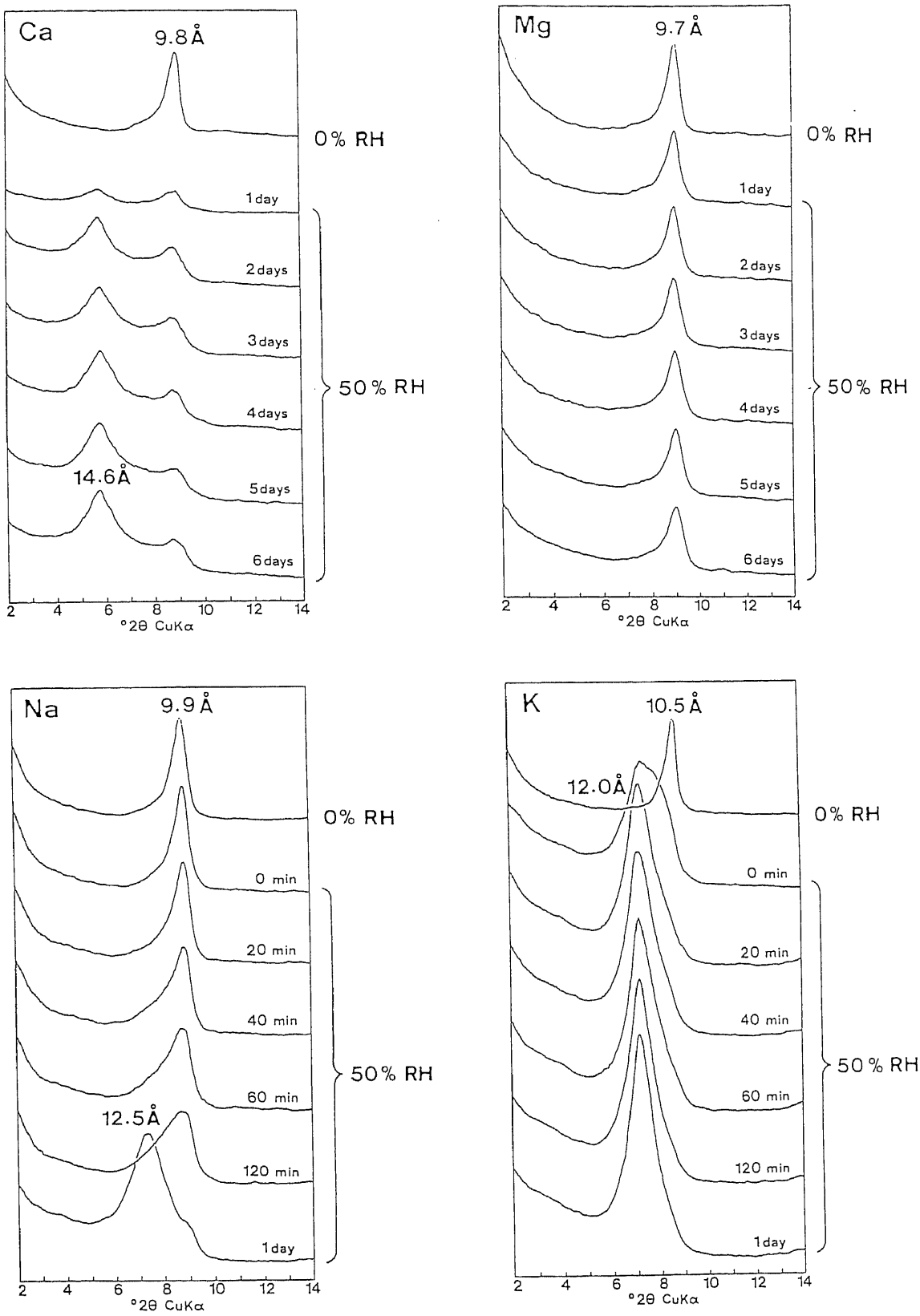

Figure 2.4. Changes in (001) reflections for homoionic beidellite from Sano mine heated at 800°C during rehydration in air at 50% RH. Ca, Mg, Na, and K represent Ca-, Mg-, Na-, and K-saturated materials, respectively. 0% and 50% RH signify relative humidity of atmosphere.

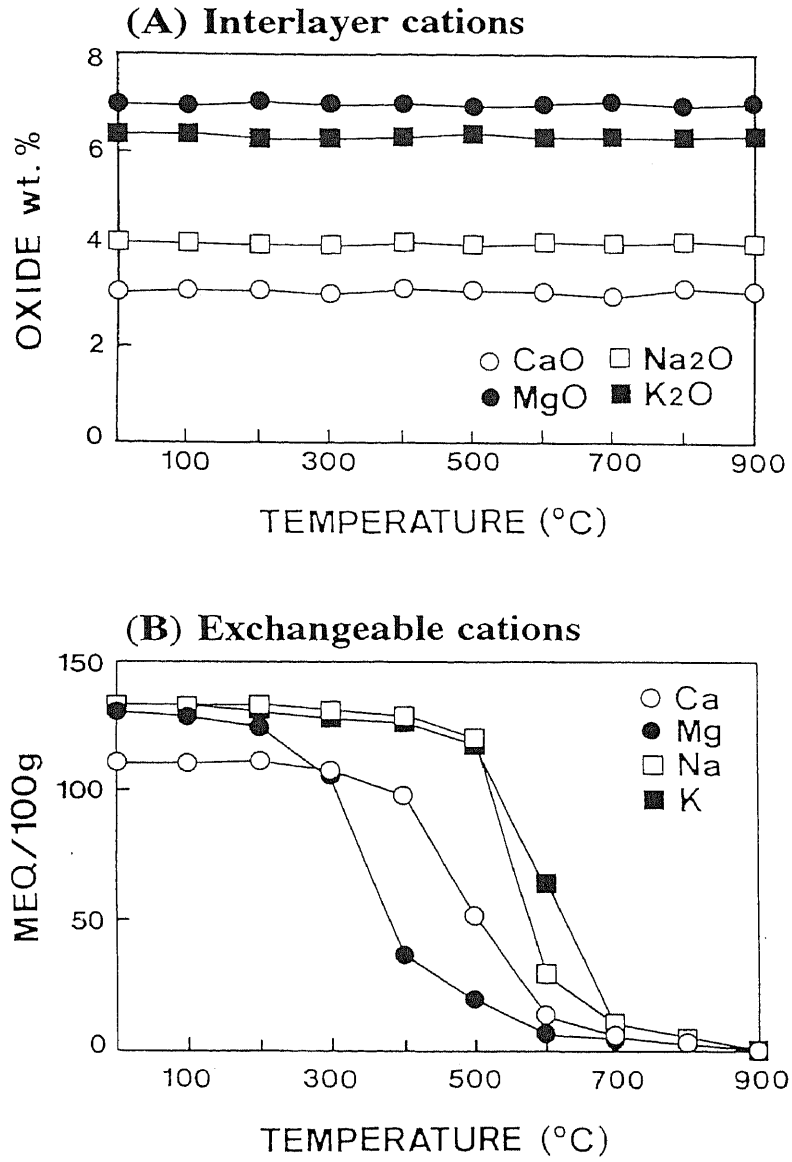

Figure 2.5. Variation of (A) oxide wt.% of CaO, MgO, Na_2O, and K_2O, and (B) exchangeable cations for homoionic montmorillonite from Cheto after heating at various temperatures.

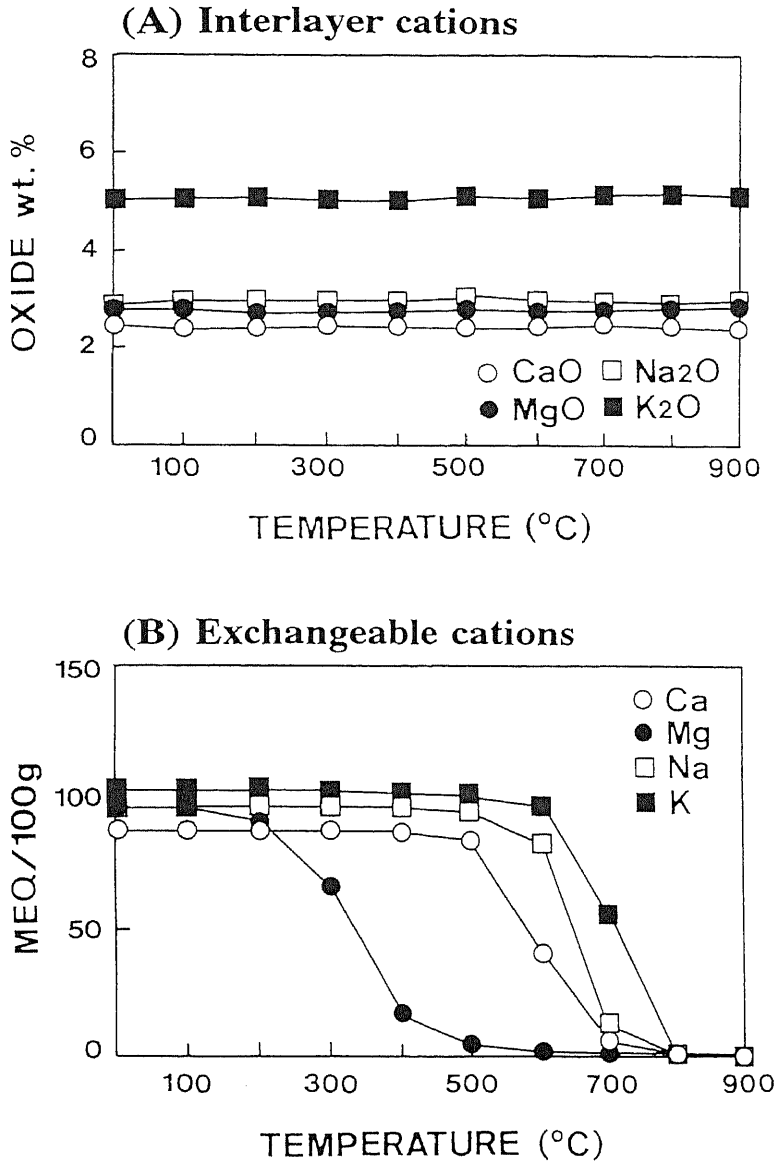

Figure 2.6. Variation of (A) oxide wt.% of CaO, MgO, Na_2O, and K_2O, and (B) exchangeable cations for homoionic smectite from Aterasawa after heating at various temperatures.

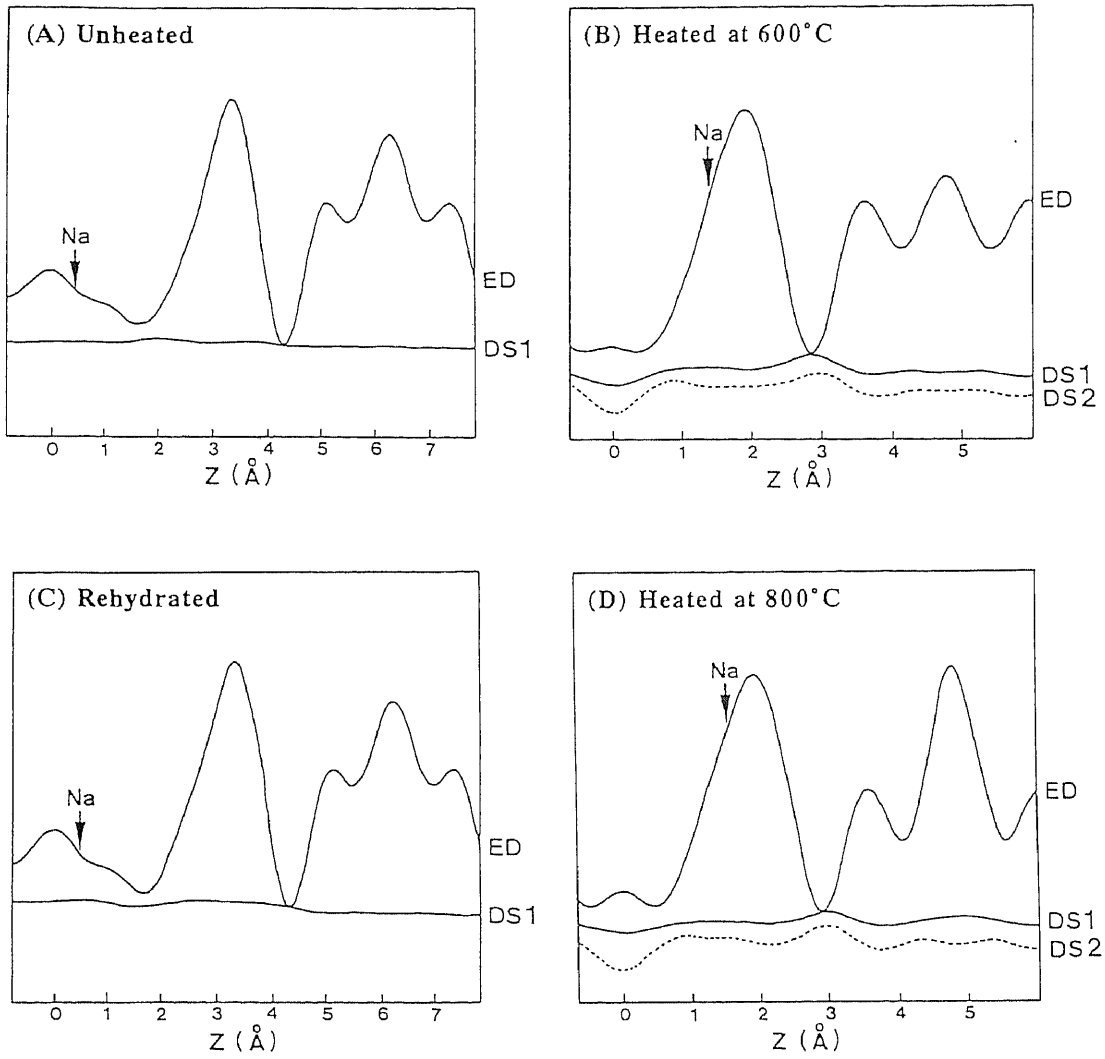

Figure 2.7. Electron density distribution and difference synthesis curves of Na-saturated smectite from Aterasawa (A) unheated, (B) heated at 600°C, (C) rehydrated after heating at 600°C, and (D) heated at 800°C. ED = electron density distribution; DS1 = difference synthesis calculated by using z-parameters obtained by the least squares refinement; DS2 = difference synthesis calculated by assuming that interlayer cations are located at the center of interlayer space.

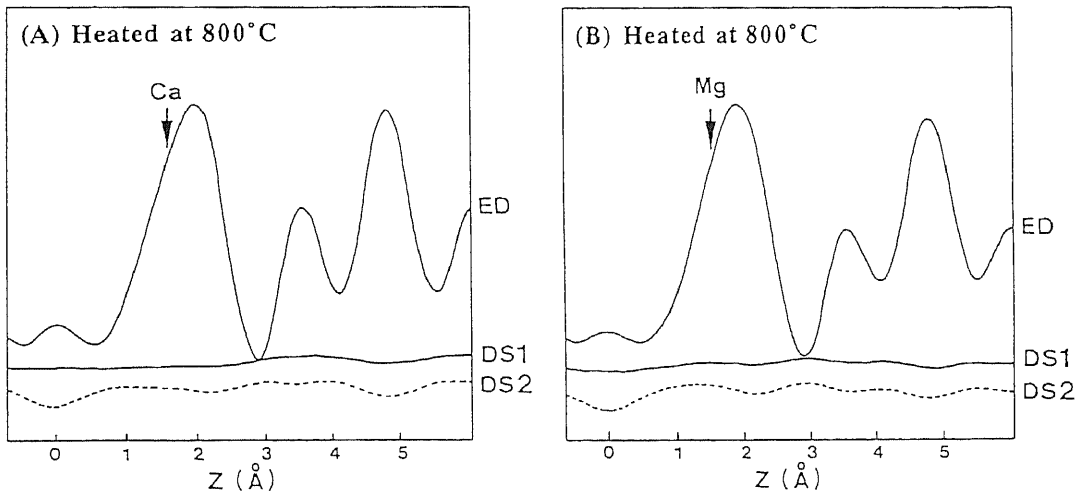

Figure 2.8. Electron density distribution and difference synthesis curves of (A) Ca- and (B) Mg-saturated smectite from Aterasawa heated at 800°C. ED = electron density distribution; DS1 = difference synthesis calculated by using z-parameters obtained by the least squares refinement; DS2 = difference synthesis calculated by assuming that interlayer cations are located at the center of interlayer space.

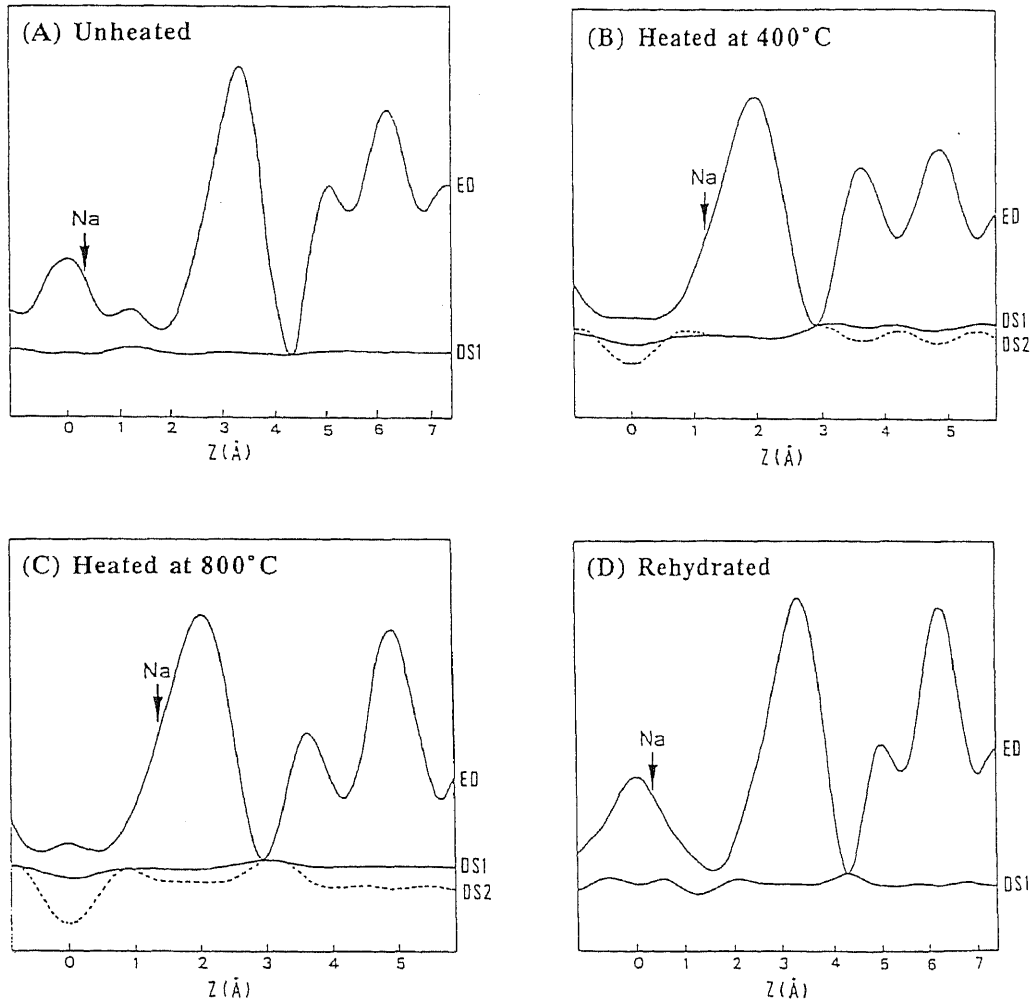

Figure 2.9. Electron density distribution and difference synthesis curves of Na-saturated beidellite (A) unheated, (B) heated at 600°C, (C) heated at 800°C, and (D) rehydrated after heating at 800°C. ED = electron density distribution; DS1 = difference synthesis calculated by using z-parameters obtained by the least squares refinement; DS2 = difference synthesis calculated by assuming that interlayer cations are located at the center of interlayer space.

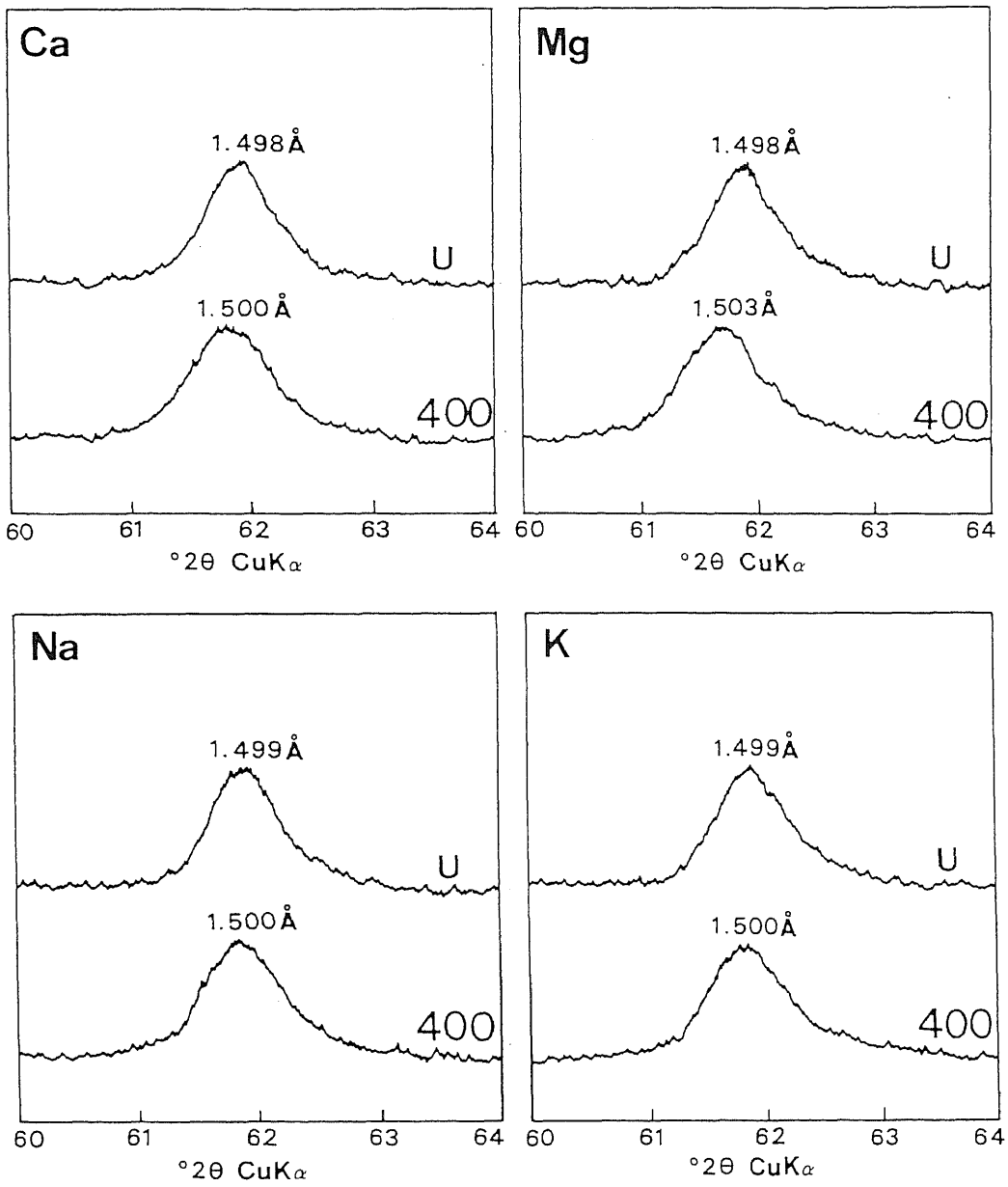

Figure 2.10. X-ray powder diffraction patterns of homoionic montmorillonite from Cheto in the region of the (060) reflection (U) before and (400) after heating at 400°C. Ca, Mg, Na, and K represent Ca-, Mg-, Na-, and K-saturated materials, respectively.

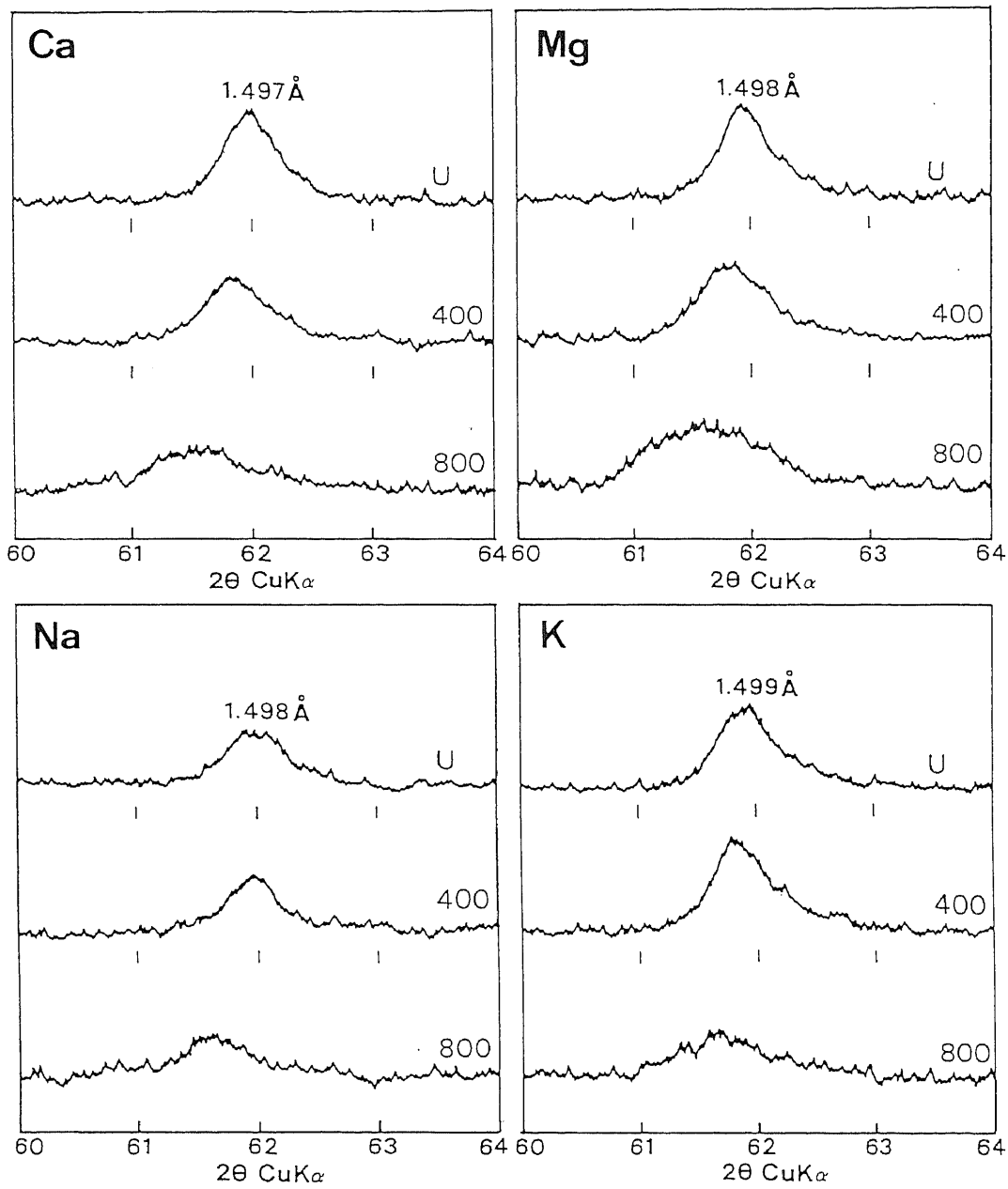

Figure 2.11. X-ray powder diffraction patterns of homoionic smectite from Aterasawa in the region of the (060) reflection (U) before and after heating at (400) 400° and (800) 800°C. Ca, Mg, Na, and K represent Ca-, Mg-, Na-, and K-saturated materials, respectively.

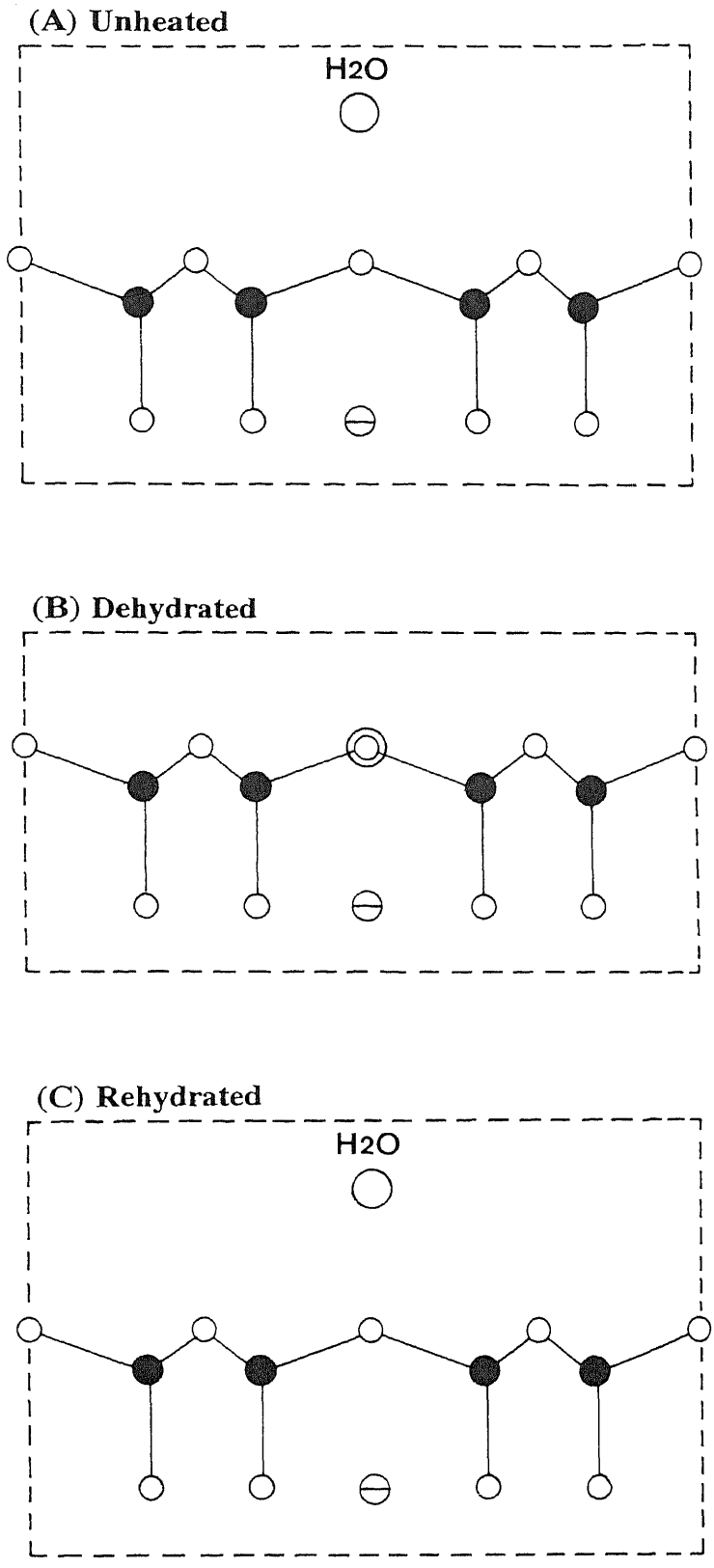

Figure 2.12. Schematic diagram showing behavior of interlayer cation during dehydration and rehydration.
◯ = interlayer cation; ● = silicon; ○ = oxygen; ⊖ =hydroxyl ion.

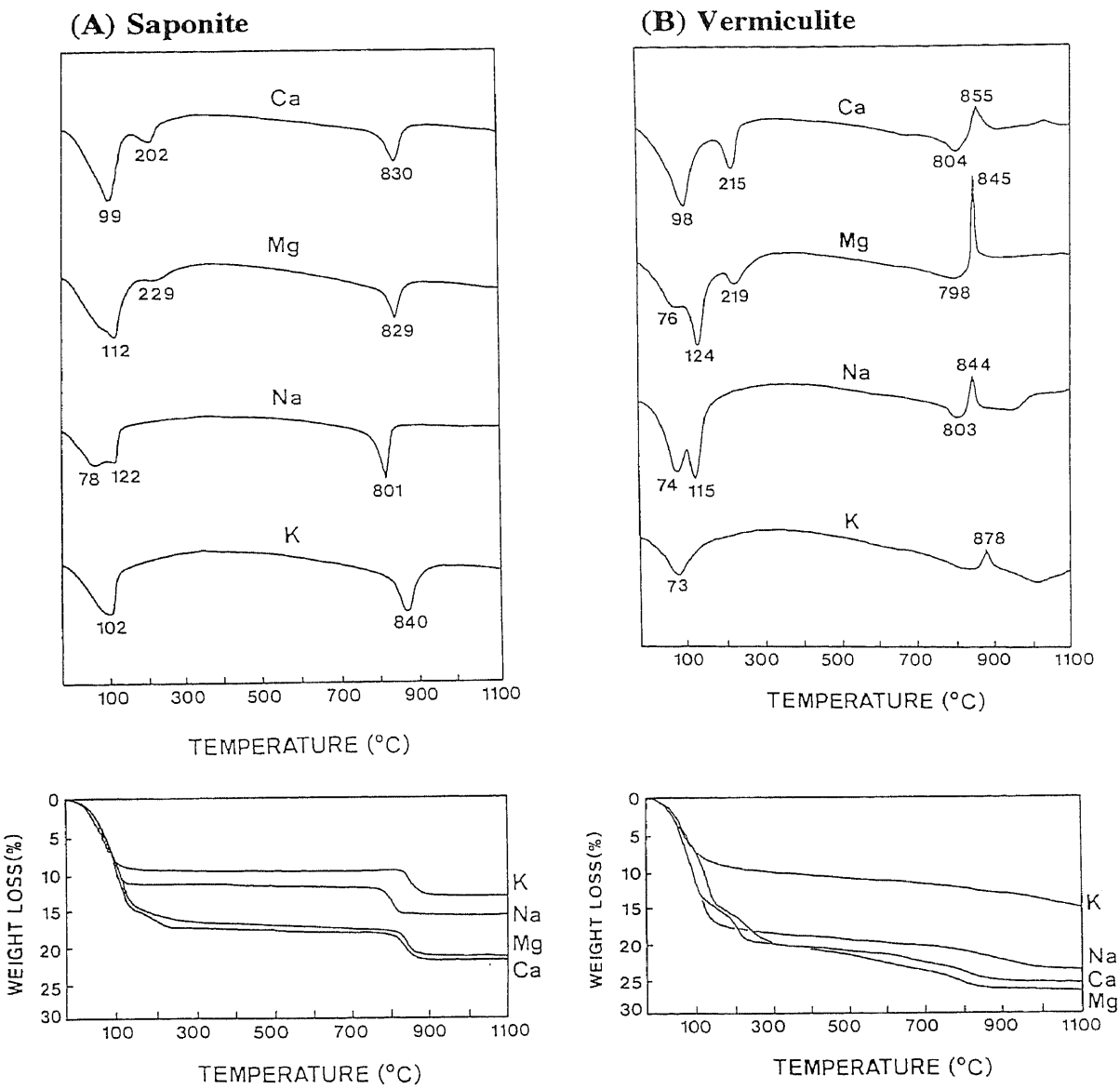

Figure 3.1. Differential thermal and thermogravimetric analysis curves of homoionic (A) saponite and (B) vermiculite. Ca, Mg, Na, and K represent Ca-, Mg-, Na-, and K-saturated materials, respectively.

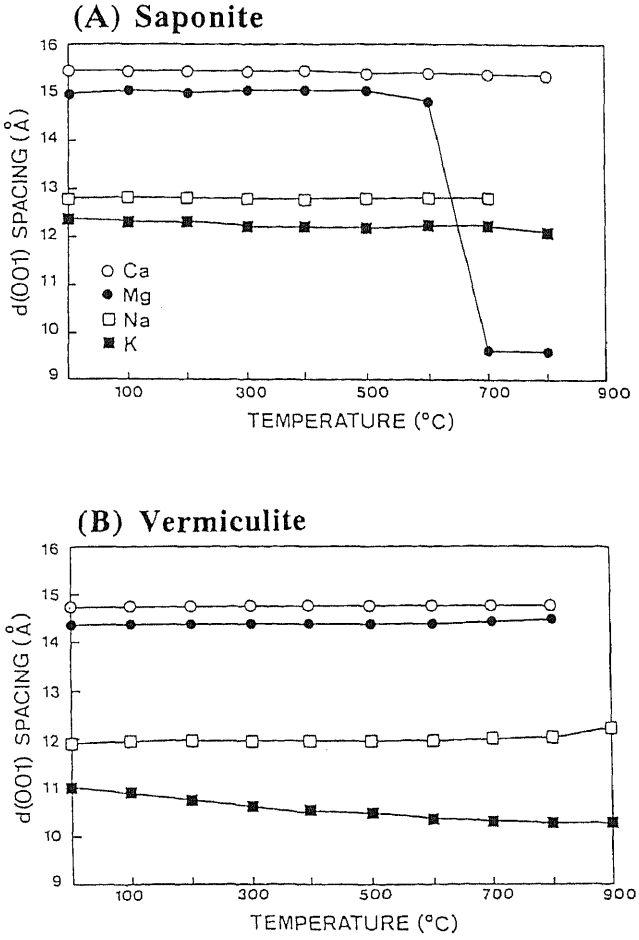

Figure 3.2. Variation of d(001) values for rehydrated homoionic (A) saponite and (B) vermiculite after heating at various temperatures.

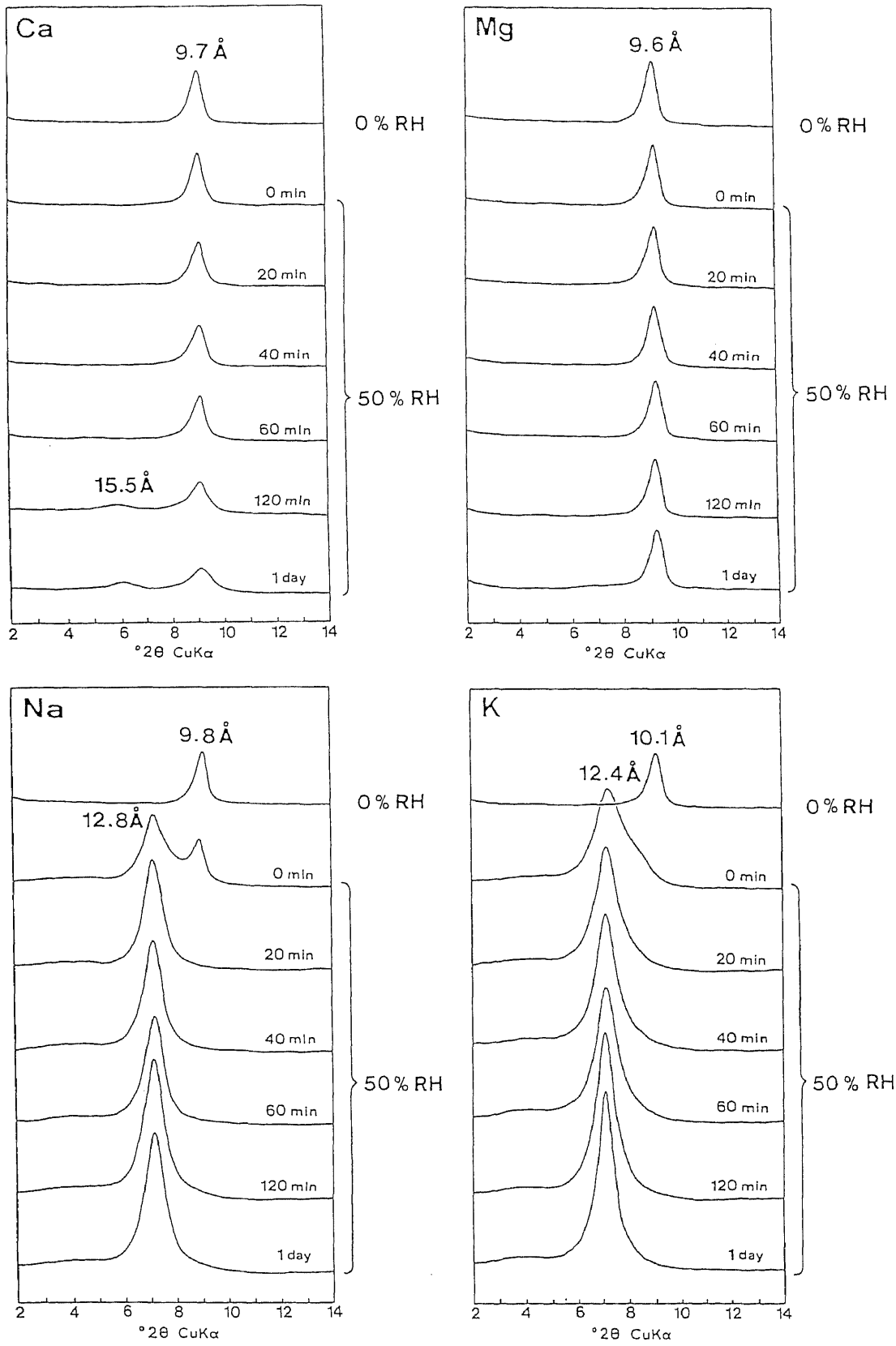

Figure 3.3. Changes in (001) reflections for homoionic saponite heated at 700°C during rehydration in air at 50% RH. Ca, Mg, Na, and K represent Ca-, Mg-, Na-, and K-saturated materials, respectively. 0% and 50% RH signify relative humidity of atmosphere.

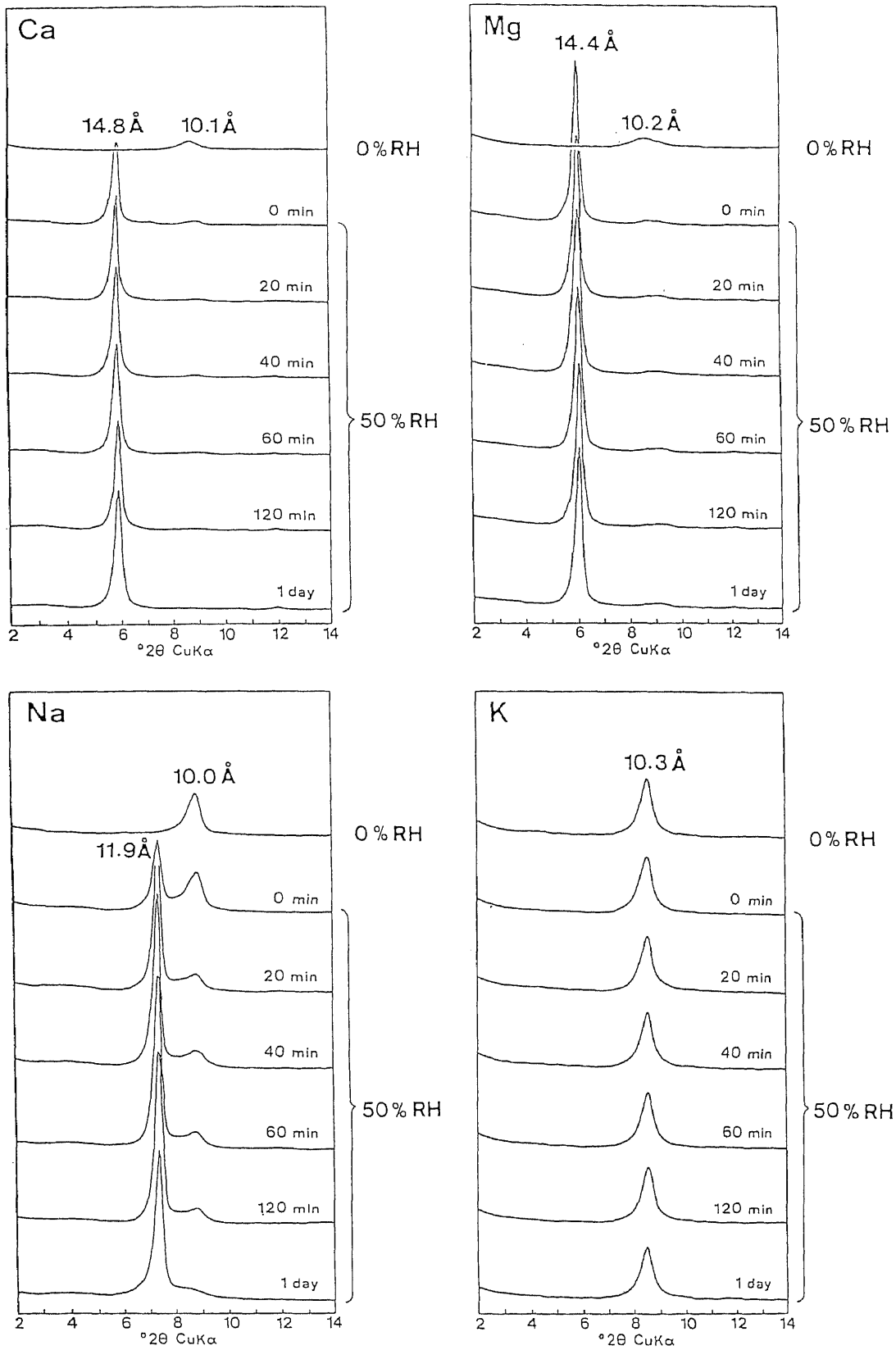

Figure 3.4. Changes in (001) reflections for homoionic vermiculite heated at 700°C during rehydration in air at 50% RH. Ca, Mg, Na, and K represent Ca-, Mg-, Na-, and K-saturated materials, respectively. 0% and 50% RH signify relative humidity of atmosphere.

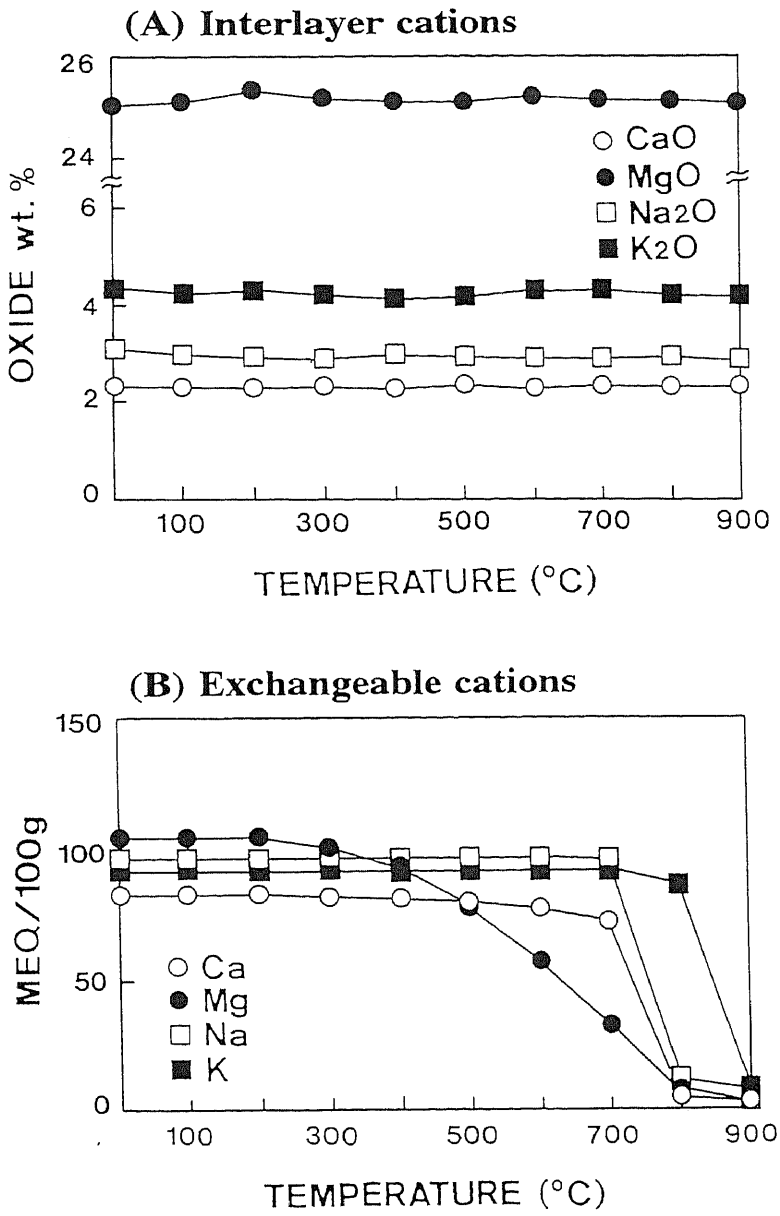

Figure 3.5. Variation of (A) oxide wt.% of CaO, MgO, Na_2O, and K_2O, and (B) exchangeable cations for homoionic saponite after heating at various temperatures.

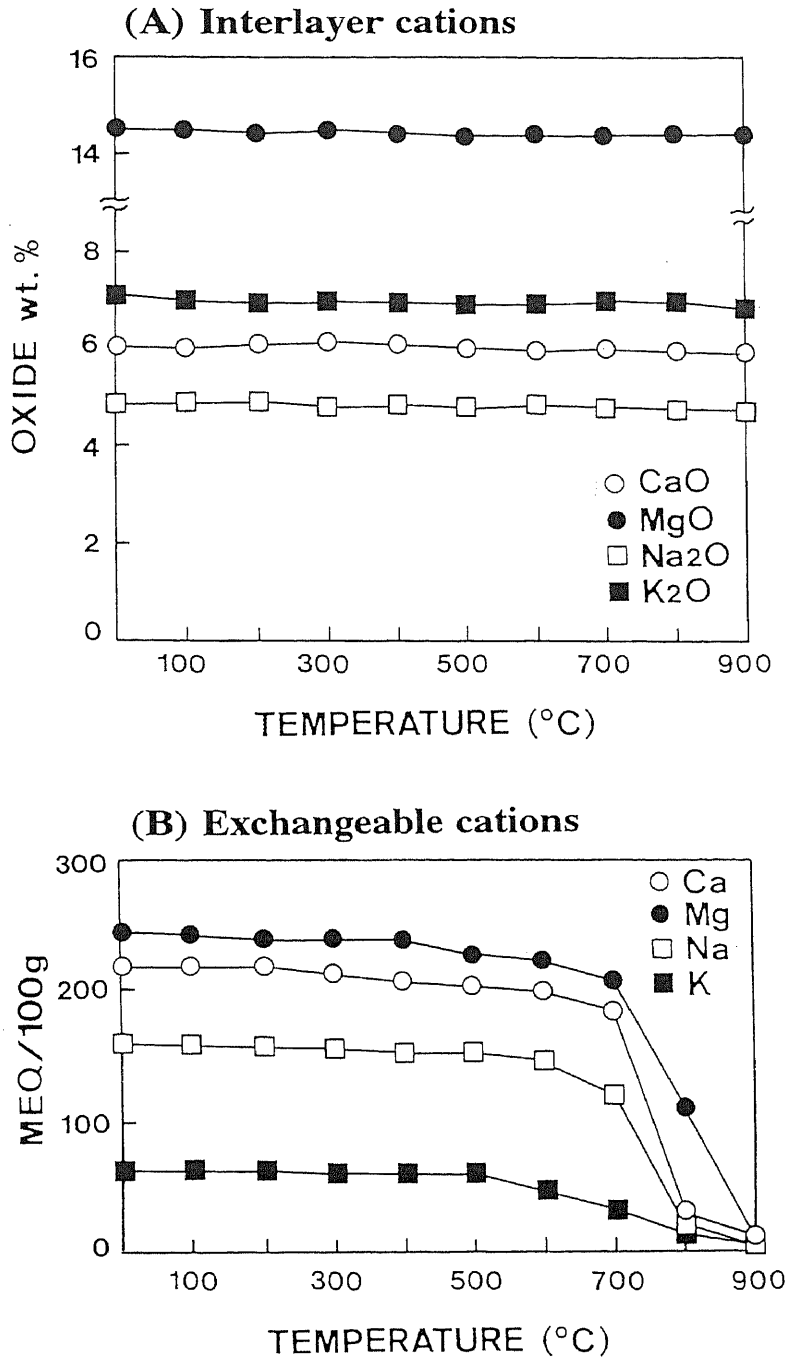

Figure 3.6. Variation of (A) oxide wt.% of CaO, MgO, Na_2O, and K_2O, and (B) exchangeable cations for homoionic vermiculite after heating at various temperatures.

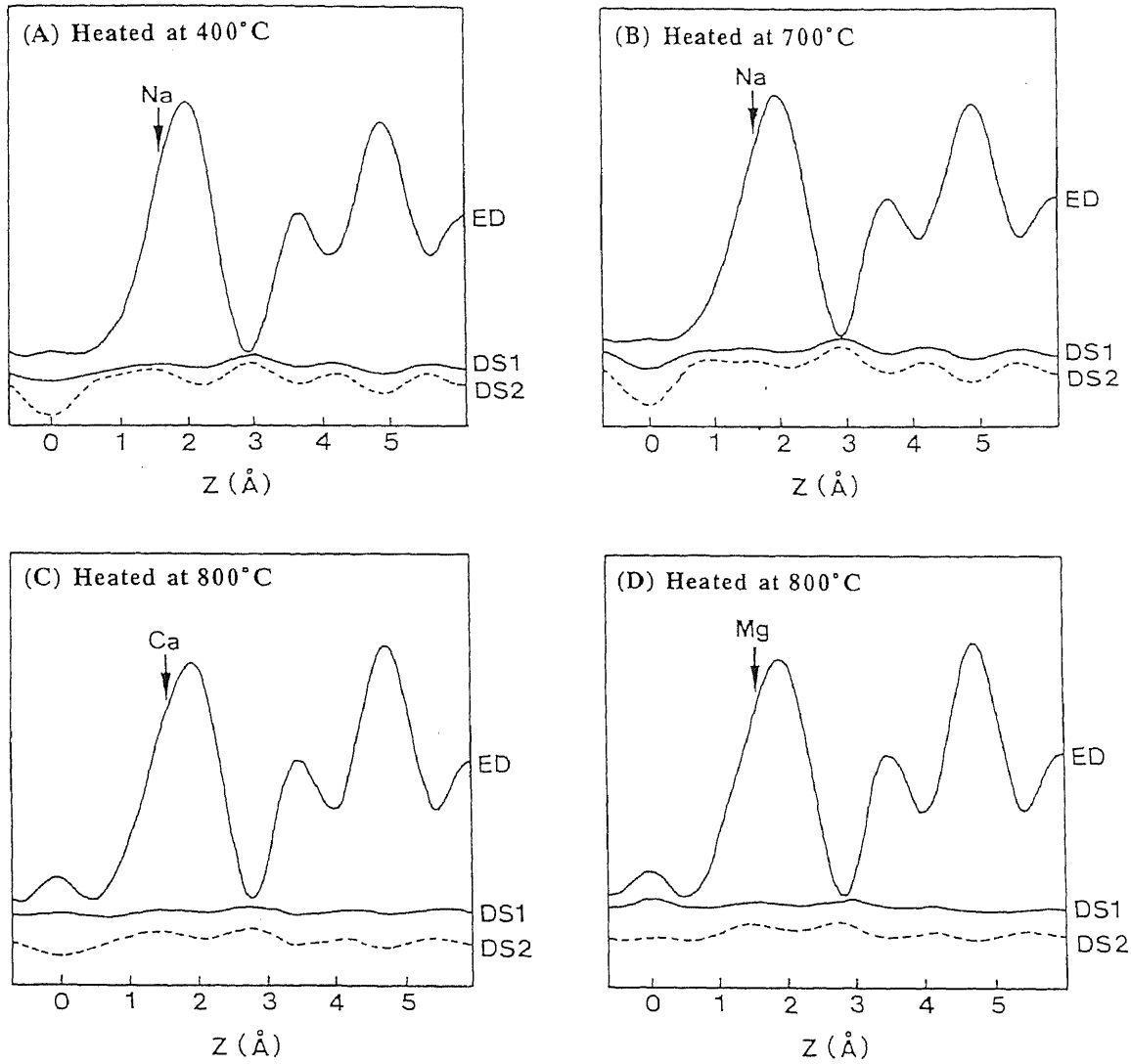

Figure 3.7. Electron density distribution and difference synthesis curves of Na-saturated saponite heated at (A) 400° and (B) 700°C, and (C) Ca- and (D) Mg-saturated saponites heated at 800°C. ED = electron density distribution; DS1 = difference synthesis calculated by using z-parameters obtained by the least squares refinement; DS2 = difference synthesis calculated by assuming that interlayer cations are located at the center of interlayer space.

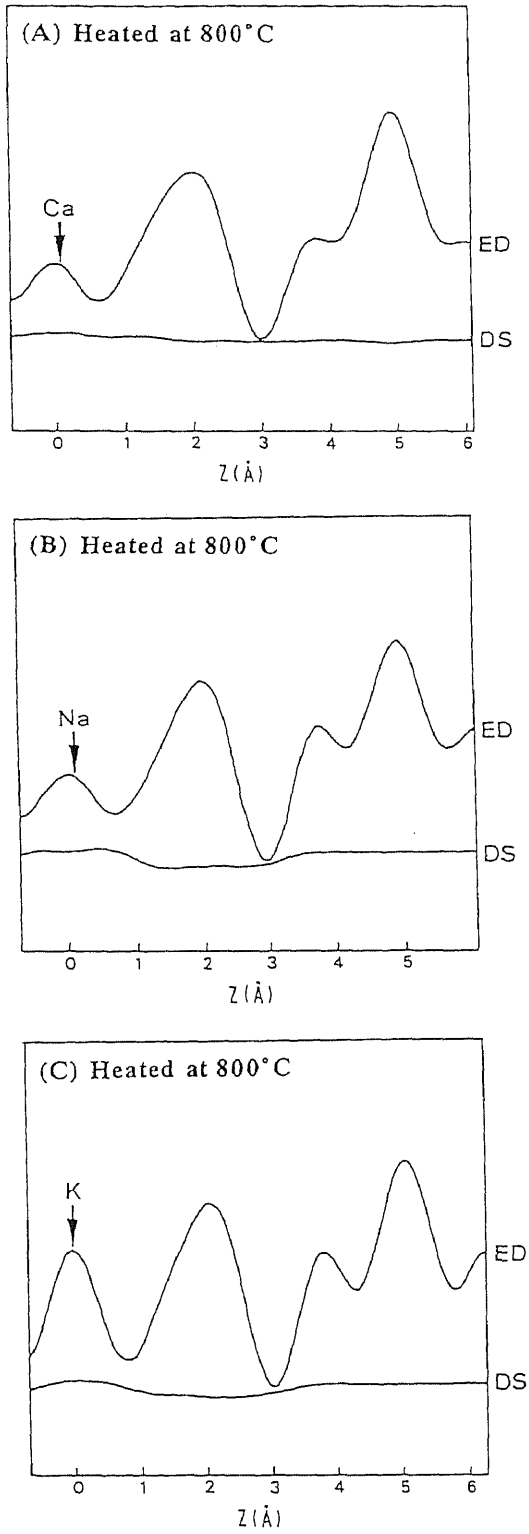

Figure 3.8. Electron density distribution and difference synthesis curves of (A) Ca-, (B) Na-, and (C) K-saturated vermiculites heated at 800°C. ED = electron density distribution; DS = difference synthesis calculated by using z-parameters obtained by the least squares refinement.

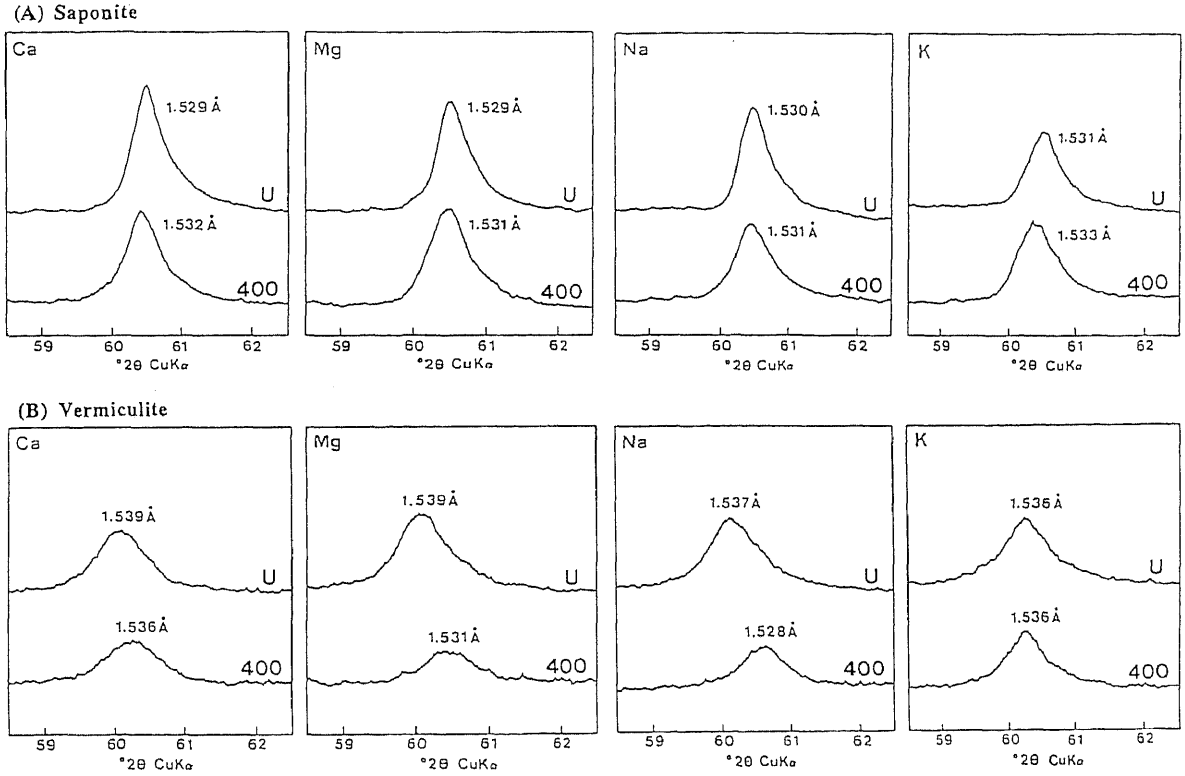

Figure 3.9. X-ray powder diffraction patterns of homoionic (A) saponite and (B) vermiculite in the region of the (060) reflection (U) before and (400) after heating at 400°C. Ca, Mg, Na, and K represent Ca-, Mg-, Na-, and K-saturated materials, respectively.

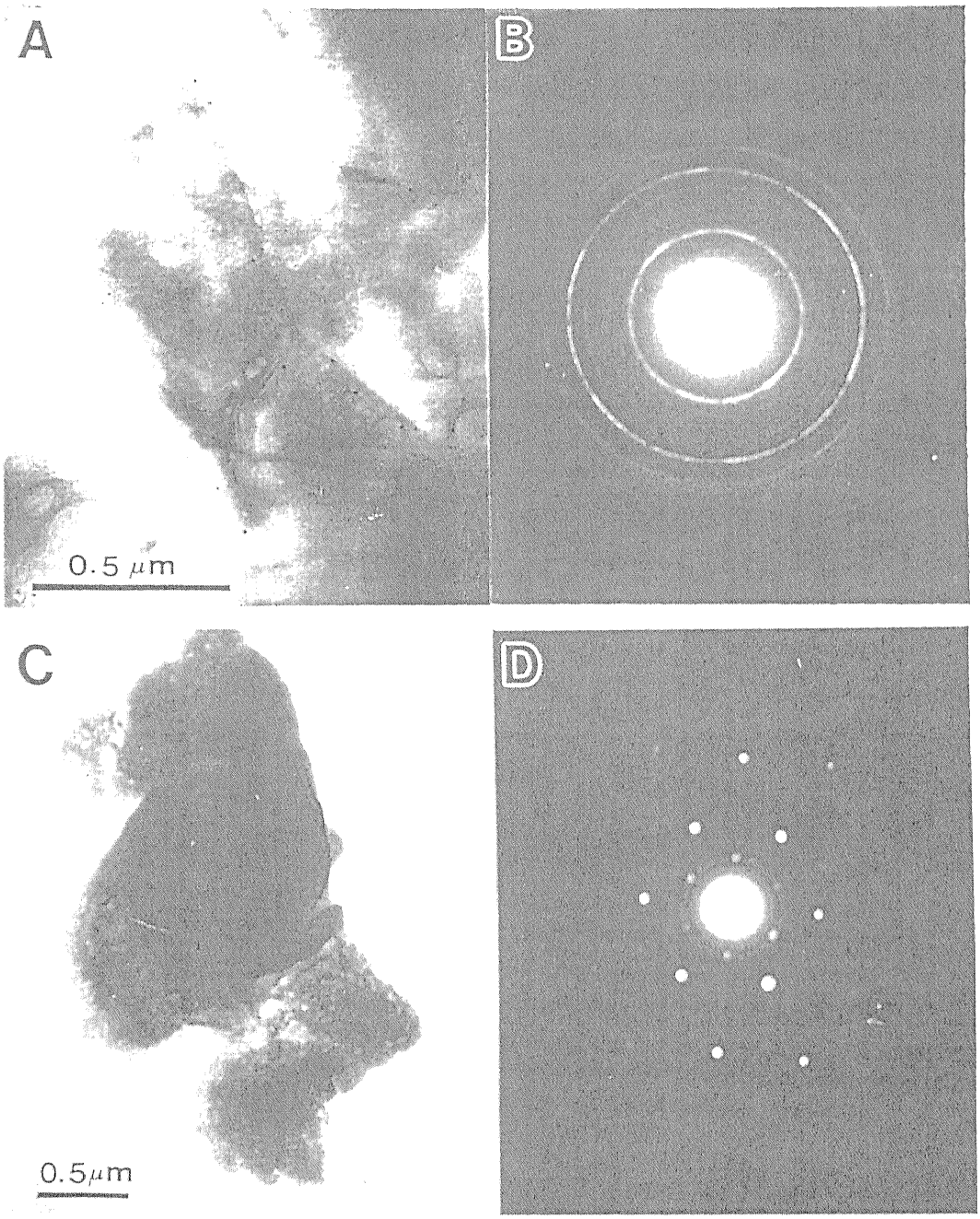

Figure 3.10. Transmission electron micrographs and electron diffraction patterns of Mg-saturated (A, B) saponite and (C, D) vermiculite.

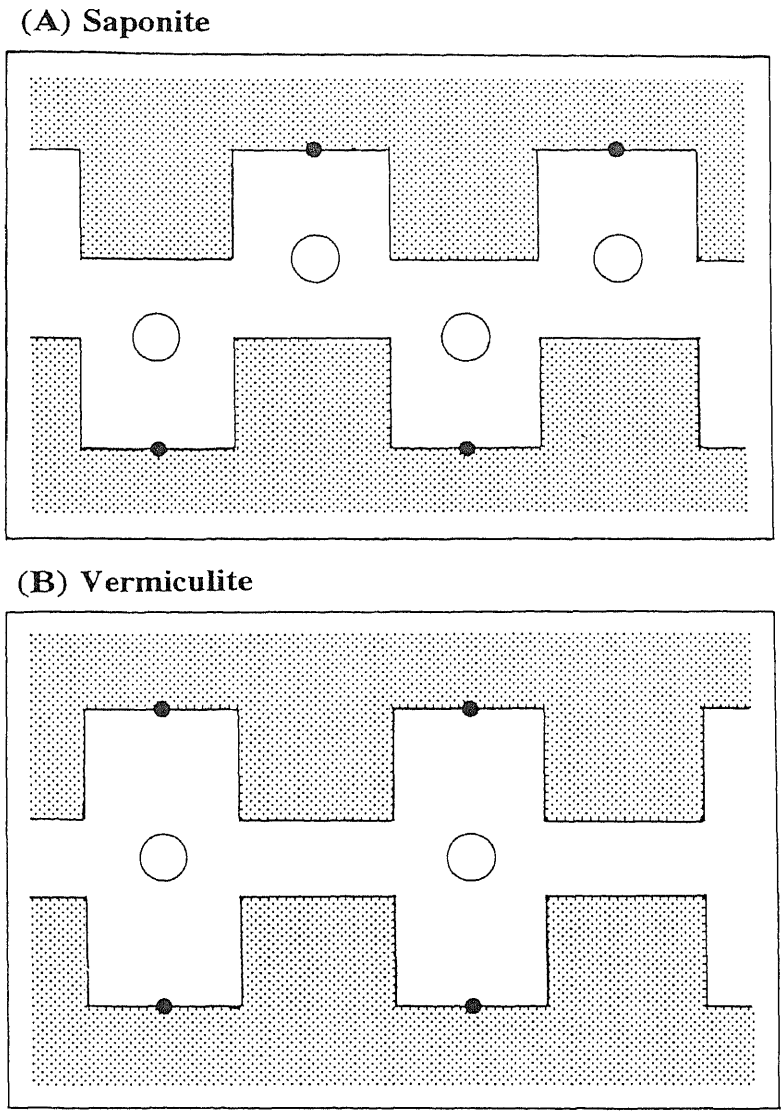

Figure 3.11. Schematic diagram showing the nature of stacking of adjacent silicate layers of dehydrated (A) saponite and (B) vermiculite, and positions of (O) interlayer cations. Shadow parts represent silicate layers.

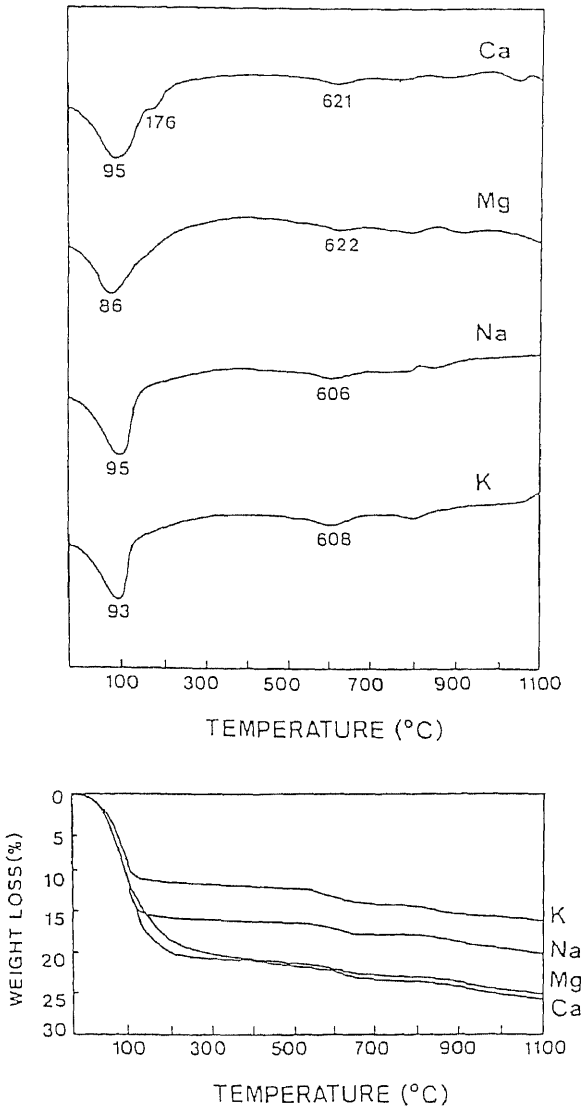

Figure 4.1. Differential thermal and thermogravimetric analysis curves of homoionic hectorite. Ca, Mg, Na, and K represent Ca-, Mg-, Na-, and K-saturated materials, respectively.

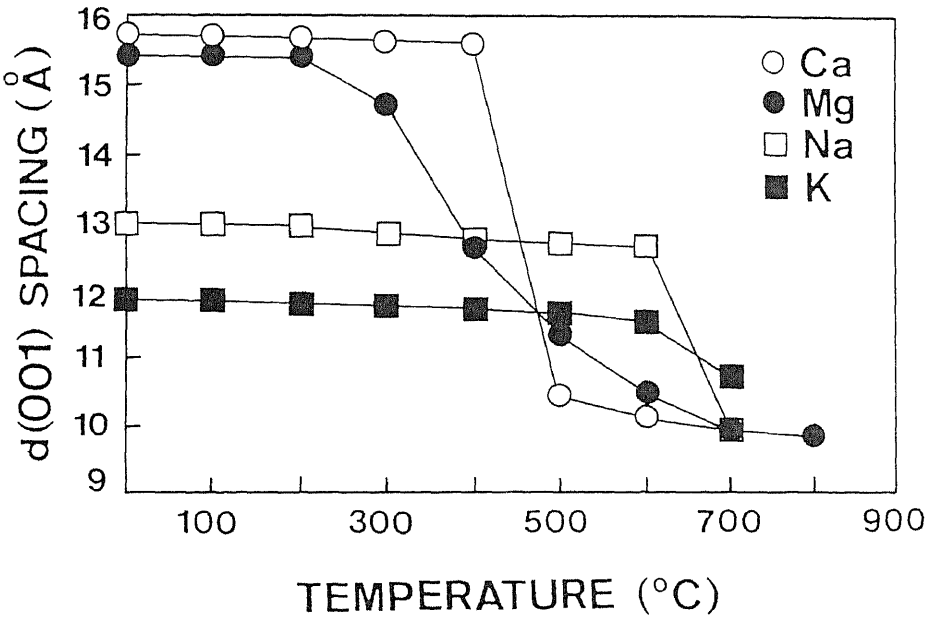

Figure 4.2. Variation of d(001) values for rehydrated homoionic hectorite after heating at various temperatures.

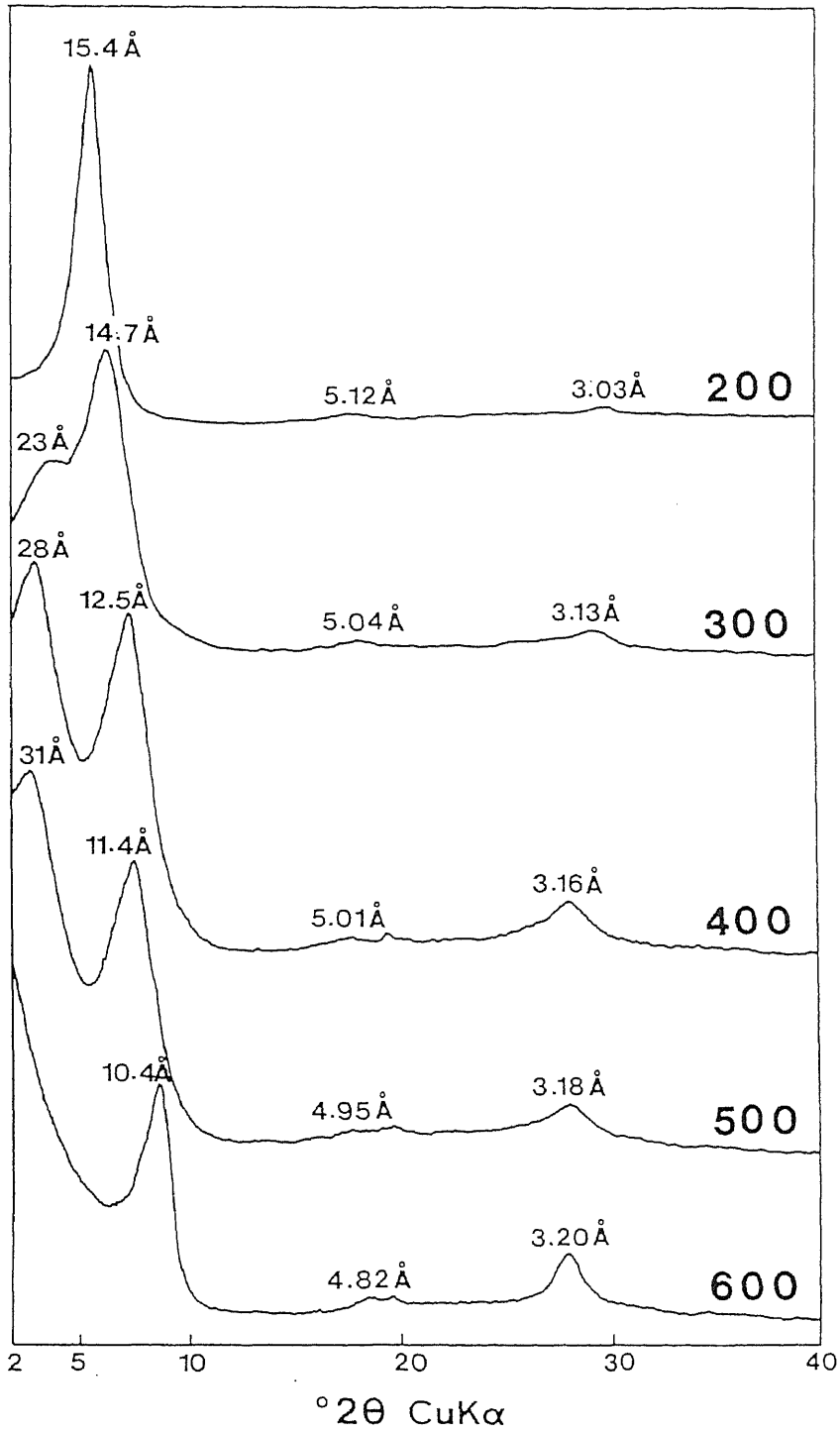

Figure 4.3. X-ray powder diffraction patterns of rehydrated Mg-saturated hectorite after heating at 200° to 600°C. The labels 200 to 600 signify heating temperatures.

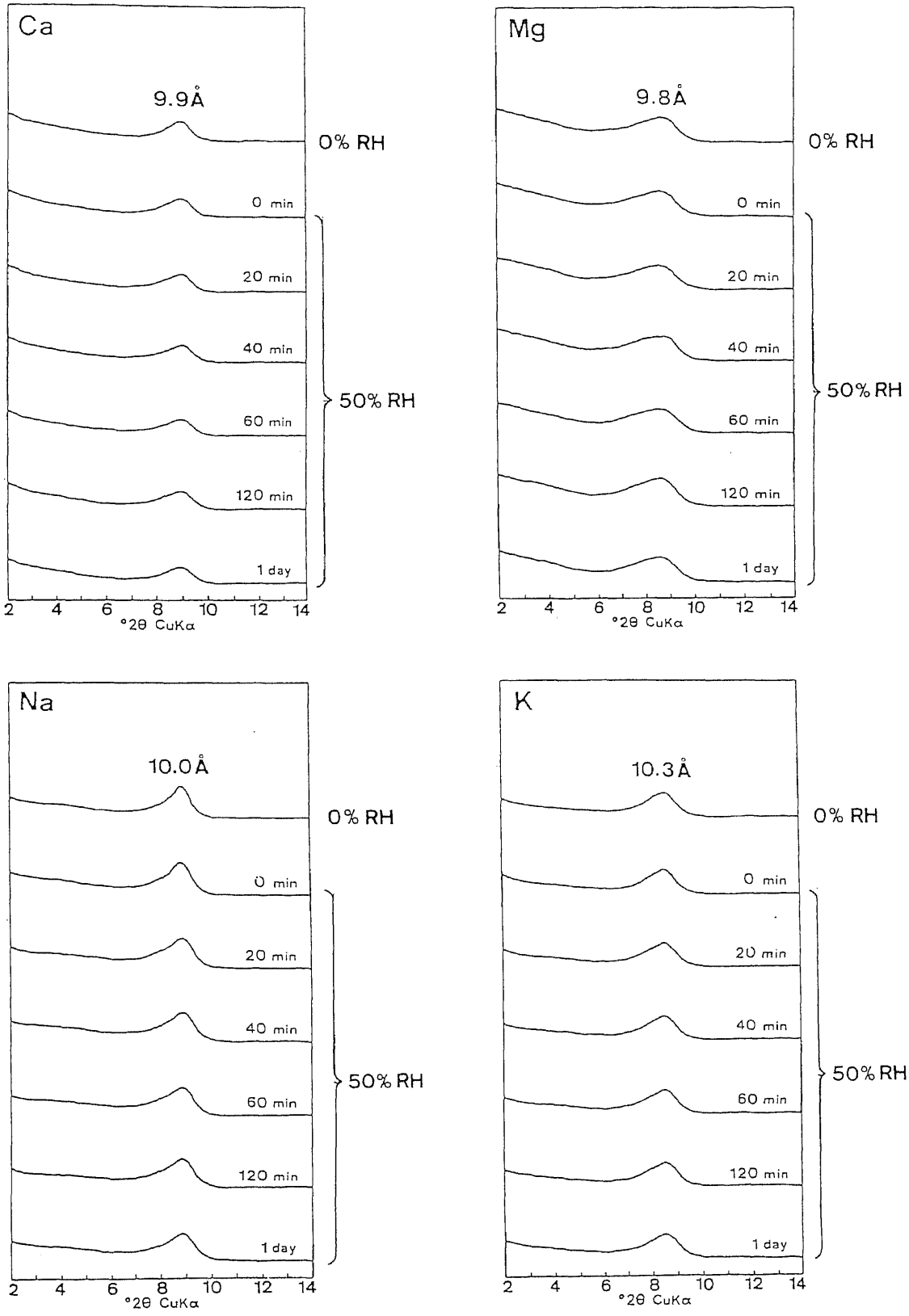

Figure 4.4. Changes in (001) reflections for homoionic hectorite heated at 400°C during rehydration in air at 50% RH. Ca, Mg, Na, and K represent Ca-, Mg-, Na-, and K-saturated materials, respectively. 0% and 50% RH signify relative humidity of atmosphere.

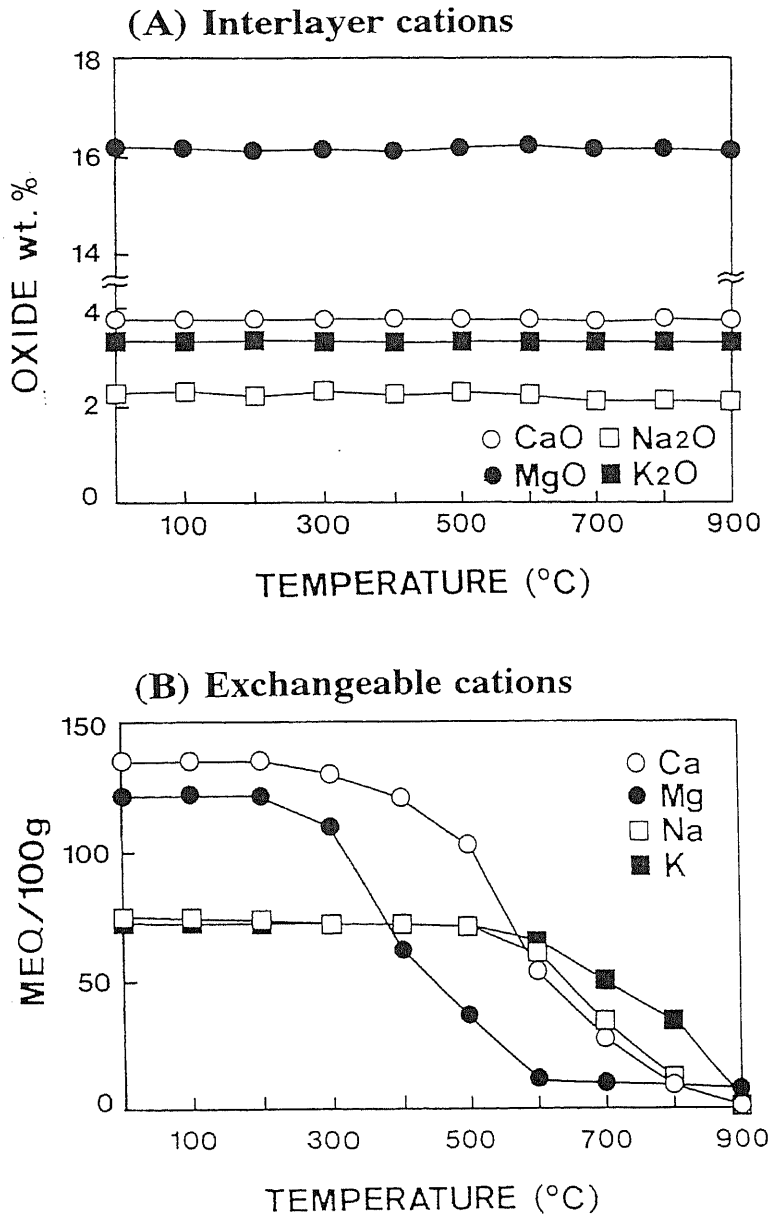

Figure 4.5. Variation of (A) oxide wt.% of CaO, MgO, Na_2O, and K_2O, and (B) exchangeable cations for homoionic hectorite after heating at various temperatures.

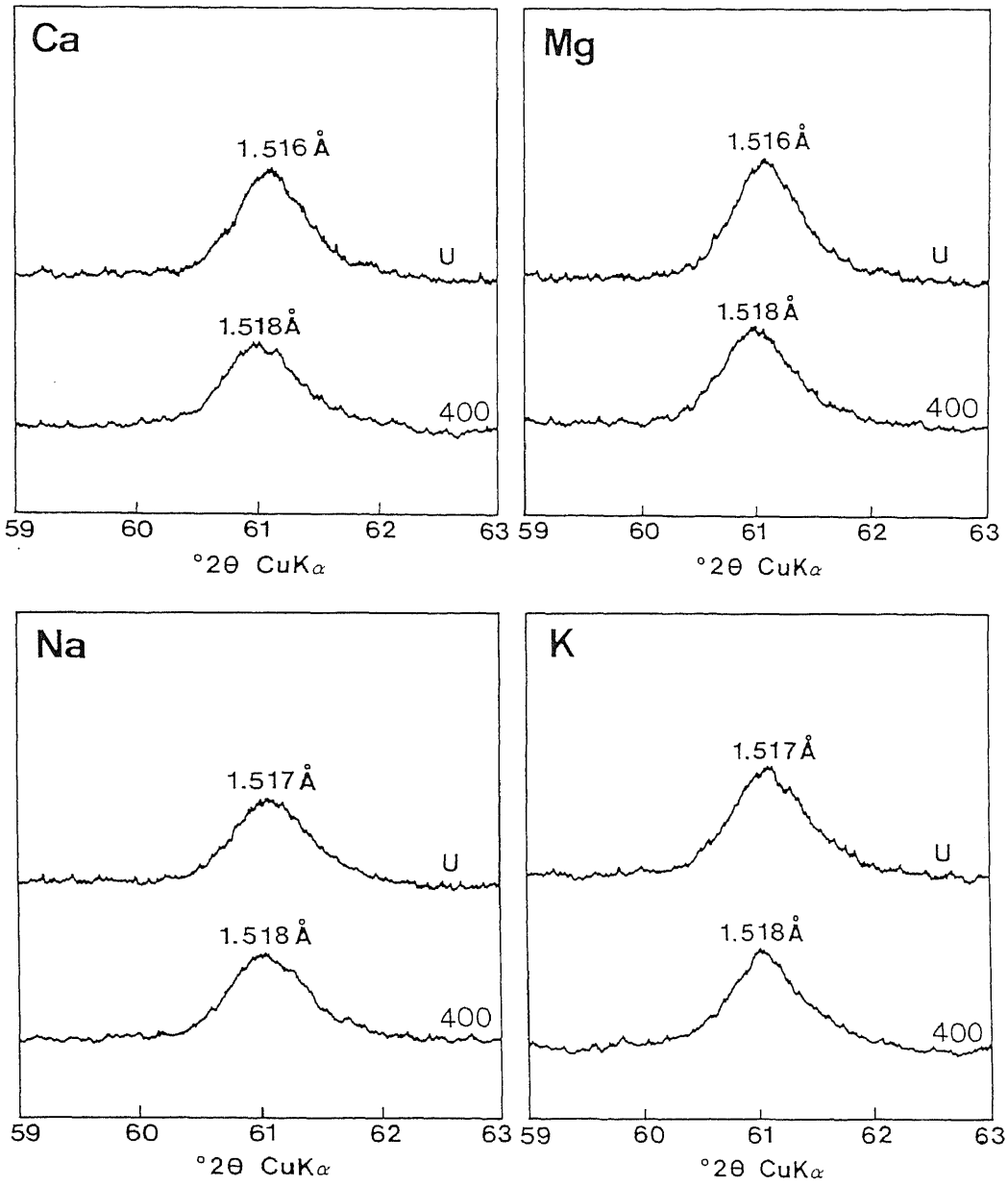

Figure 4.6. X-ray powder diffraction patterns of homoionic hectorite in the region of the (060) reflection (U) before and (400) after heating at 400°C. Ca, Mg, Na, and K represent Ca-, Mg-, Na-, and K-saturated materials, respectively.

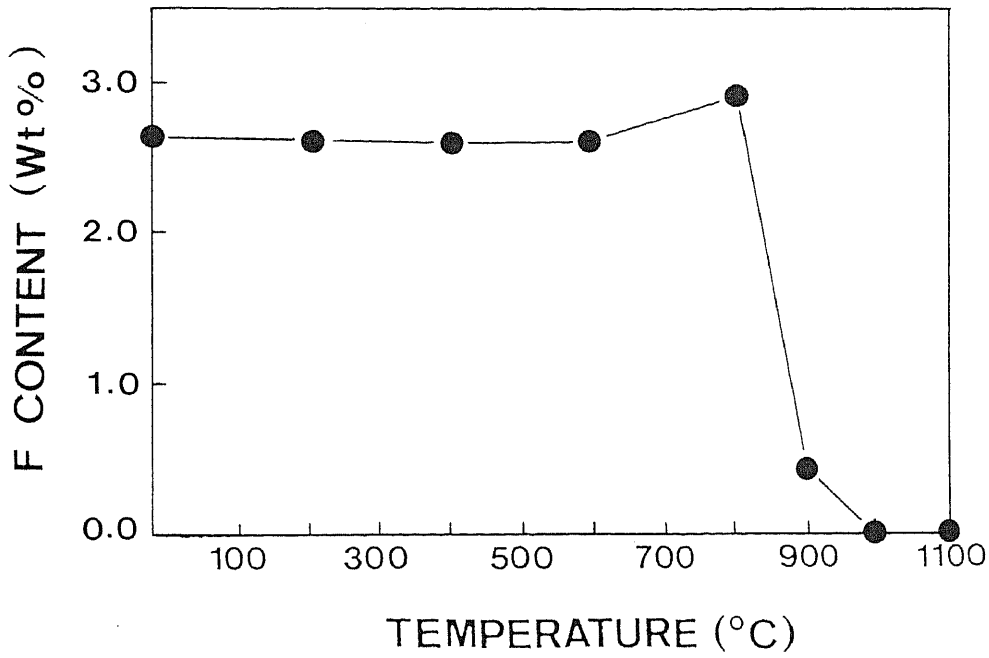

Figure 4.7. Variation of fluorine contents for Na-saturated hectorite after heating at various temperatures.

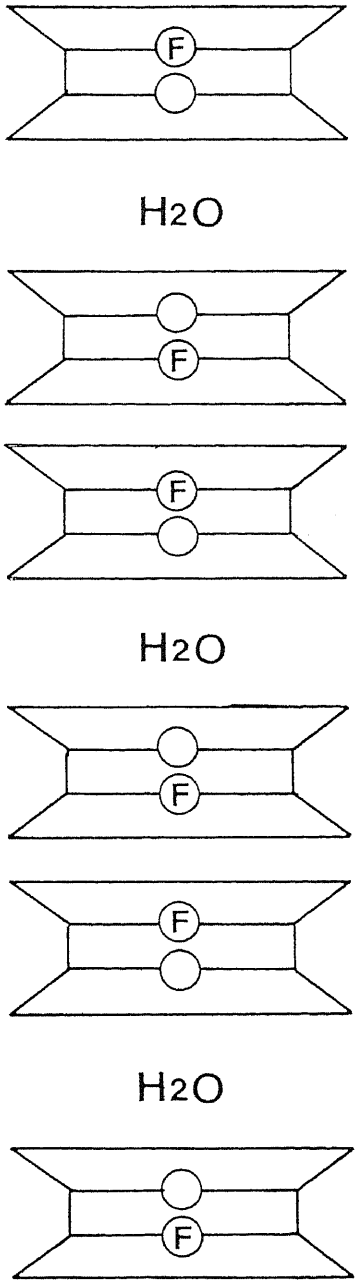

Figure 4.8. Schematic diagram showing the interstratified structure of rehydrated Mg-saturated hectorite. ◯ and Ⓕ indicate hydroxyl and fluorine ions, respectively.

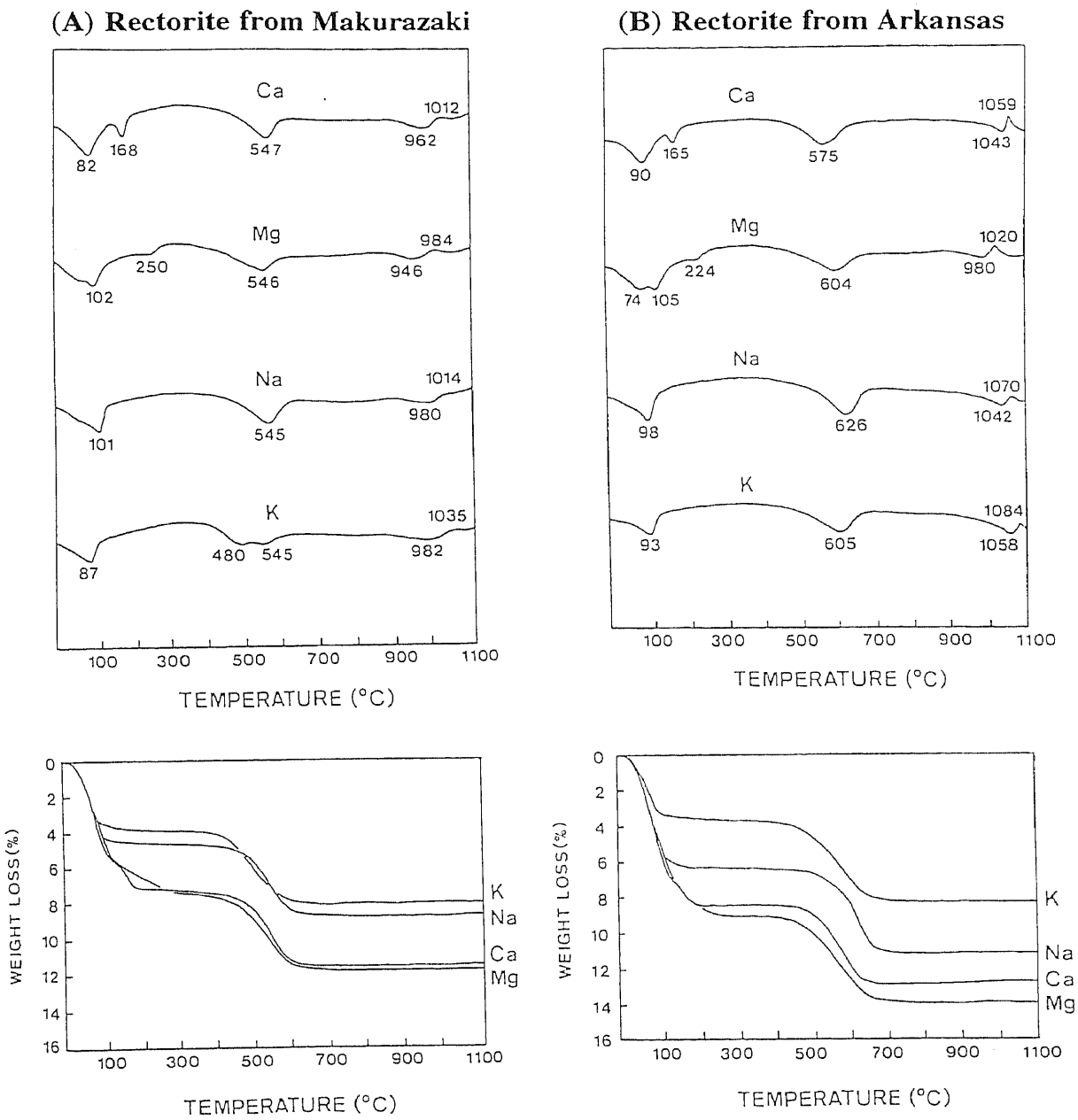

Figure 5.1. Differential thermal and thermogravimetric analysis curves of homoionic rectorites from (A) Makurazaki and (B) Arkansas. Ca, Mg, Na, and K represent Ca-, Mg-, Na-, and K-saturated materials, respectively.

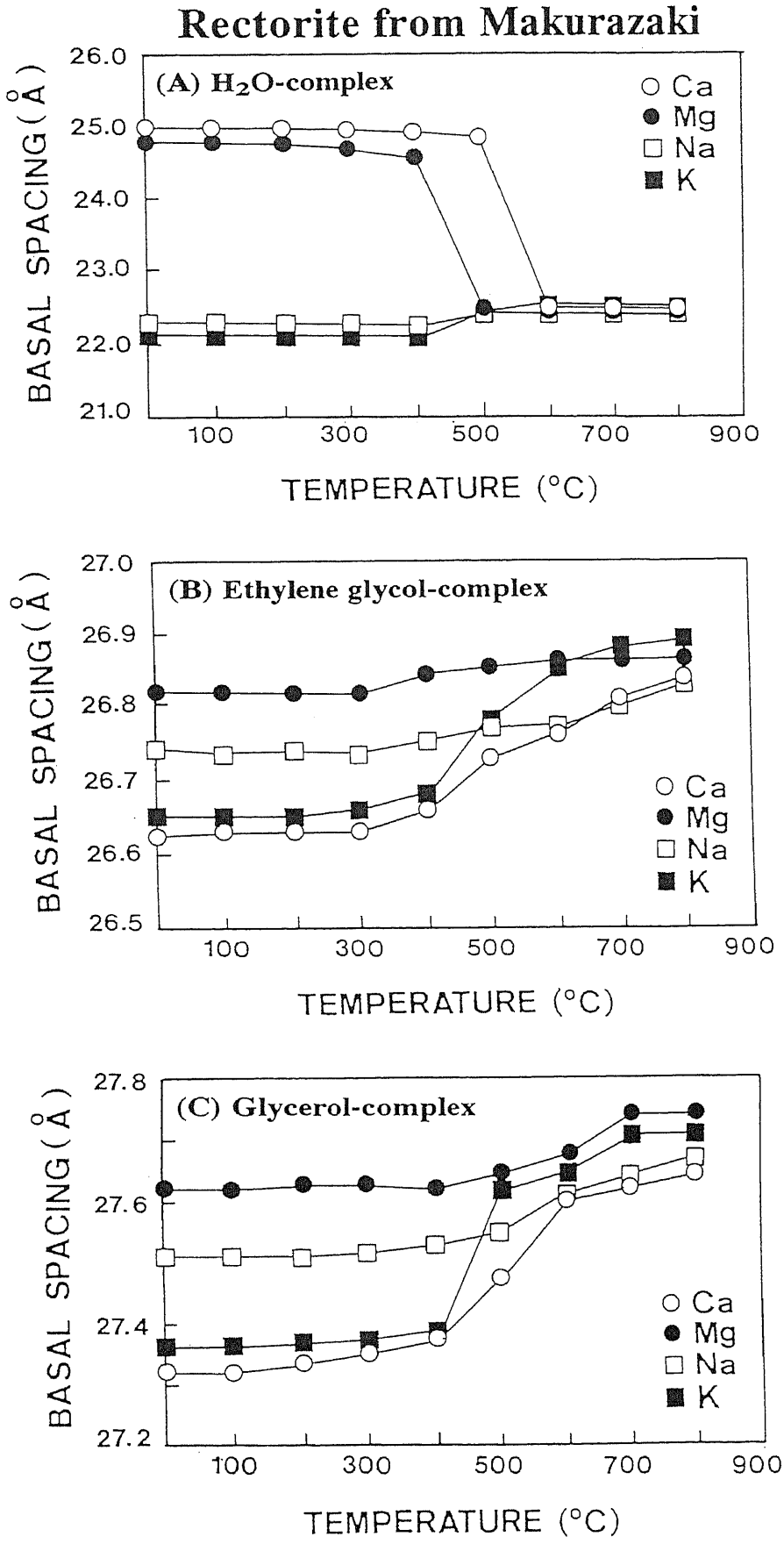

Figure 5.2. Variation of basal spacings of (A) homoionic rehydrated rectorite, and (B) ethylene glycol- and (C) glycerol-complexes of the rehydrated materials after heating at various temperatures.

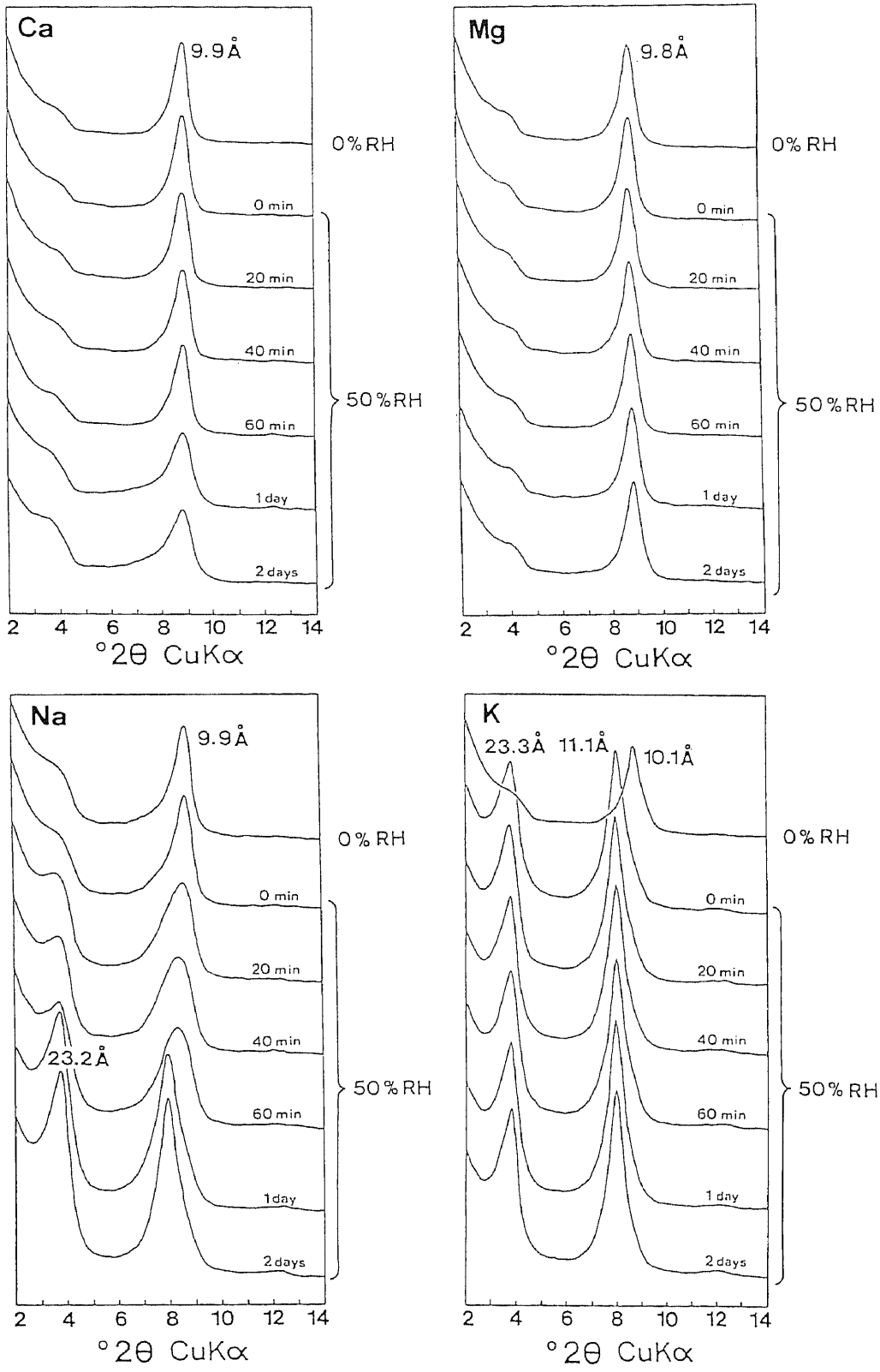

Figure 5.3. Changes in (001) reflections for homoionic rectorite heated at 800°C during rehydration in air at 50% RH. Ca, Mg, Na, and K represent Ca-, Mg-, Na-, and K-saturated materials, respectively. 0% and 50% RH signify relative humidity of atmosphere.

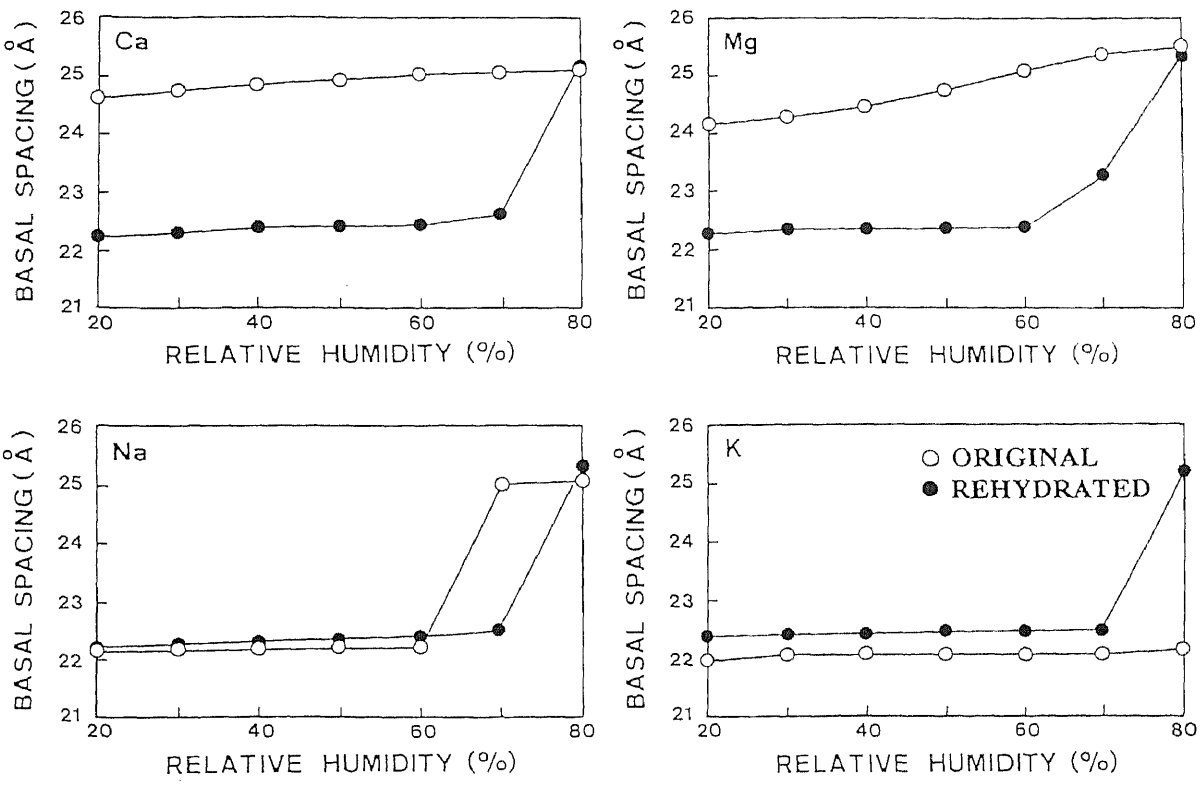

Figure 5.4. Variations of basal spacings of homoionic original rectorite and rehydrated materials after heating at 800°C with various relative humidity conditions. Ca, Mg, Na, and K represent Ca-, Mg-, Na-, and K-saturated materials, respectively.

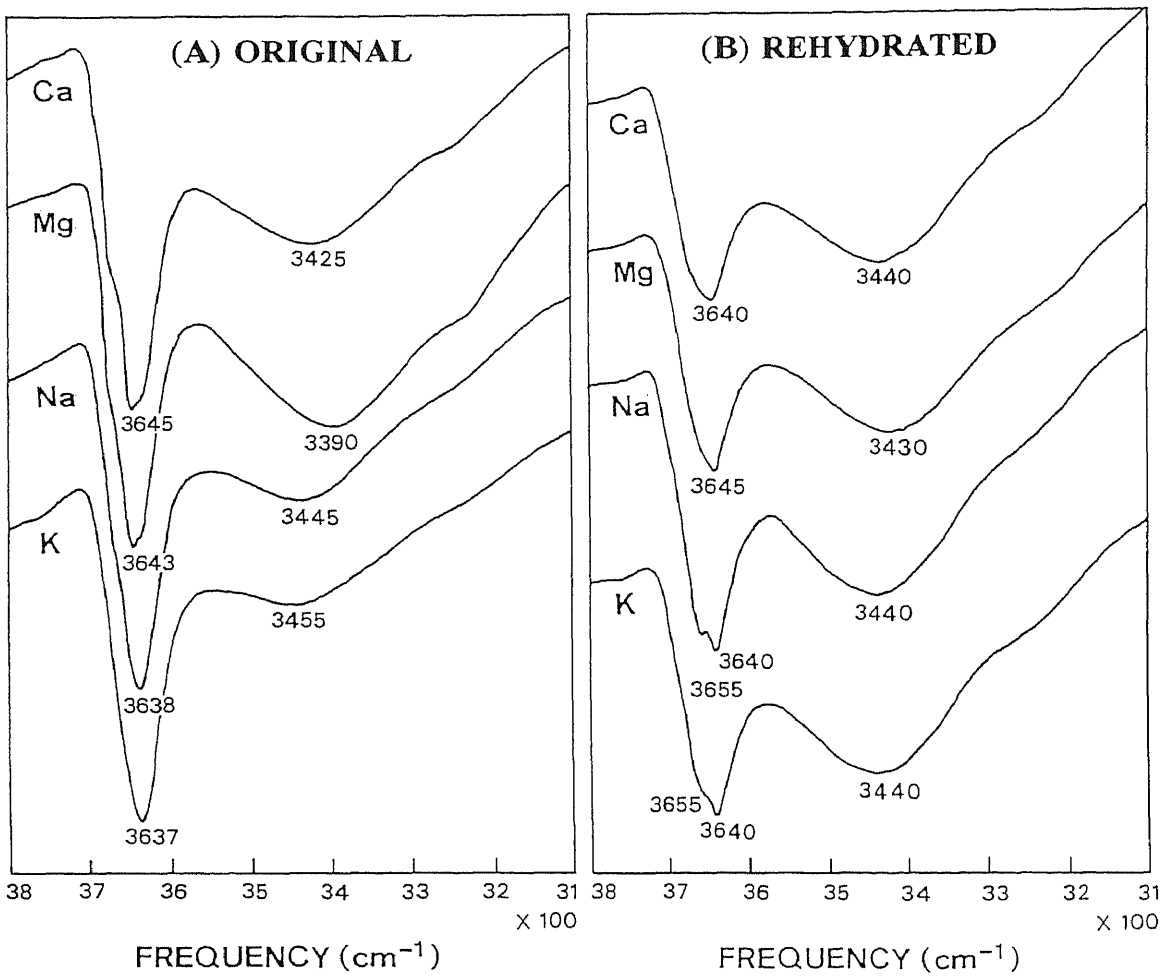

Figure 5.5. Infrared absorption spectra of (A) homoionic original rectorite and (B) rehydrated materials after heating at 800°C. Ca, Mg, Na, and K represent Ca-, Mg-, Na-, and K-saturated materials, respectively.

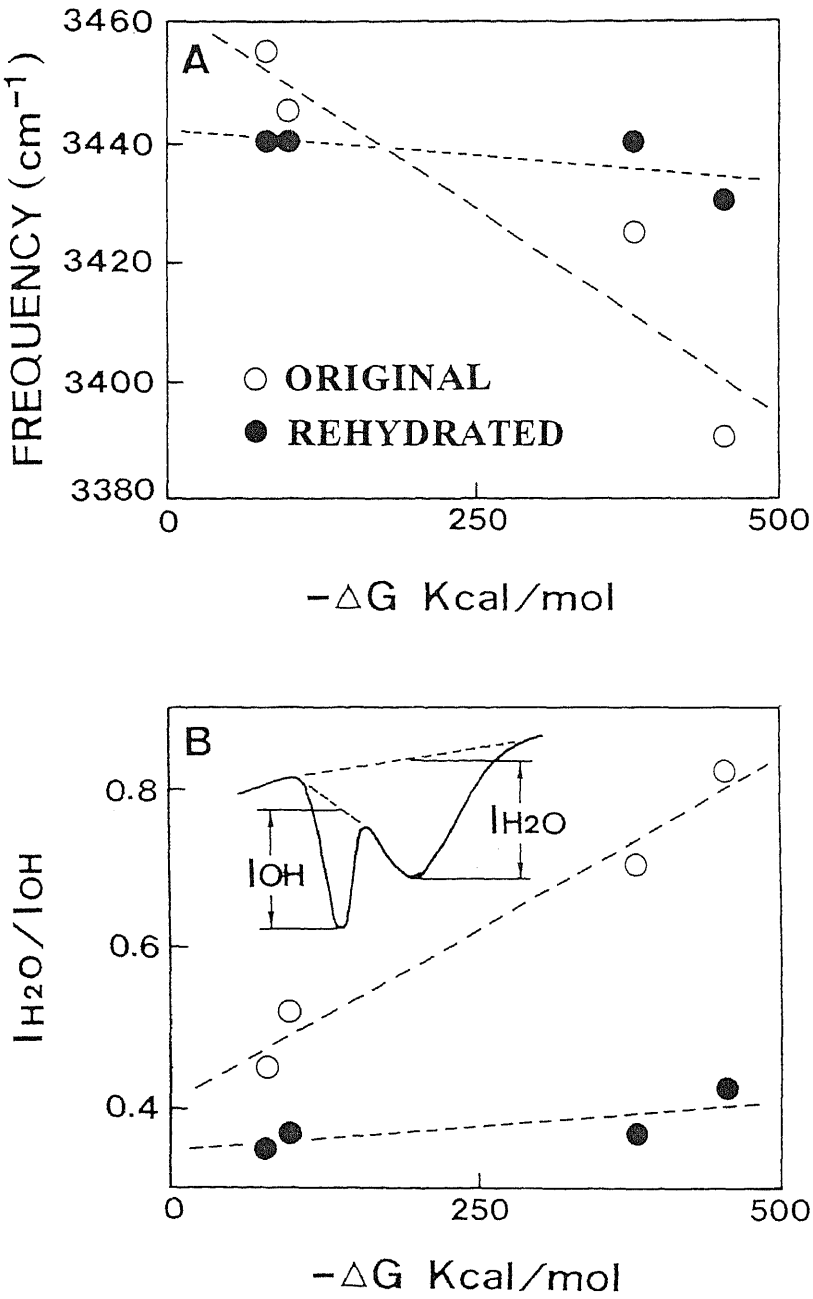

Figure 5.6. Relationship (A) between H_2O absorption frequencies and hydration energies of interlayer cations, and (B) between absorption intensity ratios of I_{H_2O}/I_{OH} and hydration energy.

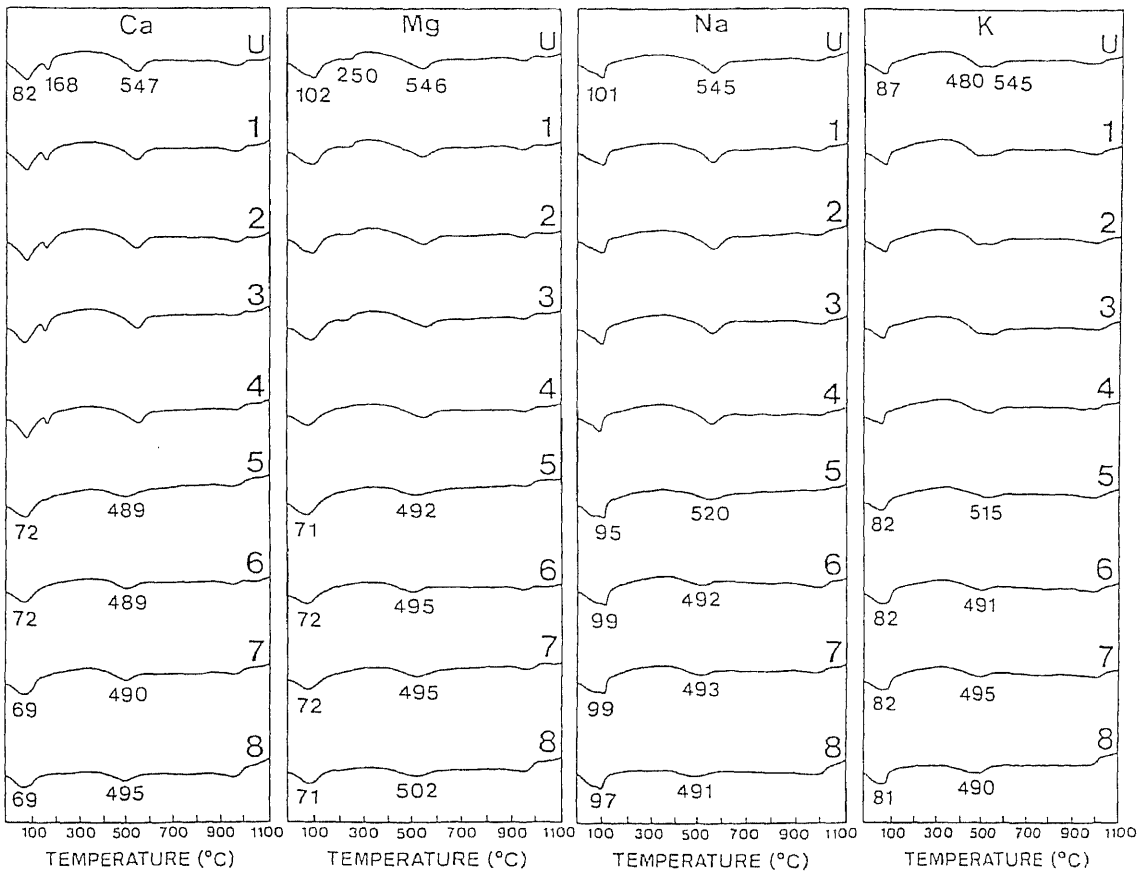

Figure 5.7. Differential thermal analysis curves of homoionic rehydrated rectorite after heating at various temperatures. Ca, Mg, Na, and K represent Ca-, Mg-, Na-, and K-saturated materials, respectively. U = unheated original samples. Numbers 1 to 8 imply heating temperatures at 100° to 800°C.

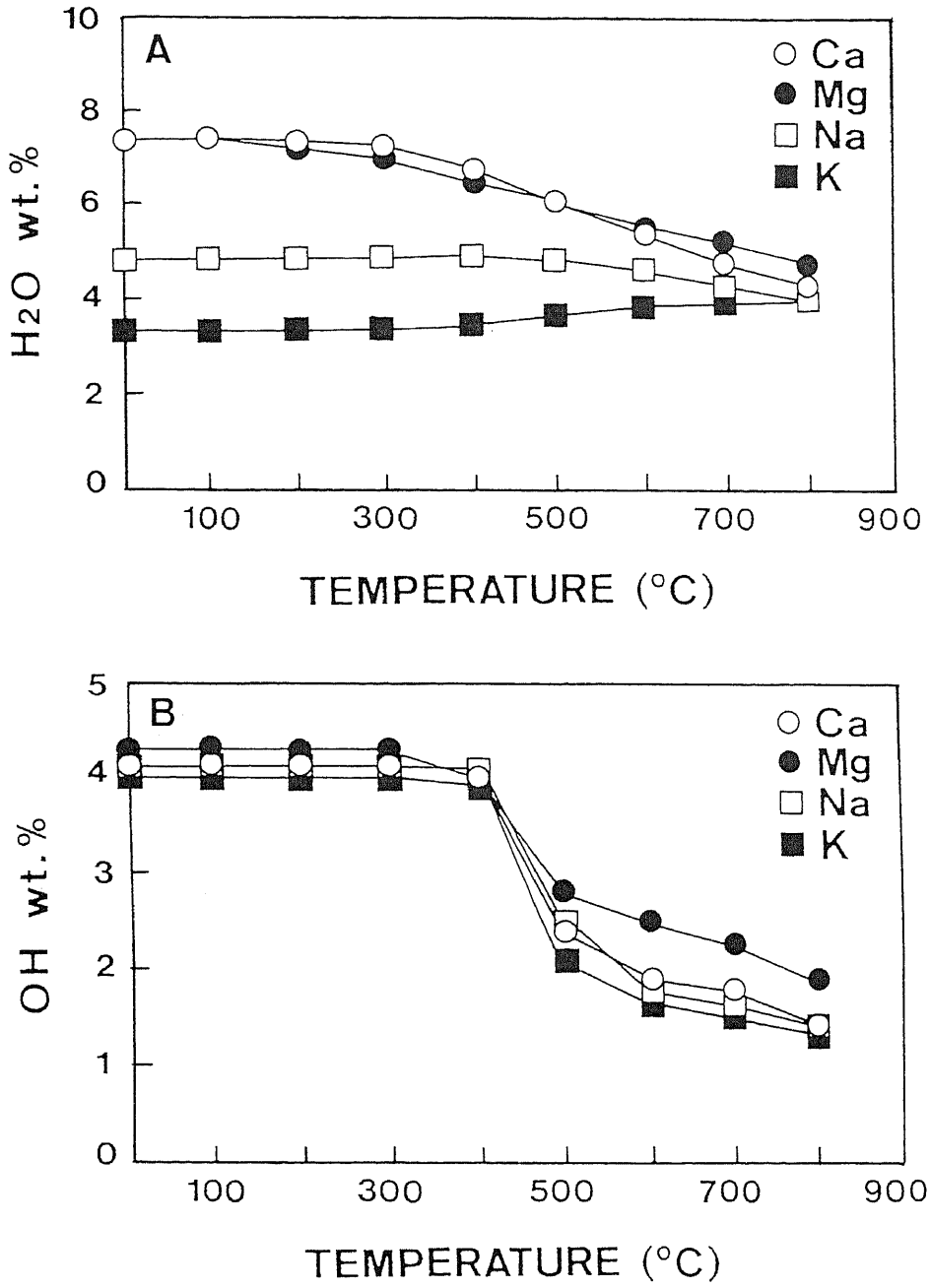

Figure 5.8. Variations of (A) H_2O wt.% and (B) OH wt.% of homoionic rehydrated rectorite after heating at various temperatures. The values of wt.% were obtained from TGA curves, in which weight losses below and above 400°C were assigned to H_2O wt.% and OH wt.%, respectively.

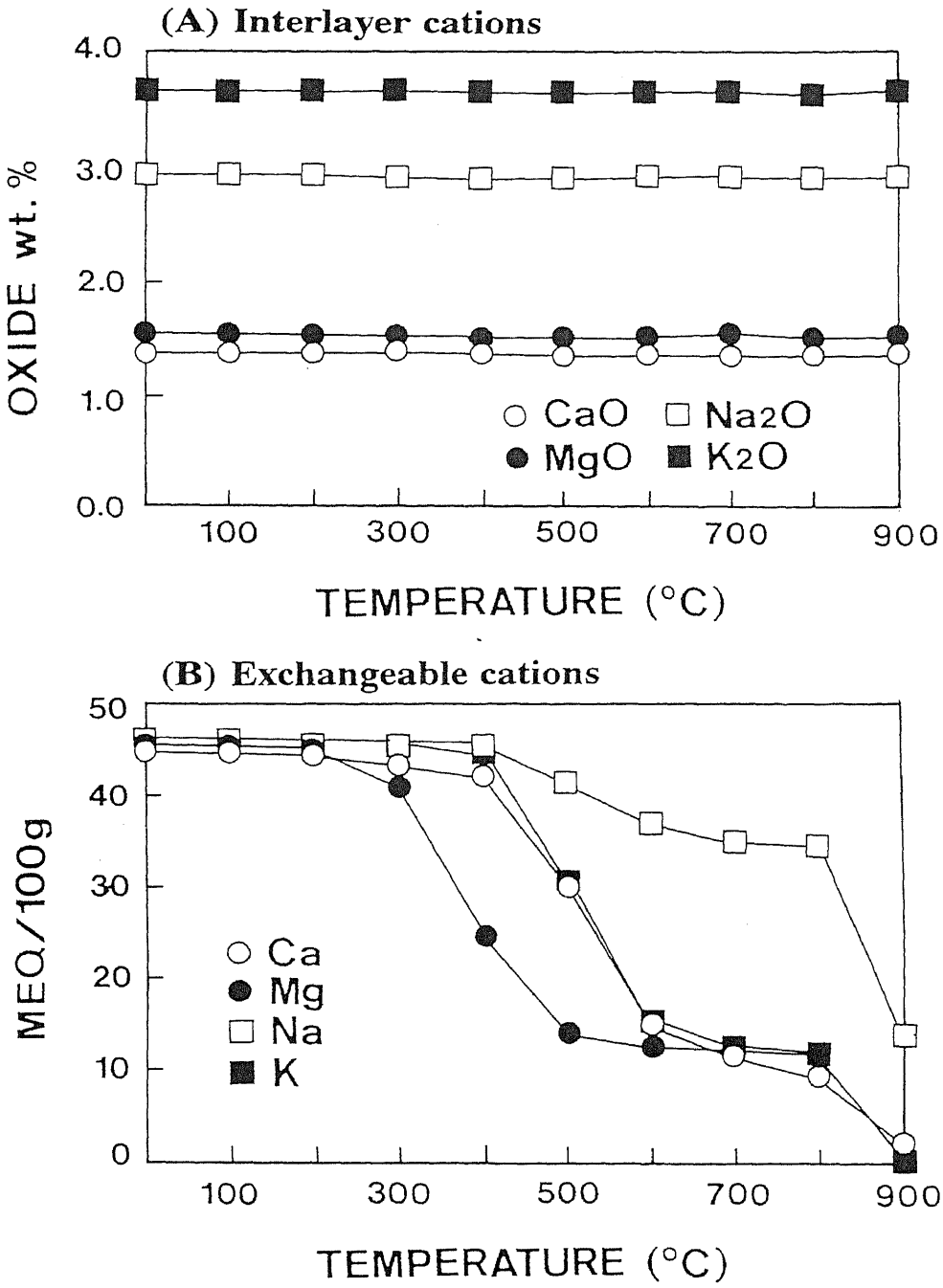

Figure 5.9. Variation of (A) oxide wt.% of CaO, MgO, Na_2O, and K_2O, and (B) exchangeable cations for homoionic rectorite after heating at various temperatures.

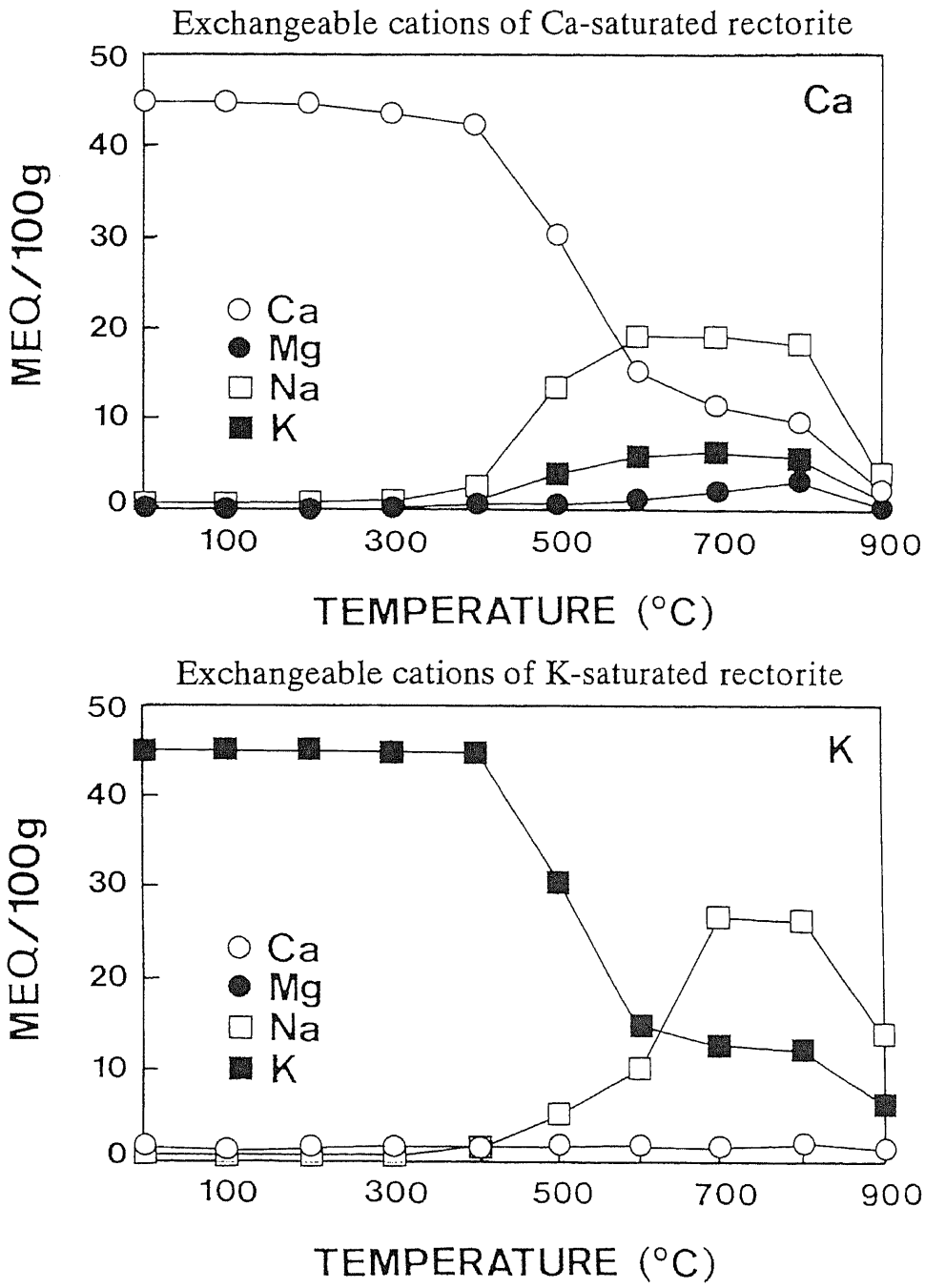

Figure 5.10. Variation of exchangeable cations of Ca- and K-saturated rectorite after heating at various temperatures.

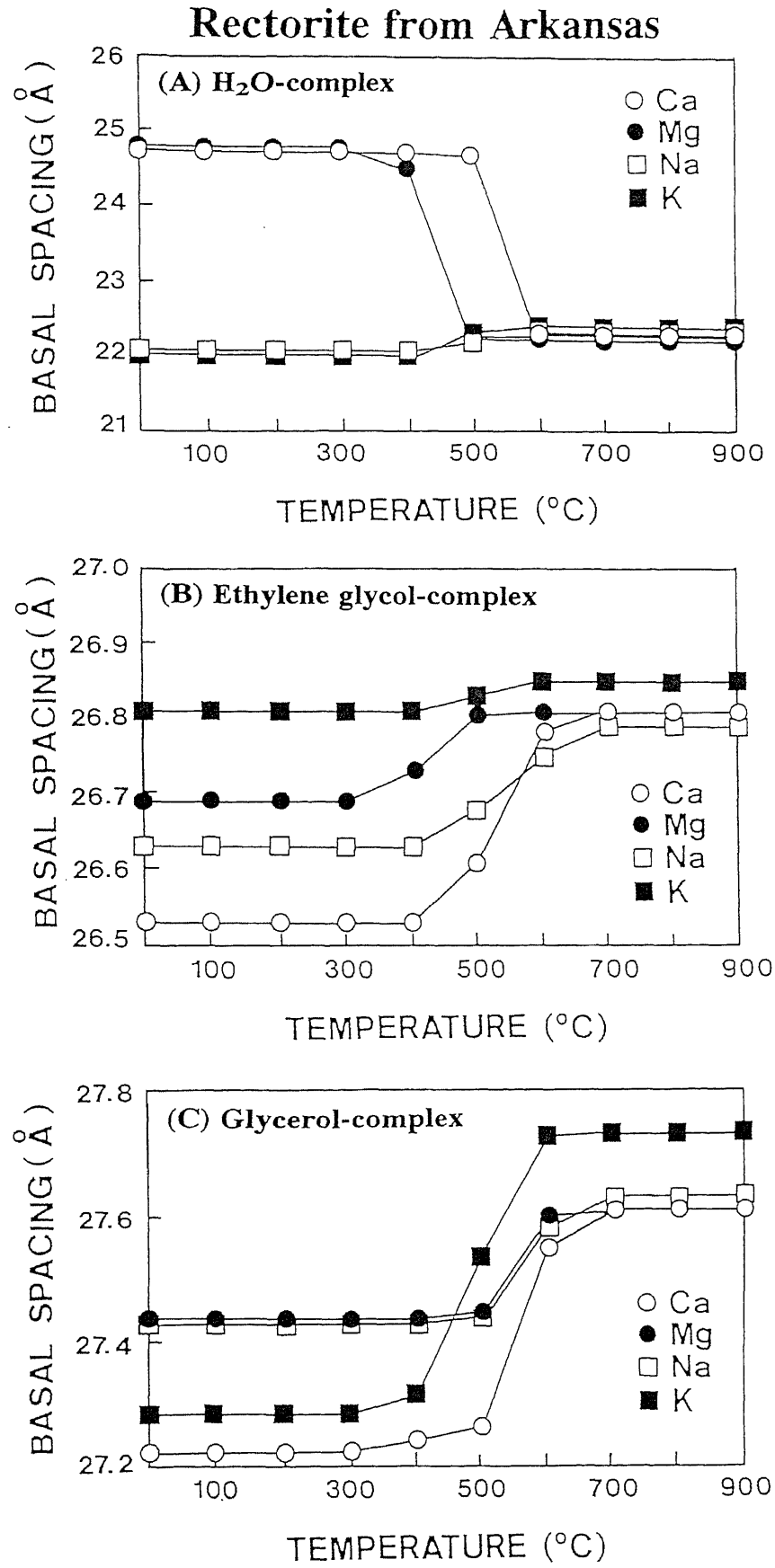

Figure 5.11. Variation of basal spacings of (A) homoionic rehydrated Arkansas rectorite, and (B) ethylene glycol- and (C) glycerol-complexes of the rehydrated materials after heating at various temperatures.

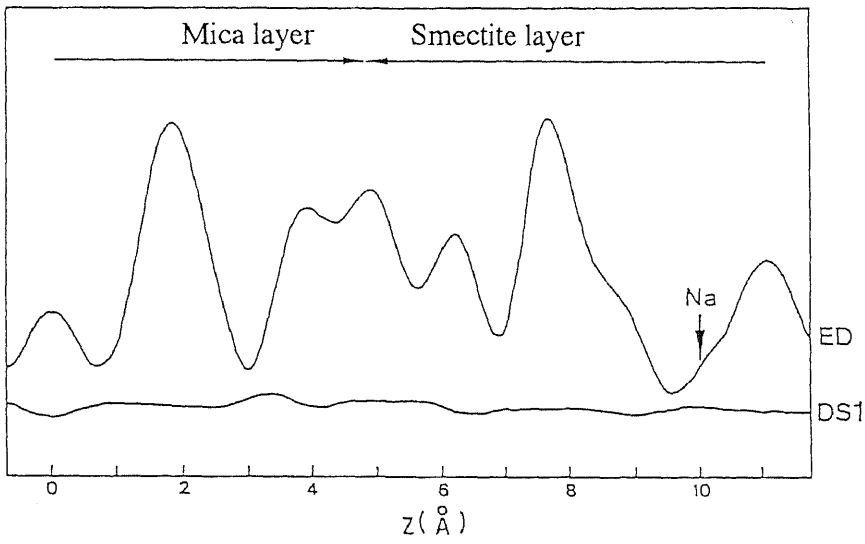

Figure 5.12. Electron density distribution and difference synthesis curves of Na-saturated rectorite. ED = electron density distribution; DS1 = difference synthesis calculated by using z-parameters obtained by the least squares refinement.

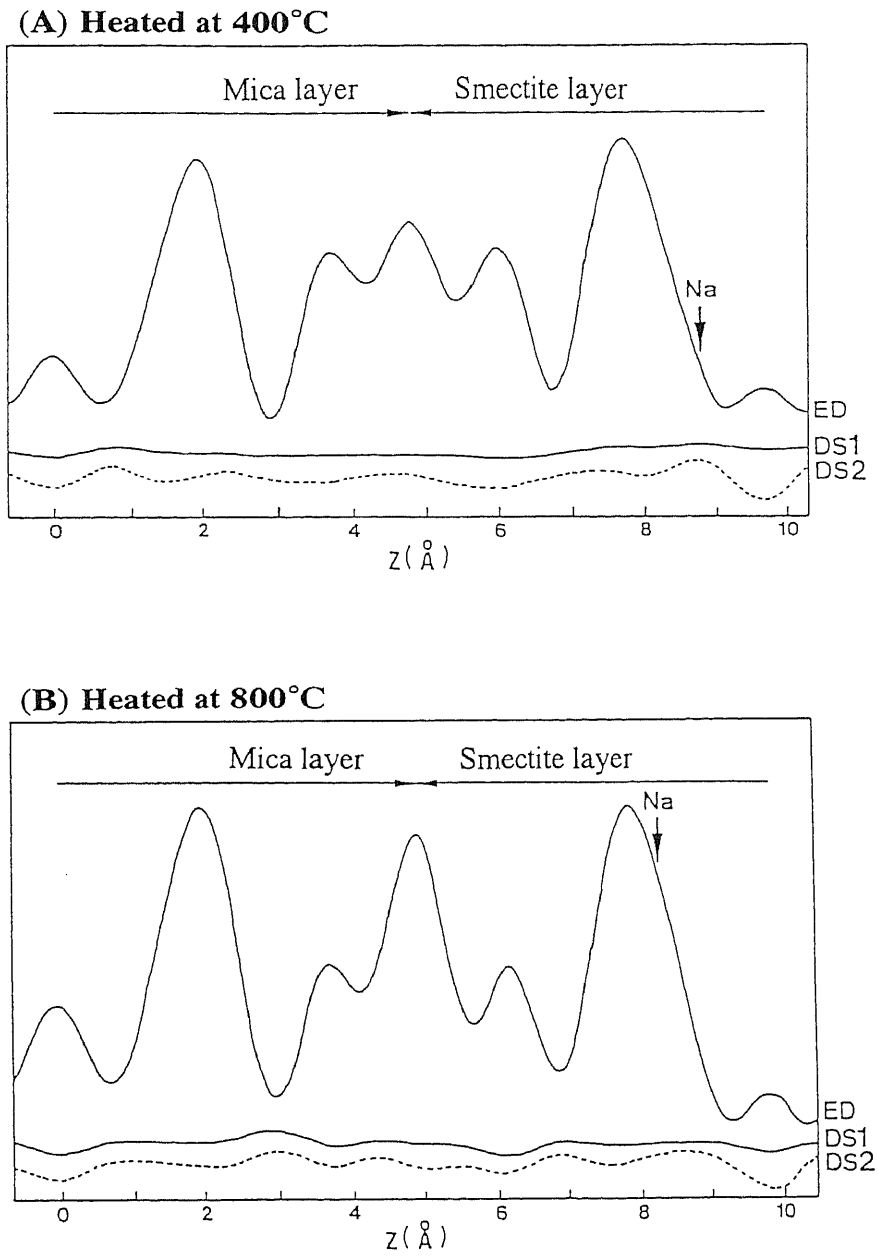

Figure 5.13. Electron density distribution and difference synthesis curves of Na-saturated rectorite heated at (A) 400° and (B) 800°C. ED = electron density distribution; DS1 = difference synthesis calculated by using z-parameters obtained by the least squares refinement; DS2 = difference synthesis calculated by assuming that interlayer cations are located at the center of interlayer space.

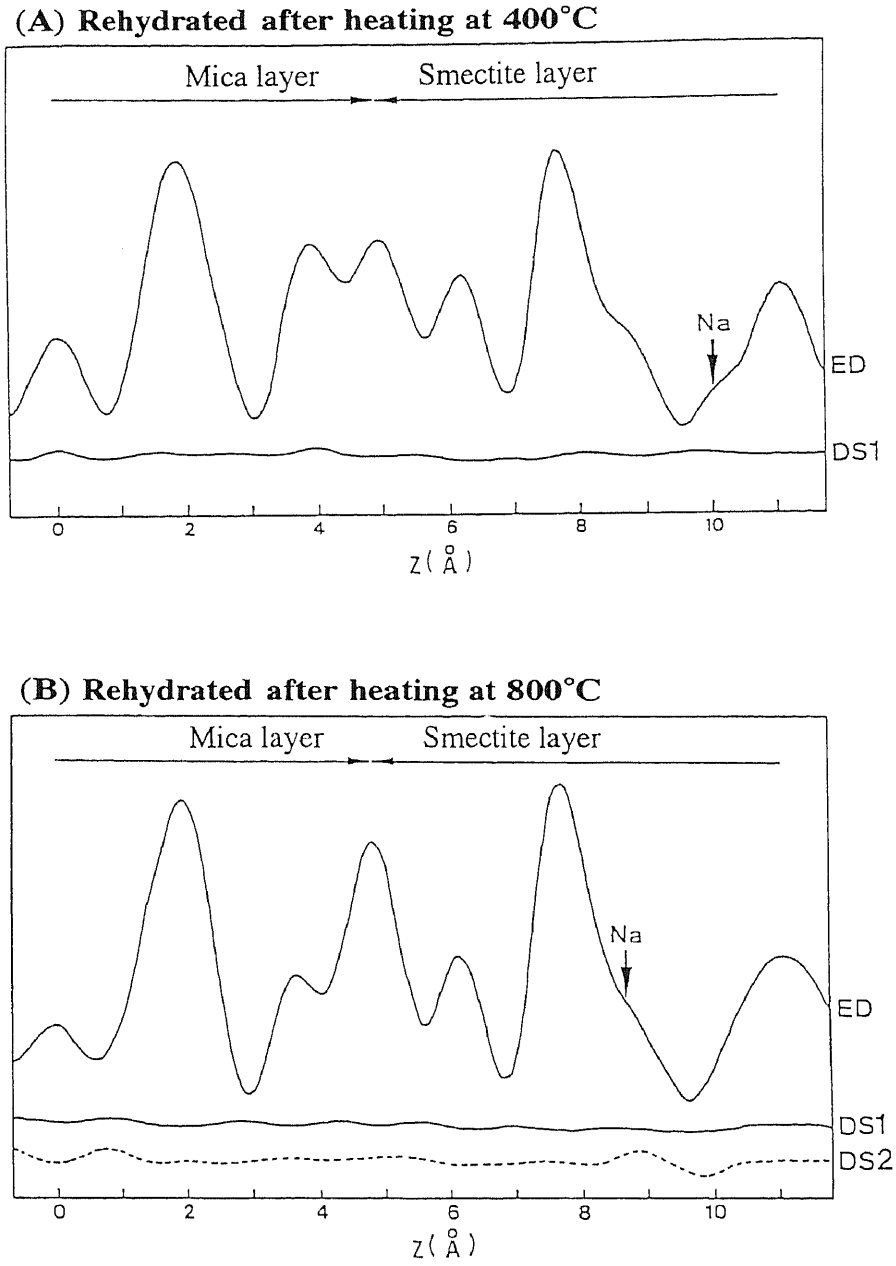

Figure 5.14. Electron density distribution and difference synthesis curves of rehydrated Na-saturated rectorite after heating at (A) 400° and (B) 800°C. ED = electron density distribution; DS1 = difference synthesis calculated by using z-parameters obtained by the least squares refinement; DS2 = difference synthesis calculated by assuming that interlayer cations are located at the center of interlayer space.